



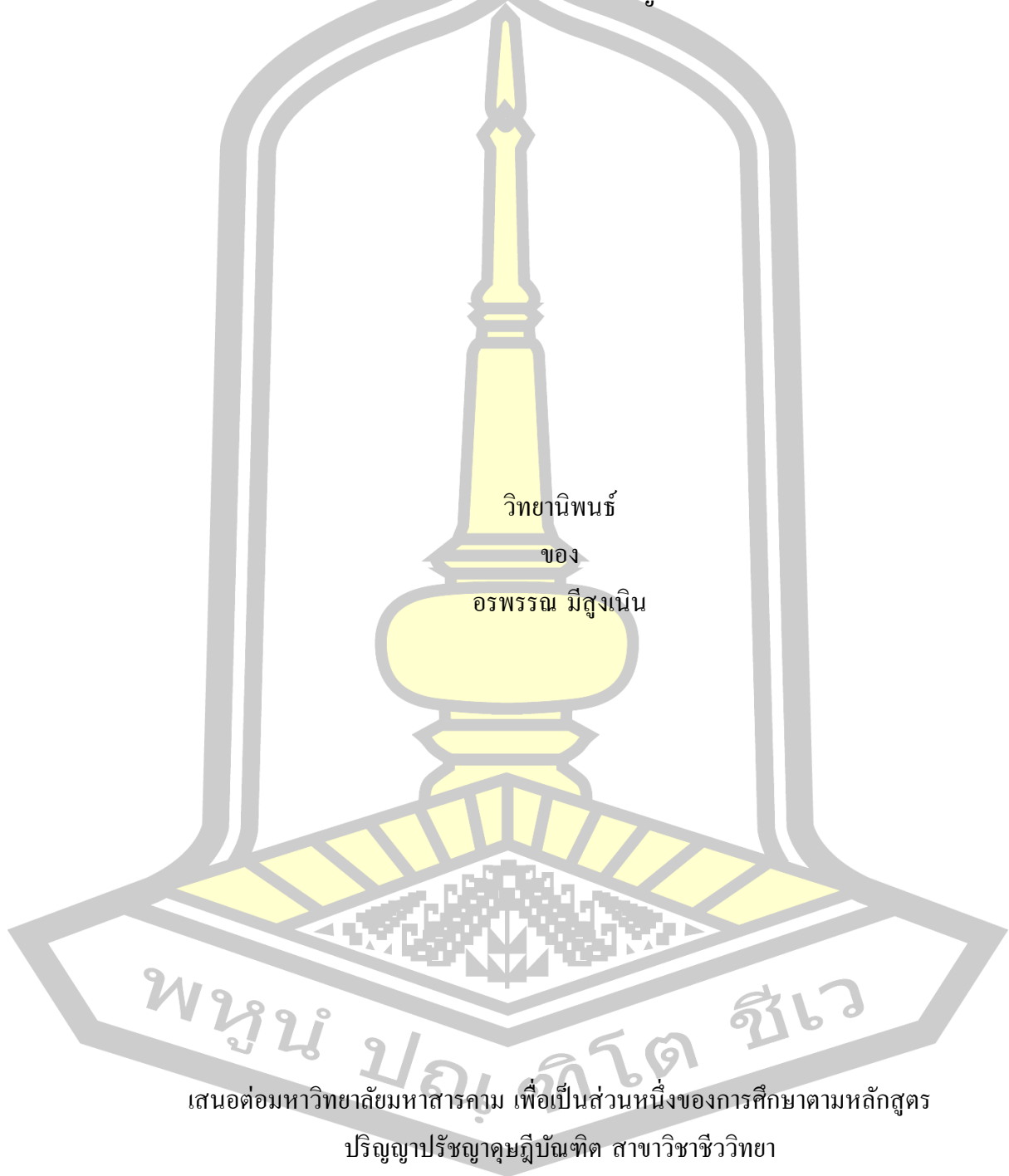
Characterization of siderophore production from *Pseudomonas aeruginosa* PDMZnCd2003 under zinc and/or cadmium conditions and the effect of crude siderophores on *Tagetes electa* L. growth

Orapan Meesungnoen

A Thesis Submitted in Partial Fulfillment of Requirements for
degree of Doctor of Philosophy in Biology
Academic Year 2017

Copyright of Maharakham University

คุณลักษณะสารไซเคอร์โรฟอร์ที่ผลิตจากแบคทีเรีย *Pseudomonas aeruginosa*
PDMZnCd2003 ภายใต้สภาวะที่มีสังกะสีและ/หรือแคดเมียม และผลกระทบของสาร
สกัดหยาบไซเคอร์โรฟอร์ต่อการเจริญเติบโตของดาวเรือง



เสนอต่อมหาวิทยาลัยมหาสารคาม เพื่อเป็นส่วนหนึ่งของการศึกษาตามหลักสูตร

ปริญญาปรัชญาดุษฎีบัณฑิต สาขาวิชาชีววิทยา

ปีการศึกษา 2560

สงวนลิขสิทธิ์เป็นของมหาวิทยาลัยมหาสารคาม

Characterization of siderophore production from *Pseudomonas aeruginosa* PDMZnCd2003 under zinc and/or cadmium conditions and the effect of crude siderophores on *Tagetes electa* L. growth



Orapan Meesungnoen

A Thesis Submitted in Partial Fulfillment of Requirements
for Doctor of Philosophy (Biology)

Academic Year 2017

Copyright of Mahasarakham University



The examining committee has unanimously approved this Thesis ,
submitted by Miss Orapan Meesungnoen , as a partial fulfillment of the requirements
for the Doctor of Philosophy Biology at Maharakham University

Examining Committee

Chairman

(Asst. Prof. Dr. Wiyada
Mongkolthanaruk)

Advisor

(Asst. Prof. Dr. Woranan
Nakbanpote)

Co-advisor

(Asst. Prof. Dr. Piyanete
Chantiratikul)

Committee

(Assoc. Prof. Dr. Aphidech Sangdee
)

Committee

(Asst. Prof. Dr. Piyaporn Saensouk)

Maharakham University has granted approval to accept this Thesis as a
partial fulfillment of the requirements for the Doctor of Philosophy Biology

(Prof. Dr. Pairoj Pramual)

Dean of the Faculty of The Faculty of
Science

(Asst. Prof. Dr. Krit Chaimoon)

Dean of Graduate School

Day.....Month.....Year.....



TITLE Characterization of siderophore production from *Pseudomonas aeruginosa* PDMZnCd2003 under zinc and/or cadmium conditions and the effect of crude siderophores on *Tagetes electa* L. growth

AUTHOR Orapan Meesungnoen

ADVISORS Assistant Professor Dr. Woranan Nakbanpote
Assistant Professor Dr. Piyanete Chantiratikul

DEGREE Doctor of Philosophy **MAJOR** Biology

UNIVERSITY Mahasarakham **YEAR** 2017
University

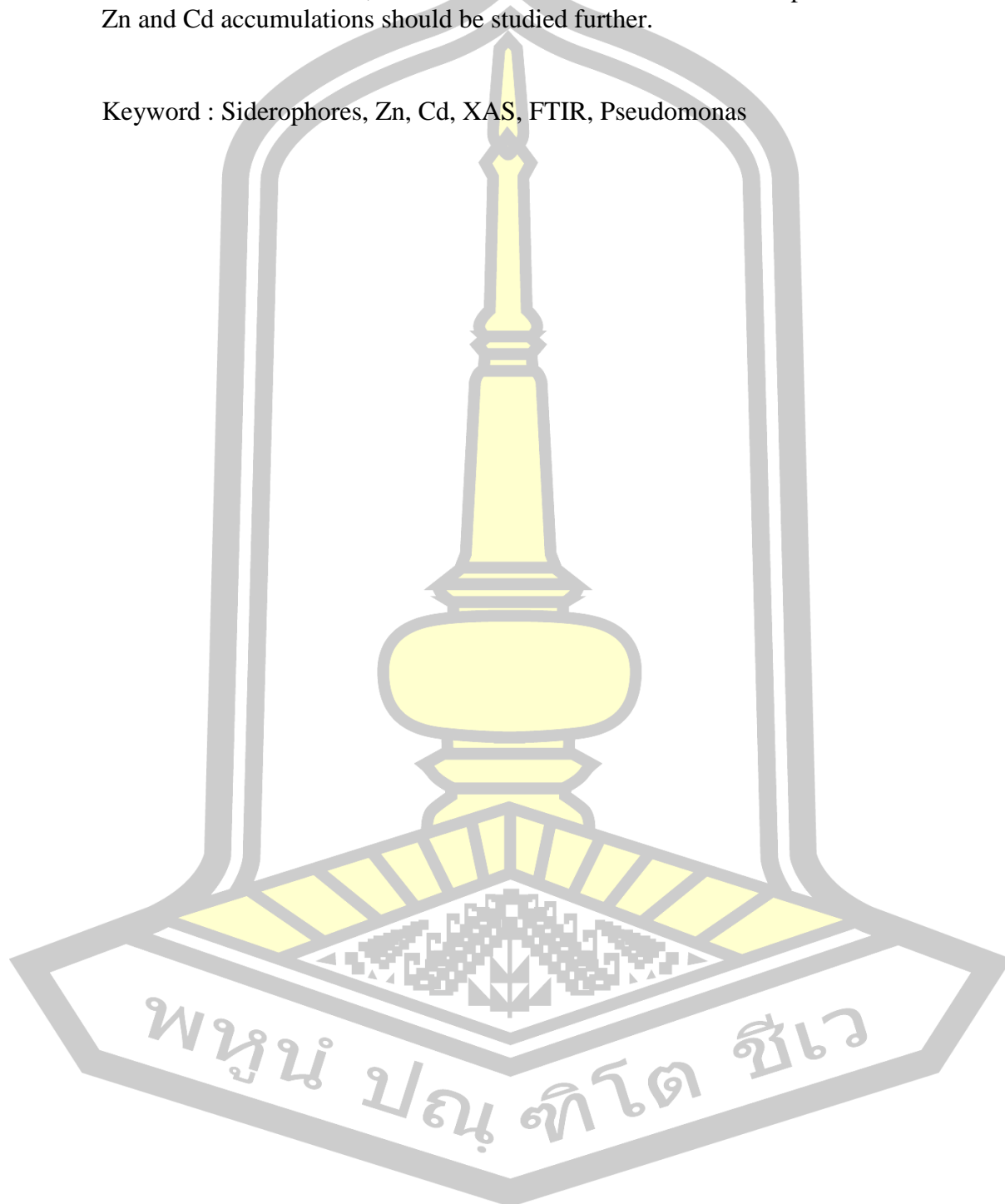
ABSTRACT

Pseudomonas aeruginosa PDMZnCd 2003 is a plant growth-promoting and Zn and Cd tolerant bacteria. This bacterial strain produced siderophores in nutrient broth (NB) (control) and NB separately containing with Zn, Cd, and Zn plus Cd. The siderophores were produced along with its bacterial growth curves. UV/visible scanning spectrophotometer of the supernatants in a range of 200-800 nm indicated that pyochelin was in control and all metals treatments, whereas pyoverdine was in the Cd and Zn plus Cd treatments. Siderophores from the medium supernatants (pH-8) and the supernatants adjusted pH to 2 (pH-2) were extracted by partition solvent extraction with ethyl acetate and *n*-butanol. Thin layer chromatographic (TLC) patterns showed pyochelin, pyoverdine and pseudomonine containing in the crude extracts. Pyochelin, pyoverdine chromophore, pyocyanin and pyridine-2,6-dithiocarboxylic acid (PDTC) were identified by liquid chromatography couple with mass spectrometry (LC-MS). S K-edge XANES spectra of pH-2 and pH-8 crude extracts determined by X-ray absorption fine structure (XAFS) and sulfur peak fitting indicated that multi-oxidation state of sulfur in reduced form were in the crude siderophore extracts. Fourier transform infrared (FTIR) spectroscopy and the principle component analysis showed the difference in functional groups of oxygen (O) and sulfur (S) between pH-2 and pH-8 crude extracts. Zn K-edge XANES spectra and Cd K-edge XANES spectra analyzed with linear combination fit (LCF) indicated to their oxidation state +2, and the pH adjustment from 8 to 2 decreased the amount of Zn and Cd in the pH-2 crude extracts. Zn K-edge EXAFS and Cd K-edge EXAFS spectra indicate to O/S coordination bonding with Zn and Cd in the pH-8 crude extracts. This research clearly showed that Zn and Cd induced *P. aeruginosa* PDMZnCd2003 to produce more than one type of siderophores. In which, Cd induced the bacterium to produce pyoverdine for relieving the Cd toxicity.

A pot experiment was carried out by growing marigold (*Tagetes electa* L.) in a Zn/Cd contaminated soil and each plant groups were separately treated with ethylenediaminetetraacetic acid (EDTA), citric acid and crude siderophore. The results showed that the providing of EDTA, citric acid and the crude siderophore improved the growth of marigold in the Zn/Cd contaminated soil. Especially,

siderophore enhanced the chlorophyll content in the plants' leaves. The EDTA increased solubility of Zn and Cd in the soil and supported Zn and Cd accumulation in shoot parts. However, citric acid and siderophore were not improved the Zn and Cd accumulation. Therefore, the unclear effect of the crude siderophore extracts on the Zn and Cd accumulations should be studied further.

Keyword : Siderophores, Zn, Cd, XAS, FTIR, Pseudomonas



ACKNOWLEDGEMENTS

I would like to express my sincere and deep gratitude to Assist. Prof. Dr. Woranan Nakbanpote, my thesis advisor, for her enlightening suggestions, untiring support and affectionate encouragement throughout this study. We are also immensely grateful to Assist. Prof. Dr. Piyanete Chantiratikul for their comments on an earlier version of the research progresses. I am particularly grateful to Assoc. Prof. Dr. Aphidech Sangdee, Department of Biology for plant pathogenicity test, Dr. Kanjana Thumanu, the Synchro-tron Light Research Institute (SLRI) for comment and suggestion on Fourier transform infrared spectroscopy, Asst. Prof. Dr. Widchaya Radchatawedchakoon, Department of Chemistry, Faculty of Science, Mahasarakham University for suggestion in the solvent extraction, Dr. Yanling Hua, Center for Scientific and Technological Equipment, Su-ranaree University of Technology for Liquid chromatography–mass spectrometry (LC-MS) analysis.

I am particularly grateful to Professor Dr. Akiko Hokura, Department of Green and Sustainable Chemistry, Tokyo Denki University, Chiyoda, Tokyo, Japan for supporting the research work on X-ray absorption fine structure (XAFS) experiments.

This research was supported by Mahasarakham University 2016. I am gratefully thanks Science Achievement Scholarship of Thailand (SAST), (20/2555), for a graduate study scholarship.

This study would not have been possible to be completed without assistance and willpower from my parents and friends in the Sustainable Development Laboratory (SDL). In addition, I really wish to thank the officers in the Faculty of Science and Faculty of Graduate Studies for good coordination of activities for the whole time.

พูนุ ปณุกิตติชัย

Orapan Meesungnoen

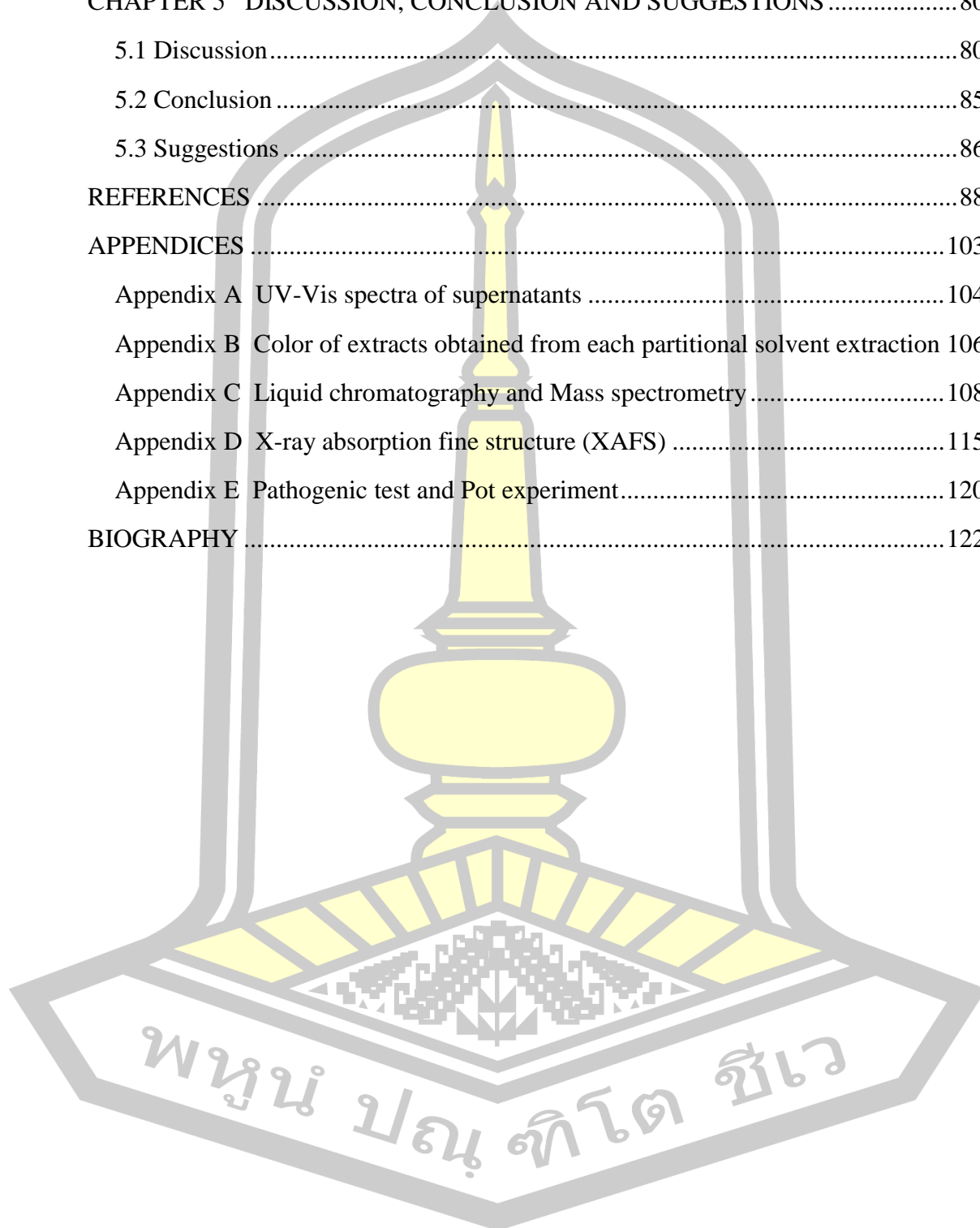
TABLE OF CONTENTS

	Page
ABSTRACT.....	D
ACKNOWLEDGEMENTS.....	F
TABLE OF CONTENTS.....	G
List of Table.....	K
List of Figures.....	L
CHAPTER 1 INTRODUCTION.....	1
1.1 Background.....	1
1.2 Objectives.....	4
1.3 Advantages of this study.....	4
CHAPTER 2 LITERATURE REVIEW.....	5
2.1 Introduction.....	5
2.2 Zinc and Cadmium.....	7
2.2.1 Zinc (Zn).....	7
2.2.2 Cadmium (Cd).....	7
2.3 Phytoremediation of heavy metal contamination.....	8
2.4 Microbial-assisted phytoextraction.....	9
2.4.1 Plant growth-promoting bacteria (PGPB).....	9
2.4.2 Siderophore-producing bacteria (SPB).....	11
2.5 Biology and chemistry of siderophore.....	15
2.6.1 Siderophore biosynthesis.....	15
2.5.2 Siderophore transport system.....	17
2.5.3 Siderophore structures.....	19
2.5.3.1 Hydroxamate siderophore.....	19
2.5.3.2 Catecholate siderophore.....	20
2.5.3.3 Carboxylate siderophore.....	20

2.5.3.4 Mixed ligand/heterocyclic-chelating siderophore	20
2.5.4 Effects of metals on siderophore production.....	21
2.6 Siderophore of <i>Pseudomonas</i> species.....	21
2.6.1 Pyoverdine (PVDs).....	23
2.6.2 Pyochelin	24
2.6.3 Pseudomonine	24
2.6.4 Yersiniabactin.....	24
2.6.5 Pyridine-2,6-bis(monothiocarboxylic acid) (PDTC).....	24
2.6.6 Quinolobactin	24
2.7 Siderophore extraction and characterization	25
2.7.1 <i>Pseudomonas</i> siderophore detection	27
2.7.1.1 Pyoverdine.....	27
2.7.1.2 Pyochelin	27
2.7.1.3 Pseudomonine	28
2.7.1.4 Yersiniabactin.....	28
2.7.1.5 Pyridine-2,6-bis(monothiocarboxylic acid) (PDTC).....	28
2.8 Marigold for heavy metal phytoremediation	28
2.8.1 Marigold	28
2.8.2 Marigold planting	29
2.8.3 Application of marigold in phytoremediation	30
CHAPTER 3 RESEARCH METHODOLOGY	32
3.1 Siderophores production, extraction and characterization.....	33
3.1.1 Bacterial cultivation under Zn and/or Cd treatments	33
3.1.2 Supernatant scanning by UV-Vis spectroscopy	34
3.1.3 Quantification of siderophore by CAS assay	34
3.1.4 Siderophore extraction	35
3.1.5 Analytical methods.....	35
3.1.5.1 Zn and Cd concentration in crude siderophore extracts	35
3.1.5.2 Thin layer chromatography (TLC)	35

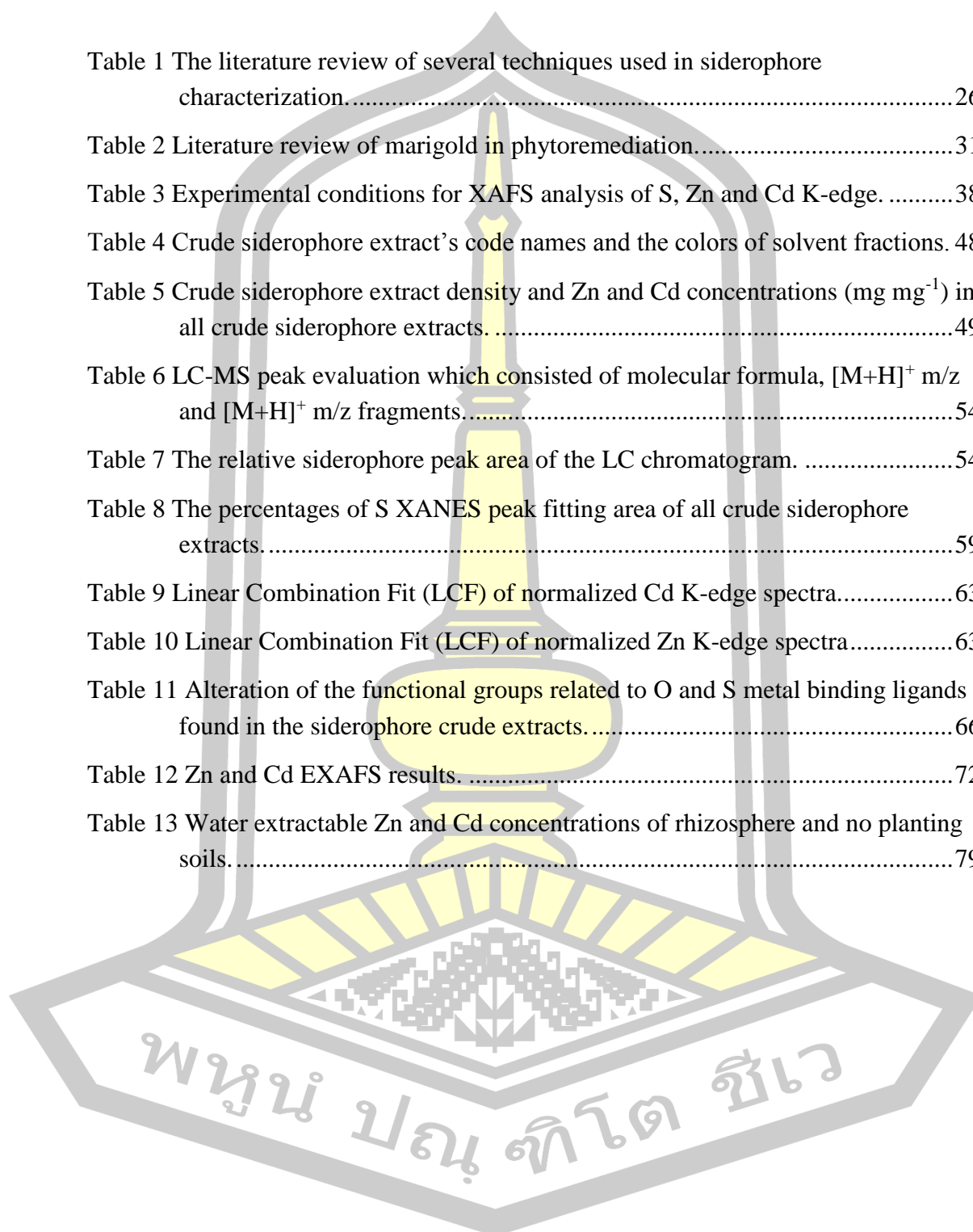
3.1.5.3 Liquid chromatography-quadrupole time-of-flight mass spectrometry (LC-QTOF MS)	37
3.1.5.4 Fourier transform infrared microspectroscopy (FTIR).....	37
3.1.5.5 X-ray absorption spectroscopy (XAS)	38
3.2 The effect of crude siderophore extract on Zn and Cd accumulation in marigold (<i>T. erecta</i> L.).	39
3.2.1 Plant pathogenicity test	39
3.2.2 Pot experiment of <i>T. erecta</i> L.....	40
3.2.3 Zn and Cd analysis	41
3.2.3.1 Total Zn and Cd extractions in shoot	41
3.2.3.2 Total Zn and Cd extractions in soil	41
3.2.3.3 Water extractable Zn and Cd in soil.....	41
3.2.4 Method validation.....	42
3.2.5 Statistical analysis	42
CHAPTER 4 RESULTS	43
4.1 Siderophore production and analysis of the productive siderophore induced by Zn, Cd, and Zn plus Cd	43
4.1.1 Bacterial growth curve and siderophore production	43
4.1.2 UV-Vis spectra of all supernatants.....	46
4.1.3 Analysis of crude siderophore extracts	48
4.1.3.1 Zn and Cd concentrations in crude siderophore extracts.....	48
4.1.3.2 Thin layer chromatography (TLC).....	50
4.1.3.3 Liquid chromatography-mass spectrometry (LC-MS)	52
4.1.3.4 X-ray absorption near edge structure (XANES)	55
4.1.3.4.1 Sulfur K-edge XANES	55
4.1.3.4.2 Zinc and cadmium K-edge XANES	60
4.1.3.5 Fourier transform infrared spectroscopy (FTIR) analysis	64
4.1.3.6 EXAFS analysis of Zn and Cd	71
4.2 The application of crude siderophores on Zn and Cd uptake in marigold.....	73
4.2.1 Plant pathogenicity test	73

4.2.2 Pot experiment.....	73
CHAPTER 5 DISCUSSION, CONCLUSION AND SUGGESTIONS	80
5.1 Discussion.....	80
5.2 Conclusion	85
5.3 Suggestions.....	86
REFERENCES	88
APPENDICES	103
Appendix A UV-Vis spectra of supernatants	104
Appendix B Color of extracts obtained from each partitional solvent extraction	106
Appendix C Liquid chromatography and Mass spectrometry	108
Appendix D X-ray absorption fine structure (XAFS)	115
Appendix E Pathogenic test and Pot experiment.....	120
BIOGRAPHY	122



List of Table

Table 1 The literature review of several techniques used in siderophore characterization.....	26
Table 2 Literature review of marigold in phytoremediation.....	31
Table 3 Experimental conditions for XAFS analysis of S, Zn and Cd K-edge.	38
Table 4 Crude siderophore extract's code names and the colors of solvent fractions.	48
Table 5 Crude siderophore extract density and Zn and Cd concentrations (mg mg ⁻¹) in all crude siderophore extracts.	49
Table 6 LC-MS peak evaluation which consisted of molecular formula, [M+H] ⁺ m/z and [M+H] ⁺ m/z fragments.....	54
Table 7 The relative siderophore peak area of the LC chromatogram.	54
Table 8 The percentages of S XANES peak fitting area of all crude siderophore extracts.....	59
Table 9 Linear Combination Fit (LCF) of normalized Cd K-edge spectra.....	63
Table 10 Linear Combination Fit (LCF) of normalized Zn K-edge spectra.....	63
Table 11 Alteration of the functional groups related to O and S metal binding ligands found in the siderophore crude extracts.....	66
Table 12 Zn and Cd EXAFS results.	72
Table 13 Water extractable Zn and Cd concentrations of rhizosphere and no planting soils.....	79



List of Figures

Figure 1 Importance of soil–plant–microbial interactions in bioremediation for the cleanup of metals and organics.....	6
Figure 2 Summarize of plant growth promoting bacteria and endophytic bacteria improve heavy metal phytoextraction.....	10
Figure 3 Plant growth-promoting mechanisms of SPB in metal contaminated soils..	13
Figure 4 Role of SPB in phytoextraction of heavy metal contaminated soils.	14
Figure 5 Pyoverdine (PVD) biosynthetic pathways.....	16
Figure 6 Three mechanisms and strategies of ferrisiderophore pathways in Gram-negative bacteria.	18
Figure 7 Metal specificities of the pyochelin and pyoverdine pathways.....	19
Figure 8 Ligands found in siderophore.....	20
Figure 9 Siderophores produced by fluorescent pseudomonads.....	22
Figure 10 The three PVDs of <i>Pseudomonas aeruginosa</i>	23
Figure 11 Pyoverdine structure.....	27
Figure 12 Some species of marigolds in Thailand.....	29
Figure 13 Research diagram for studying the effects of Zn and/or Cd on siderophore production by <i>P. aeruginosa</i> PDMZnCd2003	32
Figure 14 Research diagram for pot experiments to study the application of siderophores and other chelating agents on Zn and Cd accumulation in marigold (<i>T. erecta</i>).....	33
Figure 15 The steps of partition solvent extraction in this study and code name of crude siderophore extracts obtained in each steps.....	36
Figure 16 Relative growth.	44
Figure 17 Supernatant colors.	45
Figure 18 UV-Vis spectra of <i>P. aeruginosa</i> PDMZnCd2003's supernatants.....	47
Figure 19 TLC chromatogram detected under UV 360 nm.	51
Figure 20 LC chromatogram of the crude siderophore extracts.	53
Figure 21 X-ray fluorescent (XRF) spectra.	56
Figure 22 Normalized S K-edge XANES absorption spectra.....	57

Figure 23 Normalized S K-edge XANES peak fitting by the 7 Gaussian and Lorentzian peaks.....	58
Figure 24 Zn K-edge XANES absorption spectra.	61
Figure 25 Cd K-edge XANES absorption spectra.	62
Figure 26 The FTIR spectra of Ctrl (a), Zn (b), Cd (c) and Zn+Cd (d).....	65
Figure 27 The C=O and C-O peaks of the EtOAc (Ctrl, Zn, Cd and Zn+Cd) consisted of score plot (a), loading plot (b) and the average of normalized FTIR spectra (c).	67
Figure 28 The S=O and S-O peaks of the EtOAc (Ctrl, Zn, Cd and Zn+Cd) consisted of score plot (a), loading plot (b) and the average of normalized FTIR spectra (c).	68
Figure 29 The C=O and C-O peaks of the BuOH fractions (Ctrl, Zn, Cd and Zn+Cd) consisted of score plot (a), loading plot (b) and the average of normalized FTIR spectra (c).....	69
Figure 30 The S=O and S-O peaks of the BuOH fractions (Ctrl, Zn, Cd and Zn+Cd) consisted of score plot (a), loading plot (b) and the average of normalized FTIR spectra (c).....	70
Figure 31 Bacterial detection on shoot from non-inoculation.	73
Figure 32 Fresh weight (g) of leave (a), flower (b), stem (c) and root (d) in each treatments.	74
Figure 33 Dry weight (g) of leave (a), flower (b), stem (c) and root (d) in each treatments.	75
Figure 34 Index of relative chlorophyll content in each treatments.	75
Figure 35 Total Zn (a) and Cd (a) concentrations in leave of marigold in each treatments.	76
Figure 36 Total Zn (a) and Cd (b) concentrations in rhizosphere soil of marigold in each treatments.	76
Figure 37 Shoot fresh weight (a) and dry weight (b) of marigold in each treatments.	77
Figure 38 Total Zn (a) and Cd (b) concentrations in shoot of marigold in each treatments.	78

CHAPTER 1

INTRODUCTION

1.1 Background

Gynura pseudochina (L.) DC., a Zn/Cd hyperaccumulative plant, was found in a Zn mining area of Padang Industry, Mae Sot, Tak province, Thailand. This perennial plant was reported on tolerance and accumulation of a high Zn and Cd concentration (Phaenark et al. 2009; Nakbanpote et al. 2010; Panitlertumpai et al. 2013). Rhizospheric bacteria can enhance the uptake and accumulation of heavy metals in phytoremediation processes (Rajkumar et al. 2012). *Pseudomonas aeruginosa* PDMZnCd2003 was isolated from the rhizospheric soil of *G. pseudochina* growing in the zinc mine. This bacterial isolate tolerated to Zn and Cd, and it had plant growth-promoting abilities of indole-3-acetic acid (IAA) production, nitrogen fixation and phosphate solubilization even under the metals stress (Meesungnoen et al. 2009). In addition, Zn and/or Cd in nutrient broth induced *P. aeruginosa* PDMZnCd2003 to secrete parrot and yellow-green chemicals, which probably indicated to some siderophores (Meesungnoen et al. 2012). Siderophores are a group of naturally chelating agent produced by microorganism to chelate iron (Fe) and other metals. In which, *Pseudomonas* species normally produce pyoverdines, yellow-green siderophores (Cornelis and Matthijs 2007; Meyer 2007).

Effects of various heavy metals on bacterial siderophore production have been studied. The siderophore production of *Bacillus amyloliquefaciens* NAR38.1 was increased when cultured in glucose mineral salts medium without Fe and under heavy metals stress of Zn, cobalt (Co), molybdenum (Mo) and manganese (Mn). However, the abiotic stress from Cd, copper (Cu), arsenic (As), lead (Pb) and aluminum (Al) affected to decrease siderophore production (Gaonkar and Bhosle 2013). Uranium (U) induced siderophore production in marine cyanobacteria *Synechococcus elongatus* BDU 130911 even in Fe minus U dosed [Fe(-)U(+)] medium (Rashmi et al. 2013). An addition of Pb induced siderophore production of a

Pb resistant *P. aeruginosa* 4EA, but a high Pb treatment significantly declined in its siderophore production (Naik and Dubey 2011). However, a significant negative correlation was observed between the amount of siderophores produced by bacteria isolated from heavy metal contaminated soil and the amount of heavy metal (Hussein and Joo 2014).

Some analytical techniques used for studying and characterizing siderophores are UV-Vis spectroscopy, thin layer chromatography (TLC), Fourier transform infrared spectroscopy (FTIR), high-performance liquid chromatography (HPLC) and liquid chromatography-mass spectrometry (LC-MS). Siderophores of *Arthrobacter luteolus* were characterized as enterobactin in catecholate type by HPLC analysis, UV-Vis spectra and FTIR peaks (Emmanuel et al. 2012). Pyocyanin, pyochellin and 1-hydroxy-phenazine were detected by LC-MS/MS in the *P. aeruginosa* BRp3's crude siderophore extracts (Yasmin et al. 2017). *Rhizobium leguminosarum*'s siderophores were trihydroxamates, because supernatant of the bacterial culture was turned to orange color by ferric perchlorate reagent, and UV-Vis spectrum of the supernatant showed a broad spectral peak with a λ_{\max} at 450 nm (Carson et al. 2000). Using various spectroscopic methods of UV-Vis spectroscopy, extended X-ray absorption fine structure (EXAFS) and electron paramagnetic resonance (EPR) could solved the stoichiometry and coordination of the Fe (III) complexes of pyochelin, these results were consistent with the role of pyochelin in the uptake of Fe by FptA receptor protein in the outer membrane of *P. aeruginosa* (Tseng et al. 2006). The complexation properties of azotochelin with a series of oxoanions Mo (VI), W (VI) and V (V) and divalent cations Cu(II), Zn(II), Co(II) and Mn(II) were investigated by potentiometry, UV-Vis spectroscopy and X-ray absorption fine structure (XAFS) (Bellenger et al. 2007). A systematic density functional theory study supported by EXAFS and the infrared spectroscopic data were conducted to explain the structure and vibrational spectra of aqueous desferrioxamine B (DFOB) metal complexes vary with transition metal ions (Kruft et al. 2013).

Metal availability and mobility of metals in soil are important keys to improve uptake and accumulation of the metal in plants (Bhargava et al. 2012; Bolan et al. 2014). The efficiency of these plants can be increased by adding chelating agents. Application of ethylenediaminetetraacetic acid (EDTA), a synthetic chelator,

affected to increase bioconcentration factor (BCF) and translocation factor (TF) of Cd in marigold (*Tagetes patula*) and impatiens (*Impatiens walleriana*) (Wei et al. 2012). Comparison in the ability of citric acid (CA), oxalic acid (OA), nitrilotriacetic acid (NTA) and EDTA showed that CA>EDTA>OA>NTA for phytoremediation of U tailings by Indian mustard (*Brassica juncea* L.) (Jagetiya and Sharma 2013). Nevertheless, synthetic chelators, especially EDTA, are barely degraded in environments and the remains can be leached to ground water (Sun et al. 2001; Wu et al. 2004; Zhang et al. 2010). In addition, the synthetic chelators have negative effects or toxicity on plants and microorganisms (Krujatz et al. 2012). As naturally occurring chelating agents for iron, siderophores impacted to mineral dissolution and mobility (Bau et al. 2013; Voinot et al. 2013), enhanced iron uptake and prevented pathogens damage in plants (Miethke and Marahiel 2007). Their chelation made the abiotic metals such as Al³⁺, Cd²⁺, Cu²⁺ and Ni²⁺ hardly able to inhibit the synthesis of auxins, then the potential effects of auxins increased the plant growth-promoting and enhance the phytoremediation (Dimkpa et al. 2008). In addition, siderophores can promote phytoextraction (Rajkumar et al. 2010). Siderophores such as desferrioxamine B (DFOB), pyoverdine, pyochelin supplied Fe and other metals to plants (Yehuda et al. 2012; Nagata et al. 2013; Radzki et al. 2013).

The applications of siderophores in phytoremediation have been investigated over the synthetic chelators. Siderophores reduced toxic Cd uptake in *Streptomyces tendae* F4 whereas increased Cd uptake in sunflower (*Helianthus annuus*) (Dimkpa et al. 2009a). DFOB enhanced Cd accumulation in *Thlaspi caerulescens* (Karimzadeh et al. 2012). Plutonium (Pu)-DFOB complex was greater uptake 2-4 times than Pu-diethylenetriaminepentaacetic acid (DTPA) in *Zea mays* L. (Thompson et al. 2012). The coordination properties of pyoverdin (Pvd), produced by *P. aeruginosa* towards Cd(II) and Cu(II) indicated that stability constant of Pvd-Cu complex was much higher than that of Pvd-Cd; therefore, pyoverdine enhanced the mobility, phytoavailability and phytoextraction of Cu in tomato (*Lycopersicon esculentum* cv. St Pierre) and barley (*Hordeum vulgare* cv. Pasadena) (Cornu et al. 2014). Marigold is a suitable economical ornamental plants for phytoremediation in Thailand, because of a high demand of the cut flower (Chintakovid et al. 2008; Nakbanpote et al. 2016). Marigold had potential to remediate many toxic metals, especially Cd (Lal et al. 2008;

Liu et al. 2011a, b). Although there are many application of marigold in phytoremediation, effects of siderophores on mobility of heavy metal metals in soil and uptake of the metals in marigold have not been reported.

Therefore, this research aimed to study the productive siderophores of *P. aeruginosa* PDMZnCd2003 under Zn, Cd, and Zn plus Cd contaminated in nutrient broth (NB). Siderophore production under Zn and/or Cd treatments is quantitatively analyzed by Chrome Azurol Sulfonate (CAS) assay, and characterized by UV-Vis spectroscopy, FTIR, XAFS and LC-MS. Furthermore, the applications of crude siderophores on Zn and Cd accumulation were investigated by using marigold (*T. erecta*) as a model plant for pot experiments.

1.2 Objectives

1.2.1 Study the effect of Zn, Cd and Zn plus Cd on siderophores production of *P. aeruginosa* PDMZnCd2003.

1.2.2 Characterize the *P. aeruginosa* PDMZnCd2003 siderophores produced under Zn, Cd and Zn plus Cd treatments, by UV-Vis spectrophotometry, FTIR, XAFS and LC-MS.

1.2.3 Investigate the applications of *P. aeruginosa* PDMZnCd2003 siderophores on Zn and Cd accumulations in marigold.

1.3 Advantages of this study

1.3.1 The data obtained could explain the siderophores production from *P. aeruginosa* PDMZnCd2003 under the abiotic stress of Zn and/or Cd.

1.3.2 Bacterial cultivation, siderophore extraction and many analytical techniques used in this research could be applied to study siderophore production by other bacteria under other metals stress.

1.3.3 Application of crude siderophores from *P. pseudomonas*, which is both a plant growth promoting bacterium and a probable pathogenic bacterium, could be another way of microbial application in a phytoremediation process.

CHAPTER 2

LITERATURE REVIEW

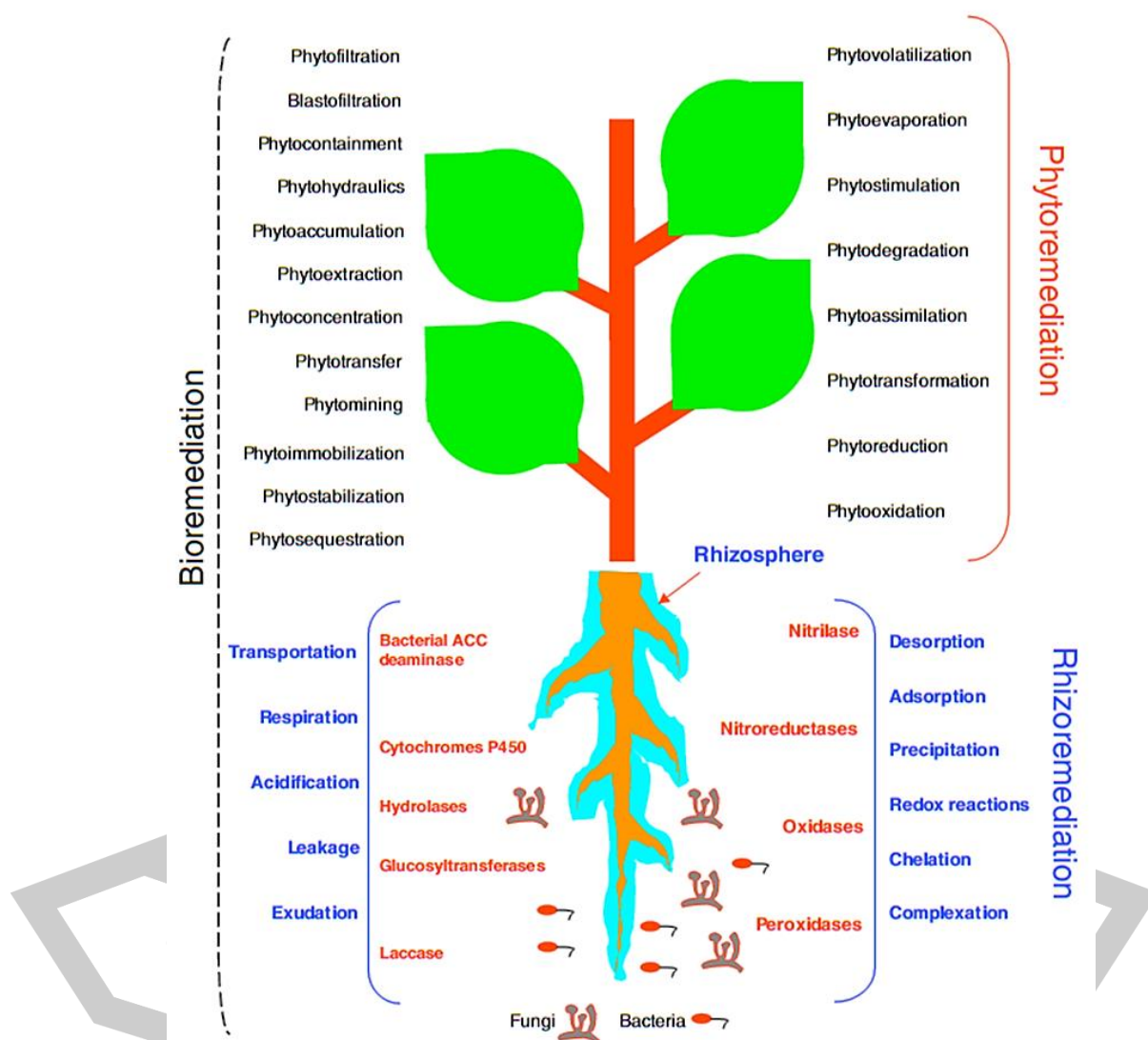
2.1 Introduction

Heavy metal pollution is the one of main worldwide problems that affect the human quality and environments. Beginning of pollution is industrialization, civilization, human activities, destroyed and utilized natural resources. The worst effects of environmental pollution have been ameliorated. Several approaches have been developed to resolve the problem. The recent concept of remediation is a sustainable technology to cover of commercial, social and environment factors (de-Bashan et al. 2012). Using green materials or living organism including plants, algae and microorganism have been interested to restore the contaminated area. The overall processes are called bioremediation. Phytoremediation is a technical term of using plants associated with microorganism (Figure 1). Advantages of phytoremediation are low cost, flexible and supplementary method for engineering-based remediation methods (Pilon-Smits 2005). To successful of phytoremediation, bacteria and fungi in rhizosphere release various metabolites and enzymes to mobilize/immobilize the metal leading to improve metal uptake and accumulation or plant growth. The microbial processes in the rhizosphere are rhizoremediation.

The common definition of rhizosphere is the surrounding root surface or cover the extended root or the soil tightly compact with the root. This area is influenced proportionally by plant root (root exudates), and there are still living activities and interaction between plant root and other organisms such as microbes and microfauna (nematodes and protozoa etc.). The complexed relationships between plants and rhizospheric organisms have been studied including microbial community, root exudates, microfauna and nutrient cycling (Hawkes et al. 2007; Standing and Killham 2007).

Microorganism such as fungi, mycorrhiza and bacteria is respected to enhance phytoremediation with the prompting plant growth and biocontrol ability.

Plant growth-promoting bacteria (PGPB) have been widely studied and applied. They have many advantages including grow fast, broad utilize of substrates, and produce benefit secondary metabolites (Tilston et al. 2010). Siderophores is a metabolites of microorganism that secreted to scavenge iron or essential elements for their growth. These compound impact phytoremediation by enhance heavy metal uptake to plants.



Reference: Ma et al. (2011)

Figure 1 Importance of soil-plant-microbial interactions in bioremediation for the cleanup of metals and organics.

2.2 Zinc and Cadmium

Heavy metal is defined base on the density as $3.5-7 \text{ g cm}^{-3}$ (Duffus 2002). However, the heavy metal definition is quite meaningless on physical property in plants and other living organisms. The metals are available to them in solution or to react with other elements or form compounds/complexes and can be solubilized, do not deal with metal state (valence state of 0). Even if chemical compound such as salt is formed, the metal density does not play any role (Appenroth 2010). Some heavy metals including (Fe), zinc (Zn), copper (Cu), manganese (Mn), and cobalt (Co) Cadmium (Cd), lead (Pb), and mercury (Hg) are essential heavy metals in organism (Nakbanpote et al. 2016). Heavy metals are not degraded biologically in soil. It occurs as free metal ions, exchangeable metal ions, soluble metal complexes (sequestered to ligands), organically bound, precipitated, or insoluble compounds such as oxides, carbonates, and hydroxides; or they may form silicate (indigenous soil content) (Kabata-Pendias and Pendias 2001).

2.2.1 Zinc (Zn)

Zn is the first element in group 12 in the periodic table. It has atomic number 30, atomic mass 65.39 (atomic mass unit, amu), melting point 419.58°C , boiling point 907.00°C and classified to be transition metal. Zn has the density 7.133 g cm^{-3} at 293 K and hexagonal in crystal structure. The common oxidation state is +2. Leakage of Zn to environment causes by the processes of Zn mining, smelter slag, chemical fertilizers, etc.

Zn is an essential element for biological metabolism. It involves in enzyme reactions, transcription factors of gene expression and zinc finger protein in the interaction of DNA structure and other protein. Many proteins consist of Zn as co-factor and co-activating function because it is stable in biological medium. Zn across cell membrane through specific Zn-protein channel (Tapiero and Tew 2003).

2.2.2 Cadmium (Cd)

Cd is an element in group 12 of periodic table. However, it is not categorized as a transition metal, because no electron is filled in d or f electron shell. It has atomic number 48, atomic mass 112.411 amu, density 8.7 g cm^{-3} , melting point

321 °C, boiling point 767 °C, oxidation state +2 (+1 in mildly basic oxide), and hexagonal close-packed crystal structure.

Cadmium has been no reported the advantages in living organism, however, marine diatoms *Thalassiosira weissflogii* was found cadmium-containing carbonic anhydrase enzymes (Lane et al. 2005). Cd is released by mining, metallurgy industry, manufactures of batteries, pigments and phosphate fertilizer. Cd are affected cell reproduction, differentiation, cause apoptosis and lead to cancer in prostate, lung and testes. Itai-Itai is well-known of Cd toxicity and developing to disease in Japan. Cd ions can induce ROS production and DNA damage. In addition, Cd can compete with other essential ions to interact with protein, enzymes or any molecules in metabolism processes especially Zn, Ca and Fe (Bertin and Averbeck 2006; Nordberg 2009).

2.3 Phytoremediation of heavy metal contamination

Heavy metals cannot degrade unlike other contaminants such as organic compounds or pesticides. Metals in soil are in form of free metal ions or soluble metal complexes, adsorbed on surface of soil particles, bound to soil organic matter such as humus, formed to oxide, hydroxide or carbonate compound and precipitation, and embedded in ore structure. Only free metal ions and metal absorbed on soil particle surface can be bioavailability (Colombo et al. 2014).

Phytoremediation is the use of plant to clean up the pollutants by physiology and metabolism of plants occurring against toxic pollutant to survive under stress environments (Ghosh and Singh 2005; Pilon-Smits 2005; Krämer 2005). Plants which growing in contaminated area develop several mechanisms for survival in metal toxicity including preventing metal uptake or accumulation inside. Plant which can accumulate a high metal concentration in its biomass called hyperaccumulator. Wild-type hyperaccumulators usually have low rate of metal uptake. The slow growth of hyperaccumulators and limitation of metal solubility in soil are problems in this approach. Artificial or genetically engineering hyperaccumulator have been developed for commercial proposes or more effectiveness. Another strategy to improve metal uptake to plant roots have been studied and found including beneficial

microorganism that enhance metal uptake and metal bioavailability (Atlas and Philp 2005).

2.4 Microbial-assisted phytoextraction

There are few researches in field experiments of soil-plant-microbes relationship. Information of the interaction between microbes and plant, the metal chemistry processes and bioaugmentation in field experiments is required before application (Lebeau et al. 2008; Ma et al. 2011; Rajkumar et al. 2012). The general information of microbial-assisted phytoremediation divided into plant growth-promoting bacteria (PGPB) and siderophore-producing bacteria (SPB) (Rajkumar et al. 2010).

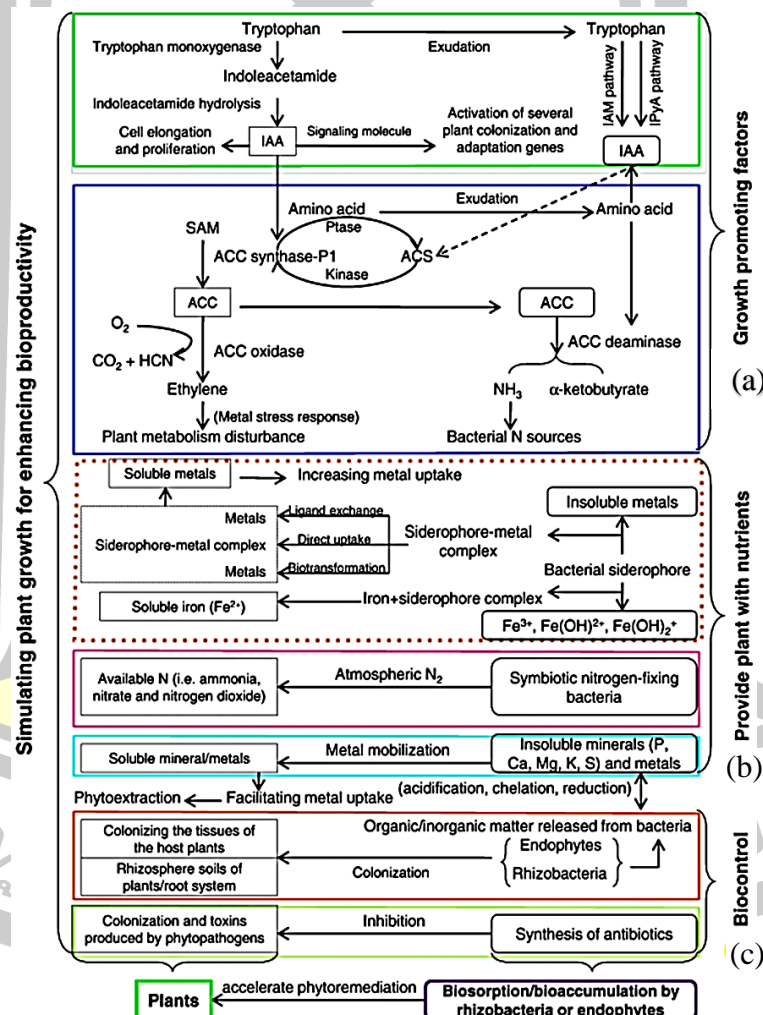
2.4.1 Plant growth-promoting bacteria (PGPB)

Microorganisms play a key role in natural and artificial ecosystem. Plant growth-promoting bacteria (PGPB) are beneficial bacteria containing plant growth promoting abilities (Figure 2(a)). PGPB synthesize phytohormones such as indole-3-acetic acid (IAA) by using tryptophan obtained from plant. IAA activate plant cell elongation and proliferation. It is a signaling molecule for bacterial colonization in plant. IAA functions are contrast with ethylene. Ethylene is involving in the tolerance of biotic and abiotic stress, inhibit cell elongation, seedling formation when it is overproduction. A 1-aminocyclopropane-1-carboxylic acid (ACC) is intermediate precursor in ethylene biosynthesis pathway and IAA is altered to 1-aminocyclopropane-1-carboxylate synthase (ACS) for ACC biosynthesis. PGPB can utilize ACC as a nitrogen source by produce ACC deaminase enzyme (Glick 2014). Cytokinins and gibberellins are the others phytohormones found in PGPB (Gutierrez-Manero et al. 2001; Arkhipova et al. 2007).

Figure 2(b) shows that PGPB enhance nutrient providing such as nitrogen by nitrogen fixation. Phosphorus, magnesium and insoluble minerals are provided to plant by many processes including acidification, chelation and redox reaction. Iron is an essential element for living organism and exists as insoluble ferric state (Fe^{3+}). Bacteria synthesize siderophores to scavenge iron and other elements and defense plant's pathogen by competition or limitation of available iron (Sayed et al. 2008). It

improve IAA biosynthesis by reducing the oxidative stresses from heavy metals (Dimkpa et al., 2009b).

PGPB also act as biocontrol (Figure 2(c)) by producing antibiotic agents to suppress plant pathogens and activate the induced systemic resistance of plant defense mechanism (Van Loon and Bakker 2006). Extracellular enzymes or organic/inorganic compounds from PGPB enhance the plant colonization. Extracellular polymeric substances (EPS), biosurfactances and glycoprotein that secreted outside the bacterial cells can modify the soil structure and induce the plants to response on stresses (Nehl and Knox 2006).



Reference: Ma et al. (2011)

Figure 2 Summarize of plant growth promoting bacteria and endophytic bacteria improve heavy metal phytoremediation by (a) plant growth promoting factors, (b) providing nutrients to plants and (c) acting as biocontrol.

2.4.2 Siderophore-producing bacteria (SPB)

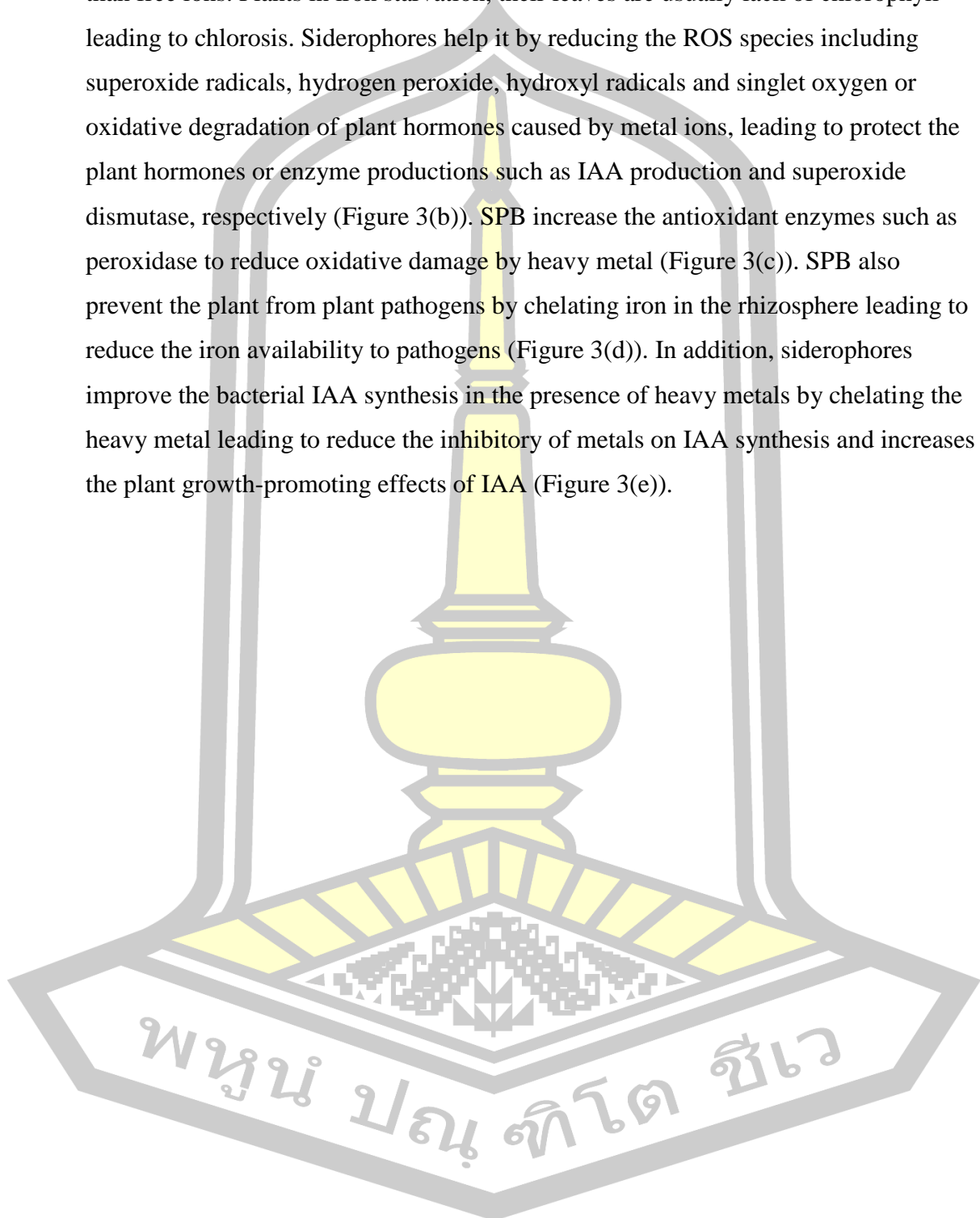
Some heavy metals in soil is slightly soluble and difficult to uptake by plants. Phytoremediation, especially phytoextraction, need to increase metal uptake. The pH of rhizosphere has influenced metal behavior including bioavailability and mobility. Lower pH causes metal ion to release from soil surface and mobility. Some chelating agents such as EDTA, citrate, oxalate and malate can improve the metal availability and metal uptake by plant root (Jagetiya and Sharma 2013). EDTA enhances the Cd uptake in French marigold and impatiens (Wei et al. 2012). Jagetiya and Sharma (2013) compared chelator citric acid, oxalic acid, nitrilotriacetic acid and EDTA and found that EDTA depressed Indian mustard growth but it enhanced uranium uptake. However, the toxicity of synthetic chelators and the leaching of synthetic chelators to ground water lead to not acceptance. Addition of EDTA reduced the toxicity of Ni and Cd, but it also exhibited an inhibitory effect on growth of growth-promoting rhizobacterium *P. brassicacearum* (Krujatz et al. 2012).

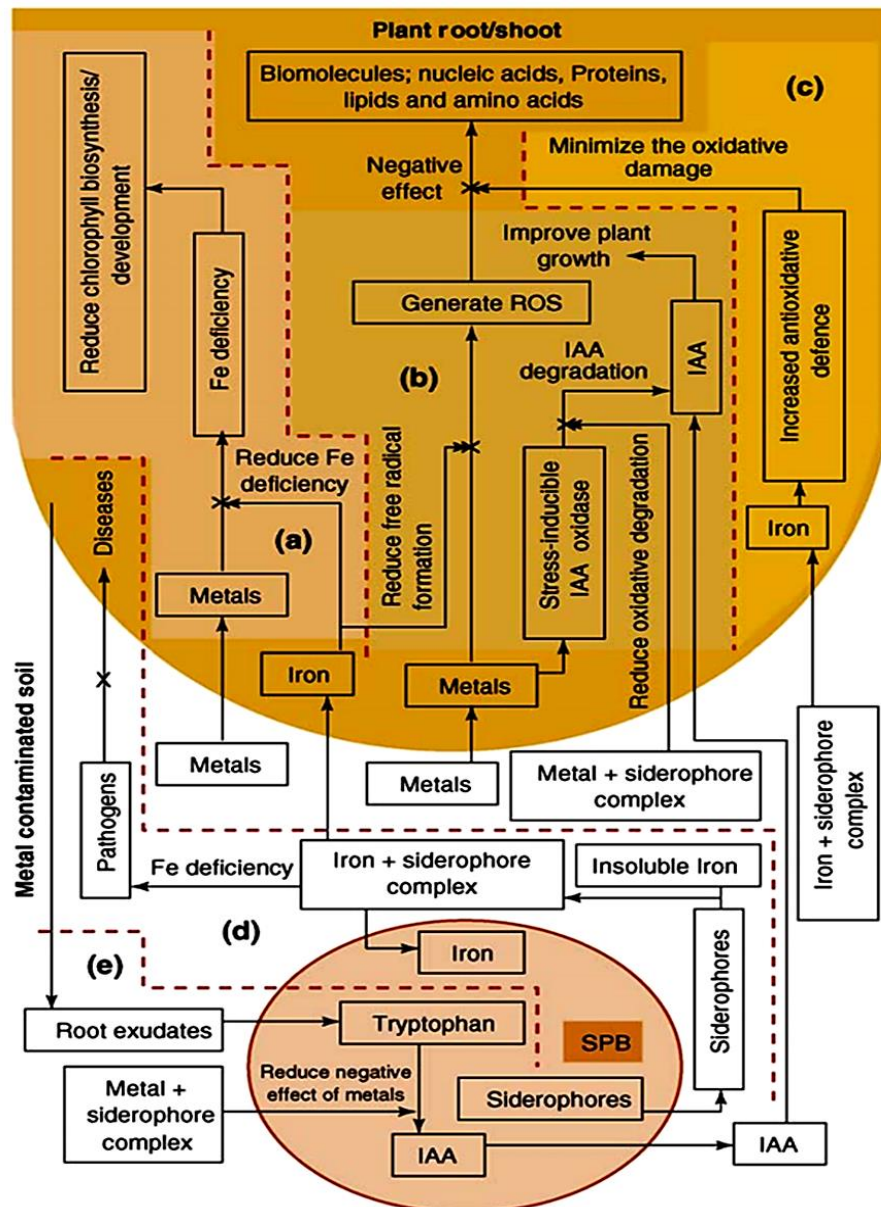
Biochelators, which are produced by plant and microorganism such as metallothioneins, organic acids and siderophores, enhance metal mobilization in rhizosphere and bulk soil. Chelating agents such as bacterial siderophores are released to scavenge metal ions leading to reduce metal toxicity by stop their mobility and reactivity. These molecules are alternative, degradable and friendly to environments.

Siderophores is important biomolecules on iron acquisition in bacteria and indirect iron supplement mechanism in plants. In addition to iron, other metal such as Zn, Cd, and Cu can be chelated by siderophores. The siderophore biosynthesis is participating in heavy metal tolerant mechanism of bacteria. Bacteria protect their cells from metal toxicity by various ways including sequestration, exclusion or efflux system, complexation, detoxification and compartmentalized in vacuole. EPS also prevent bacterial cells from metal ions by binding them with anionic functional groups or ligands (sulfhydryl, carboxyl, hydroxyl, sulfonate, amine and amide groups) (Nies 1999; Meesungnoen et al. 2012).

SPB assist phytoremediation by enhance metal availability and also indirectly promote plant growth. The mechanism of SPB on plant tolerant are summarized in Figure 3. Plant growing in contaminated area or extreme environment have negative effects on growth, physiology and the iron deficiency (Figure 3(a)).

SPB can reduce its effects on plants by chelating or transform them to lower toxic than free ions. Plants in iron starvation, their leaves are usually lack of chlorophyll leading to chlorosis. Siderophores help it by reducing the ROS species including superoxide radicals, hydrogen peroxide, hydroxyl radicals and singlet oxygen or oxidative degradation of plant hormones caused by metal ions, leading to protect the plant hormones or enzyme productions such as IAA production and superoxide dismutase, respectively (Figure 3(b)). SPB increase the antioxidant enzymes such as peroxidase to reduce oxidative damage by heavy metal (Figure 3(c)). SPB also prevent the plant from plant pathogens by chelating iron in the rhizosphere leading to reduce the iron availability to pathogens (Figure 3(d)). In addition, siderophores improve the bacterial IAA synthesis in the presence of heavy metals by chelating the heavy metal leading to reduce the inhibitory of metals on IAA synthesis and increases the plant growth-promoting effects of IAA (Figure 3(e)).

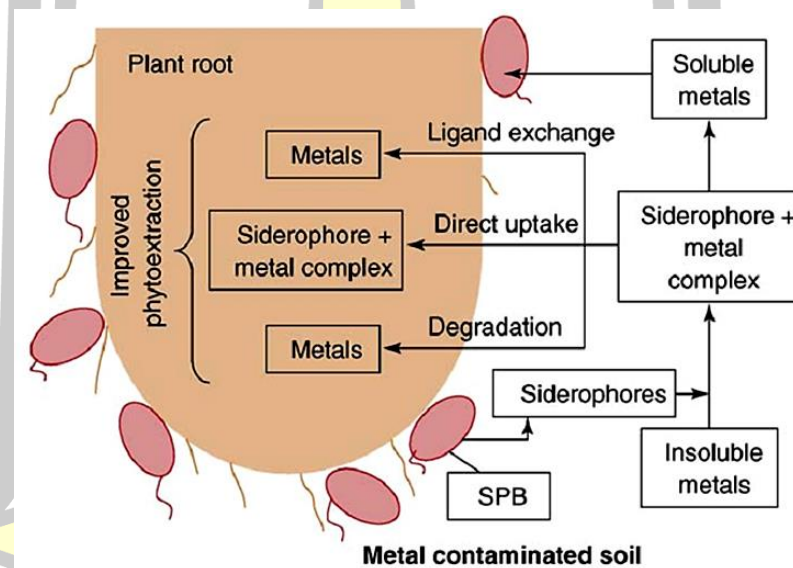




Reference: Rajkumar et al. (2010)

Figure 3 Plant growth-promoting mechanisms of SPB in metal contaminated soils. Metal accumulation in plant tissues negatively affects Fe uptake and chlorophyll biosynthesis (a). SPB alleviate metal-induced oxidative stress in plants and reduce the oxidative degradation of indole-3-acetic-acid (IAA) by reducing the formation of free radicals (b). SPB also minimize negative effects of reactive oxygen species (ROS) by increasing peroxidase (POD) activity (c). Siderophores protect the plant from microbial pathogens by chelating iron in the rhizosphere and thus reducing its availability to pathogens that are reliant on this metal (d). Siderophores promote bacterial IAA synthesis in the presence of heavy metals by chelation, which in turn reduces the inhibitory capacity of these metals on IAA synthesis and potentially increases the plant growth-promoting effects of IAA (e).

SPB can enhance phytoextraction by increasing metal accumulation in plant biomass. Siderophores chelate metal ions bearing on soil particles and become to metal-siderophore complexes. The root transported mechanisms of siderophores have various ways to improve metal accumulations. SPB release siderophores into rhizosphere and thus chelate to insoluble metal ions to form siderophore-metal complex. There are 3 pathways to import siderophore-metal complex into root (Figure 4); (i) degradation the complex and uptake the metal into the root, (ii) direct uptake the whole siderophore-metal complex molecule passes through the root membrane, and (iii) ligand exchange between the metal ion in the siderophore-metal complex and the ligands on the cell membrane, the free siderophores was released or degraded by cell membrane-enzymatic systems. The metal ion in the siderophore-metal complex can alter to be soluble metal and is uptake by SPB again (Rajkumar et al. 2010).



Reference: Rajkumar et al. (2010)

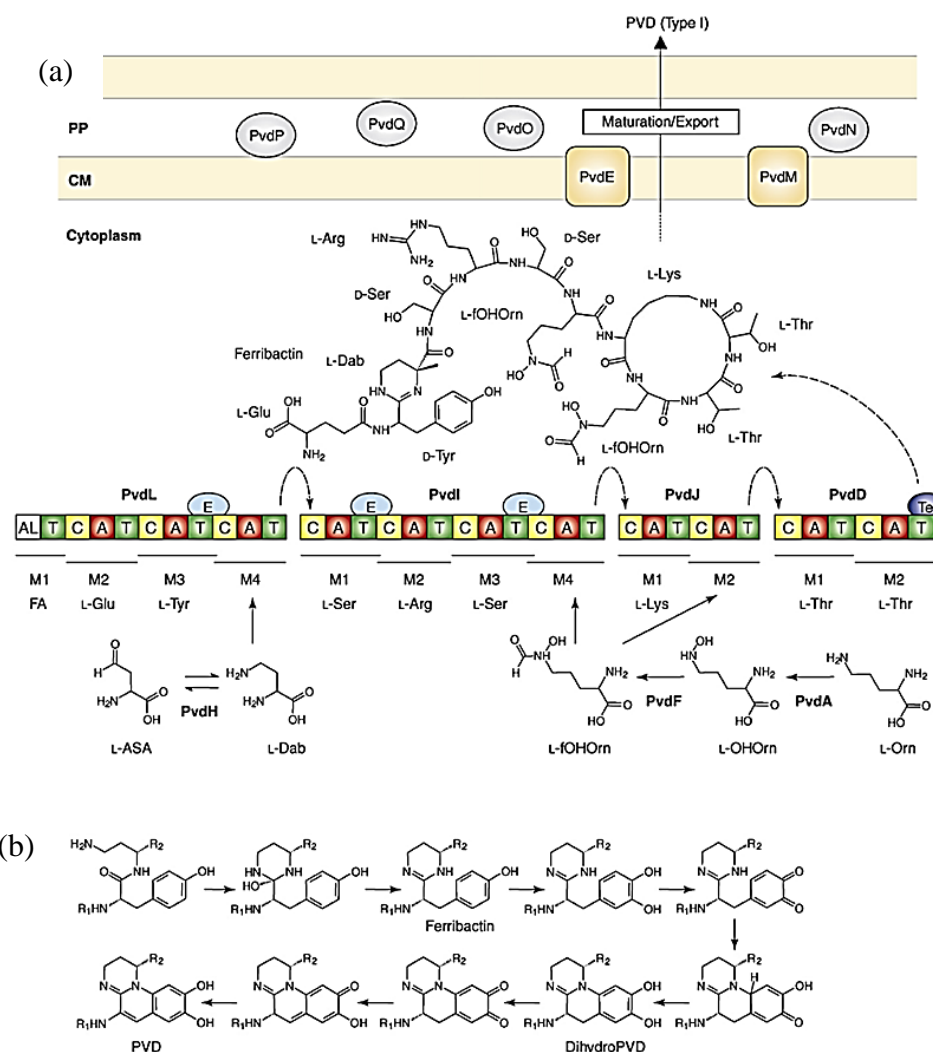
Figure 4 Role of SPB in phytoextraction of heavy metal contaminated soils. Siderophores produced by SPB solubilize insoluble heavy metal-bearing minerals by chelation. Plants can uptake metals from metal–siderophore complexes by root processes including chelate degradation and release the metals, the direct uptake of siderophore–metal complexes or by a ligand exchange reaction.

2.5 Biology and chemistry of siderophore

Siderophores is a naturally iron chelators produced from microorganism, and they can across or active transport through the cell membrane. Siderophores are secondary metabolites that can chelate Fe or other ions such as Al, Zn, Cu, Cd or rare earth elements (REEs). In which, the concentrations of iron or other ions affect the regulation of siderophores biosynthesis (Raymond and Dertz 2004; Meyer 2007; Visca et al. 2007).

2.6.1 Siderophore biosynthesis

The biosynthetic pathway of siderophores are involve in aerobic metabolism that oxygen molecules activated mono-, di- and *N*-oxygenases enzymes and used acid molecules from the final oxidation reactions in citric acid cycle, such as citrate, succinate and acetate. Moreover, all siderophore peptides are synthesized by non-ribosomal peptide synthetases. Siderophore synthesis is independent from the primary metabolism (Visca et al. 2007; Schalk and Guillon 2013). For example, pyoverdine (PVD) biosynthesis pathway in *P. aeruginosa* POA1 is shown in Figure 5. There are 4 largest PVD synthesis gene including *pvdL*, *pvdI*, *pvdJ* and *pvdD* for encoding peptide synthetase enzymes (Figure 5(a)). These enzymes involve the formation of peptide bond in amino acids via non-ribosomal synthesis leading to the present of amino acid residues in PVD such as D-Ser, *N*⁵-formyl-*N*⁵-hydroxyornithine (fOHOrn) and chromophore precursors. The order of amino acids in PVD involve the transfer of intermediates from PvdL via PvdI and PvdJ to PvdD and generated the peptide chain (Figure 5(a)). PvdH, PvdA and PvdF are precursor-generating enzymes. PvdH generates 2,4-diaminobutyrate (Dab) and PvdA and PvdF is catalyze synthesis of fOHOrn. Biochemical processes of PVD chromophore maturation have not yet been fully characterized. PVD precursor is synthesized and maturation in the cytoplasm. PVD exportation mechanism is not clear (Visca et al. 2007).



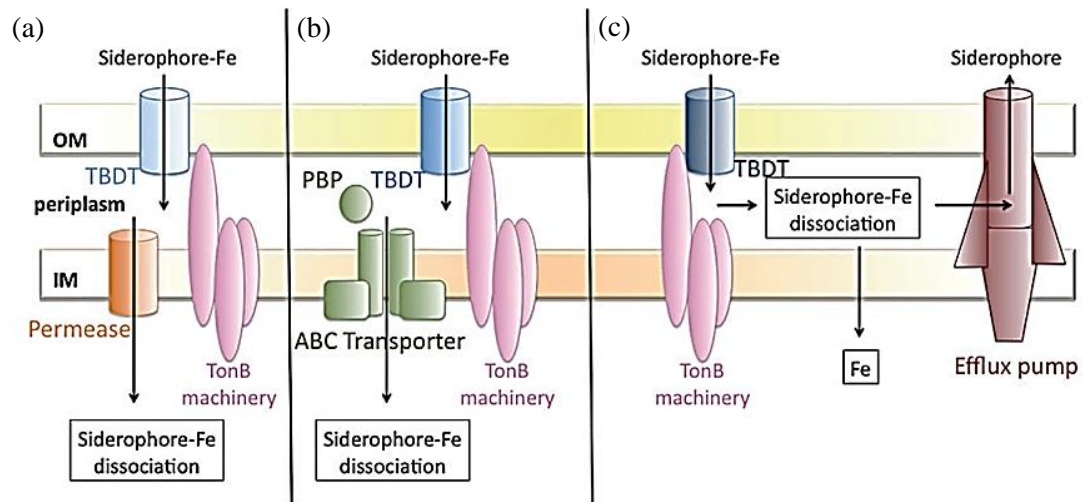
Reference: Visca et al. (2007)

Figure 5 Pyoverdine (PVD) biosynthetic pathways. Ferribactin biosynthesis and maturation in *P. aeruginosa* PAO1. Reactions catalyzed by precursor-generating enzymes (PvdH, PvdA and PvdF) are shown [bottom of part (a)]. Nonribosomal peptide synthetases (PvdL, PvdI, PvdJ and PvdD) are dissected into modular domains: A, adenylation domain; AL, acyl-CoA ligase domain; C, condensation domain; and T, thiolation domain. Ovals indicate auxiliary domains: E, epimerization domain; Te, thioesterase domain. Substrates recognized by each module (M) are indicated. The combined activity of the nonribosomal peptide synthetases results in the generation of the PVD precursor ferribactin. The probable cytoplasmic membrane (CM) and periplasmic (PP) location of proteins (PvdE, PvdM, PvdN, PvdO, PvdP and PvdQ) that have uncharacterized roles in PVD synthesis and/or export are shown. Proposed scheme for maturation of the PVD chromophore (b). Structures corresponding to ferribactin, mature PVD and the unsaturated form dihydroPVD are indicated. Abbreviations: ASA, aspartate b-semialdehyde; Dab, 2,4-diaminobutyrate; FA, fatty acid; fOHOrn, N^5 -formyl- N^5 -hydroxyornithine; OHOrn, N^5 -hydroxyornithine; OM, outer membrane; R_1 , acyl chain; R_2 , peptide chain.

2.5.2 Siderophore transport system

Siderophores in *Pseudomonas* is specific in the level of genus and species, another species cannot stole or use it. Therefore, the transport system is also developed for this competition and protecting other species theft it. The transport system have specific receptors on cell membrane, protein recognition, signaling mechanism, etc. (Smith 1998; Cornelis and Matthijs 2002; Beasley and Heinrichs 2010; Schalk et al. 2012).

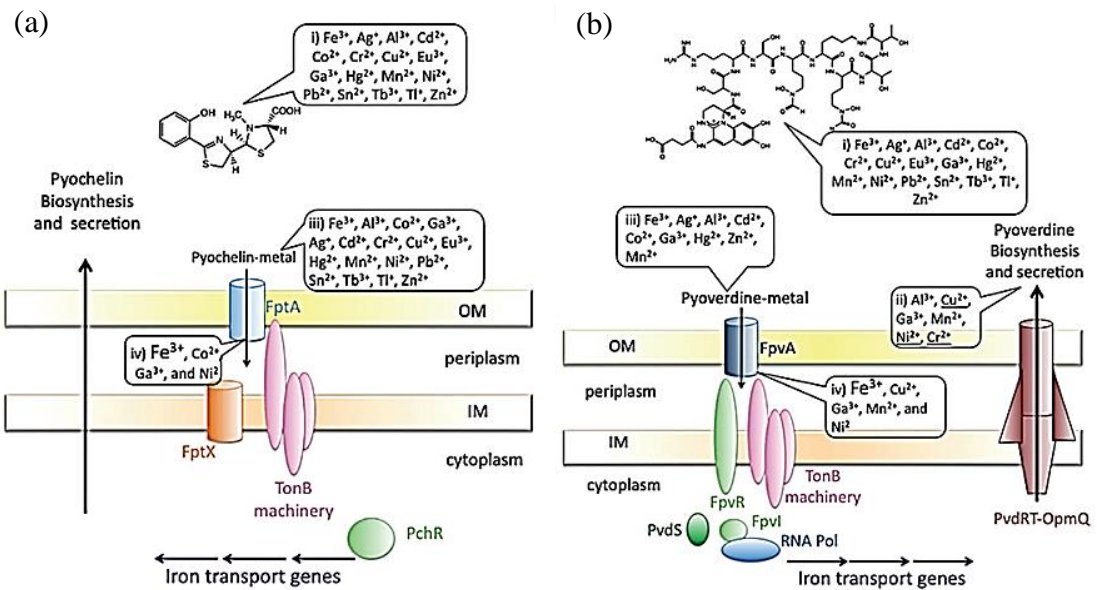
Iron chelated by siderophores is called ferrisiderophore. It is transfers to bacteria via energy-coupled transport involving TBDTs (TonB-Dependent Transporters) and the TonB complex that composed of TonB, ExbB and ExbD. The ferrisiderophore entering in the periplasm is dependent on the siderophore pathway and bacteria (Figure 6). For example, ferrichrome or ferripyochelin in *P. aeruginosa* are transported across the inner membrane by permeases (Figure 6(a)) while ferrichrome or ferrienterobactine in *Escherichia coli* are across by ABC transporters (Figure 6(b)). Iron is released into the cytoplasm by mechanisms involving either enzymatic degradation or chemical modification of the siderophore and/or iron reduction. However, iron can be released from the siderophore in the periplasm as found in pyoverdine pathway in *P. aeruginosa* (Figure 6(c)). The mechanism of ferrisiderophore dissociation in the cytoplasm found in ferrichrome and ferrienterobactin pathways in *E. coli*. Iron is released from ferrichrome in the cytoplasm in a process probably involving iron reduction followed by acetylation of the siderophore and it's recycling into the growth media. For the ferrienterobactin pathway, a cytoplasmic esterase hydrolyses the siderophore. Iron release from the siderophore in the periplasm found only in the ferripyoverdine pathway in *P. aeruginosa* and involves no chemical modification of the siderophore, but the iron is reduced and the siderophore recycled into the extracellular medium by the efflux pump PvdRT-OpmQ (Schalk et al. 2011).



Reference: Schalk et al. (2011)

Figure 6 Three mechanisms and strategies of ferrisiderophore pathways in Gram-negative bacteria. Ferrisiderophore uptake across the outer membrane (OM) involves a TonB-dependent transporter (TBDT). TBDT is specific for each siderophore. The energy provided by the proton-motive force (pmf) in the inner membrane (IM) is required for this first uptake process by TonB–ExbB–ExbD complex actions. Uptake of ferrisiderophore across the inner membrane involves either (a) specific permeases or (b) specific ABC transporters. In which, (a) and (b) show iron released from siderophore in the cytoplasm (ferrichrome and ferrirentreobactin pathways in *E. coli*). (c) shows iron released from the siderophore in the periplasm (ferripyoverdine pathway in *P. aeruginosa*) with no chemical modification of the siderophore, then the iron is reduced and the siderophore is recycled into the extracellular medium by the efflux pump PvdRT–OpmQ.

The molecular mechanism involved in the activation of pyoverdine production starts from the interaction on the cell surface between the pyoverdine-metal complexes and FpvA. Pyocheline pathway occurs in cytoplasm and involves pyochelin–metal uptake and interact with the cytoplasmic PchR regulator. TonB dependent transport is not only used in iron uptake but other biological metals in siderophore complex also use this route in Gram-negative bacteria. Therefore, the biological metals able to be transported by TonB-dependent pathways. Metal specificities of the pyochelin and pyoverdine pathways show in Figure 7. FptA and FpvA are the ferripyochelin and ferripyoverdine TBDTs. Stimulation of pyoverdine production by metals other than iron may involve the FpvR/PvdS signaling cascade activated by the pyoverdine–metal complex binding to FpvA at the cell surface.



Reference: Schalk et al. (2011)

Figure 7 Metal specificities of the pyochelin and pyoverdine pathways. Pyochelin (a) and pyoverdine (b) are the two major siderophores produced by *P. aeruginosa*. FptA and FpvA are the ferripyochelin and ferripyoverdine TBDTs. (i) Metals are bound by siderophore; (ii) metals that lead to upregulation of the siderophore in iron-limited conditions (underlined are the metals leading to upregulation in iron-supplemented conditions); (iii) metal–siderophore complexes bound to TBDT; and (iv) metal–siderophore complexes transported. Abbreviations: OM, outer membrane; IN, inner membrane. For (b), FpvR is the anti-sigma factor and FpvI and PvdS are the sigma factors involved in pyoverdine biosynthesis regulation. PvdRT-OpmQ is the efflux pump involved in pyoverdine secretion and recycling.

2.5.3 Siderophore structures

Siderophore have binding ligands consists of O atoms of hydroxamate, catechol, hydroxy-carboxylic acid, and carboxylic acid. Each ligand is bidentate with two oxygen atoms by coordinate covalent bonds. The cycling compounds facilitate the complex and chemical structural stability and resist to enzyme degradation. There are four types of siderophores including hydroxamate siderophores, catechol siderophores, carboxylate siderophores and mixed ligands/heterocyclic-chelating siderophores (Figure 8(a,b,c)). It is classified by ligand and/or functional groups which chelated iron or other ions (Krewulak and Vogel 2008).

2.5.3.1 Hydroxamate siderophore

Hydroxamate siderophores contain hydroxamic acid (Figure 8(c)) such as DFOB and Ferrichromes (Figure 8(d)).

2.5.3.2 Catecholate siderophore

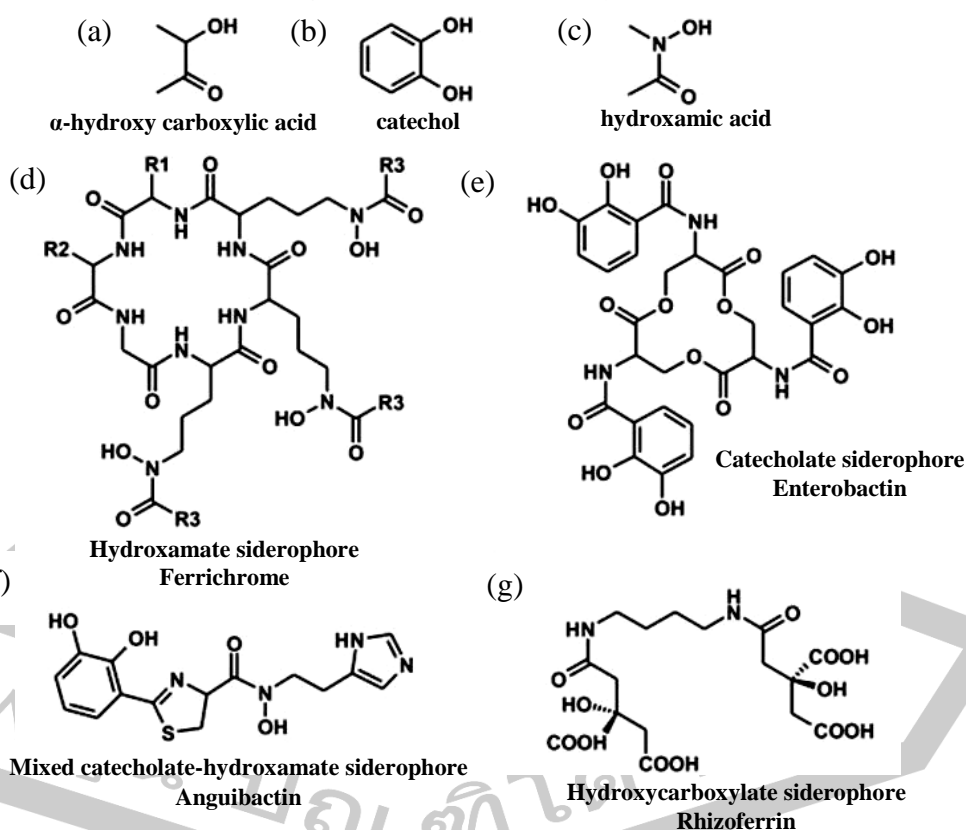
Catecholate siderophores contain catechol (Figure 8(b)) or 2,3-dihydroxybenzoate (DHB) or phenol such as enterobactin (Figure 8(e)) and salmochelin.

2.5.3.3 Carboxylate siderophore

Carboxylate siderophores contain α -hydroxy carboxylic acid (Figure 8(a)) such as staphyloferrin A and B, Rhizoferrin (Figure 8(g)).

2.5.3.4 Mixed ligand/heterocyclic-chelating siderophore

Siderophores in this group are diverse and some siderophore have aromatic ring and/or peptide chain in their structures such as pyoverdine, mycobactin and anguibactin (Figure 8(f)).



Reference: Krewulak and Vogel (2008)

Figure 8 Ligands found in siderophore including (a) α -hydroxy carboxylic acid, (b) catechol and (c) hydroxamic acid. Some siderophores in each group are (d) Hydroxamate siderophore Ferrichrome, (e) Catecholate siderophore Enterobactin, (f) Mixed catecholate-hydroxamate siderophore Anguibactin and (g) Hydroxycarboxylate siderophore Rhizoferrin.

2.5.4 Effects of metals on siderophore production

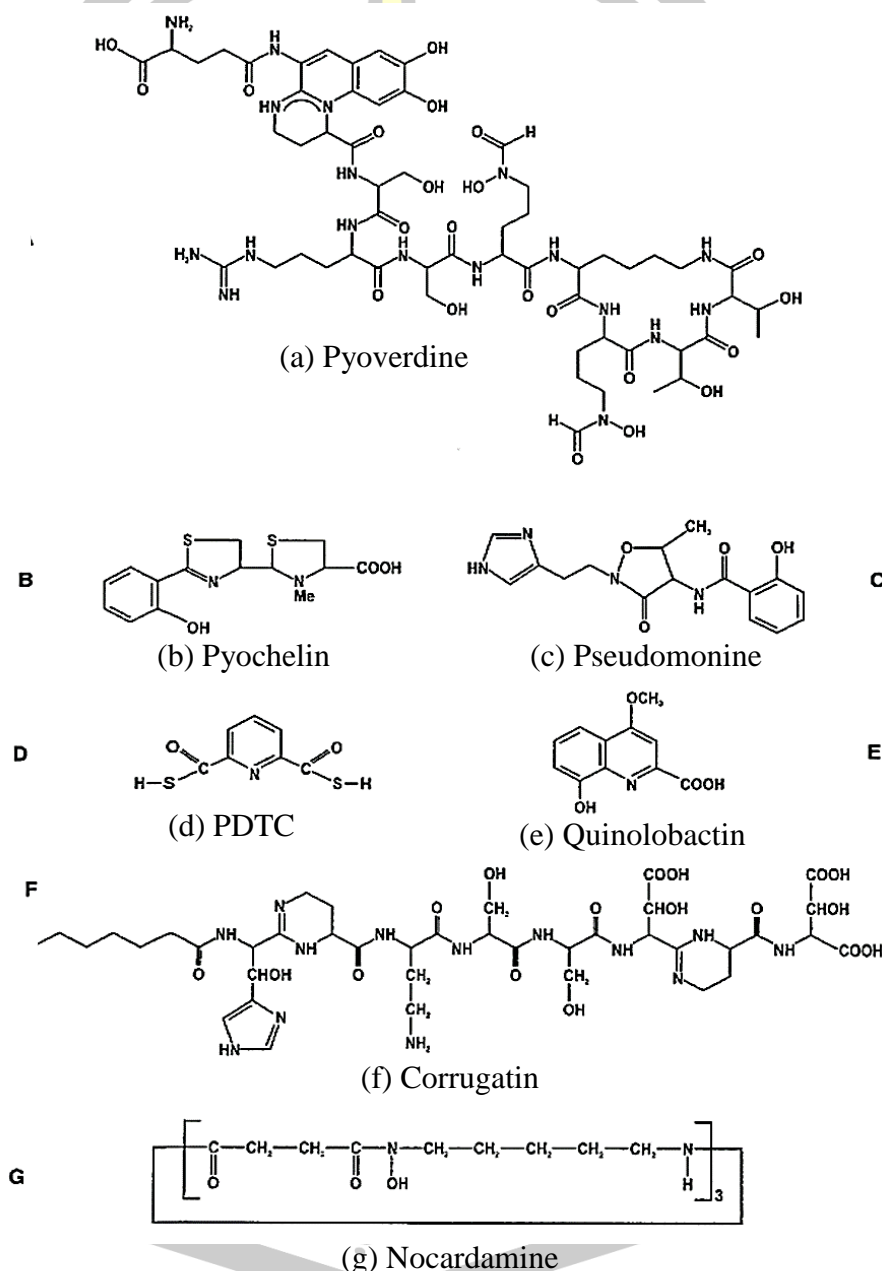
The effects of various heavy metals on heavy metal-resistant microorganism and/or PGPB have been investigated. Gaonkar and Bhosle (2013) showed the trace elements induced siderophore production whereas toxic metals decreased its production. CuO nanoparticles (NPs) inhibited pyoverdine production of *P. chlororaphis* O6 while EDTA co-inoculation enhanced its production (Dimkpa et al. 2012). Naik and Dubey (2011) reported an increase Pb reduced siderophore production. Whereas, presence of U in media increased the siderophore production by Cyanobacteria *S. elongatus* BDU130911 (Rashmi et al. 2013).

2.6 Siderophore of *Pseudomonas* species

Pseudomonas is gram negative bacteria, aerobic γ -proteobacteria, classified to family Pseudomonadaceae. They are found in wide range environmental condition such as water, air, soil and extremely environments, because they are capable to utilize various substrates for their growth. The importance of *Pseudomonas* is impact on organism to ecosystem level (Peix et al. 2009). Some strain of *P. aeruginosa* is the opportunistic human pathogen. The importance of *Pseudomonas* in human health is their highly virulent by secreted siderophores. This make the *Pseudomonas* siderophores are novel studies in medical science to prevent or decrease the virulent by siderophores (Aizawa and Aizawa 2014). Moreover, *P. syringae* discovered to be a plant pathogen (Lamichhane et al. 2014). However, siderophores produced by beneficial bacteria have been accepted to enhance of nutrient uptake to plants (Marschner et al. 2011). *P. putida* and *P. fluorescens* are well-known to be PGPB. Some soil *Pseudomonas* concern the geochemical cycling of rock or earth by secreted siderophores. Siderophores have affected the REEs solubilisation and mobility in ores or soil cycle. Therefore, siderophores from *Pseudomonas* is important role in nature (Mirleau et al. 2000; Jiricny et al. 2010) and many studies have been reported for many decade.

The parrot green color of *P. fluorescens* was found in culture media and suggested to be siderophores (Meyer and Abdallah 1978; Meyer and Hornsperger 1978). Elliott reported that pyoverdine (PVDs) is a typically pigment (yellow-green)

of fluorescent *Pseudomonas*. In addition to pyoverdines, other siderophores are produced in different growth conditions such as culture media, temperature, heavy metal and growth time (Braud et al. 2007). *Pseudomonas* siderophores are shown in Figure 9.

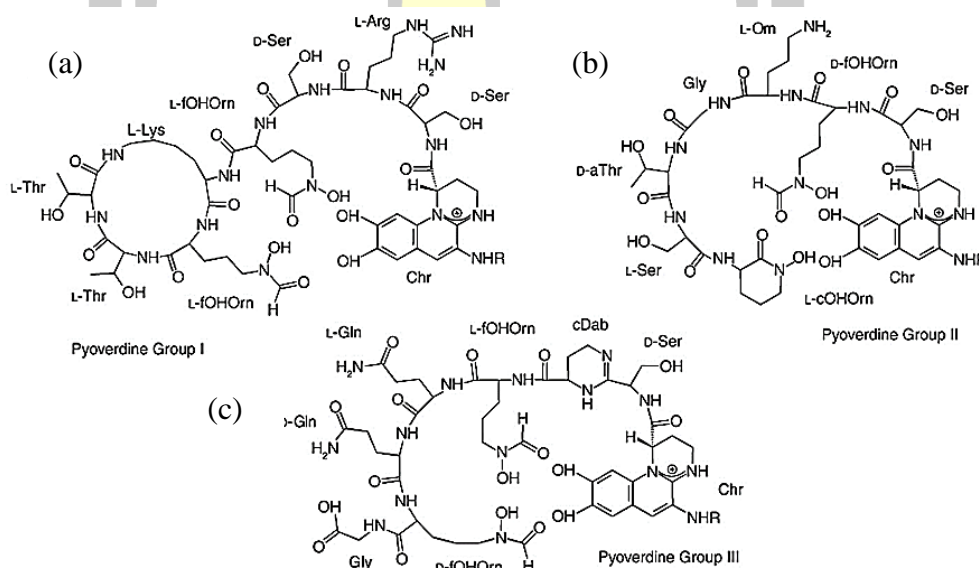


Reference: Cornelis and Matthijs (2002)

Figure 9 Siderophores produced by fluorescent pseudomonads including (a) pyoverdine, (b) pyochelin, (c) pseudomonine, (d) PDTC, (e) quinolobactin, (f) corrugatin and (g) nocardamine.

2.6.1 Pyoverdine (PVDs)

Pyoverdine are the major siderophore of the fluorescent pseudomonads. Pyoverdine or pseudobactin is consisting of quinoline chromophore, peptide chain containing 6 to 12 amino acids with half *d*-amino acids and acid (amide) side chain with dicarboxylic acid (Figure 10). The peptide chain is strain specific and varies among species. The catechol of the chromophore and two amino acids are involved in iron chelation. Bacteria uptake pyoverdine-iron complexes by specific receptor locating in the outer membrane which recognized their peptide chain (Schalk and Guillon 2013). The pyoverdine of *P. aeruginosa* is involved in virulence in animal models (Buckling et al. 2007; Mossialos and Amoutzias 2009). Pyoverdine improve the iron and metal competition, growth promotion and biocontrol because their high affinity constants for iron. These abilities are suggested playing role in bioremediation (Rajkumar et al. 2010).



Reference: Visca et al. (2007)

Figure 10 The three PVDs of *Pseudomonas aeruginosa*. (a) PVD Group I, (b) PVD Group II, and (c) PVD Group III. Abbreviations: aThr, allo-threonine; cDab, tetrahydropyrimidine ring generated by condensation of Dab with the preceding amino acid; Chr, chromophore; cOHOrn, cyclic- N^5 -hydroxyornithine; Dab, 2,4-diaminobutyrate; fOHOrn, N^5 -formyl- N^5 -hydroxyornithine.

2.6.2 Pyochelin

Pyochelin is a siderophore contain salicylic acid with a lower affinity for iron (III). Its formula is $C_{14}H_{16}N_2O_3S_2$ (molecular mass 324). There are two stereoisomeric structures (pyochelin I and II). It synthesized from chorismate and two moles of cysteine. Salicylic acid and the iron-chelator and antibiotic dihydroaeruginic acid are by-products of pyochelin. Pyochelin involved in the acquisition of trace-metals (Co and Mo) than iron (Visca et al. 1992). Salicylic acid play role in plant defense by inducing systemic acquired resistance (SAR) and biocontrol. Pyochelin of pathogenic *P. aeruginosa* is virulence in mice and humans. Ferri-pyochelin can degrade toxic organotins in the environment. Ferri-pyochelin can affect in redox-cycle especially in the presence of the *P. aeruginosa* phenazine pigment pyocyanin resulting in the production of cell-damaging active oxygen species.

2.6.3 Pseudomonine

Pseudomonine is a salicylic acid-based siderophore. Its formula is $C_{16}H_{18}N_4O_4$ (molecular mass 330). It produced when the pyoverdine is repressed.

2.6.4 Yersiniabactin

Yersiniabactin is salicylic acid based-siderophore. Its formula is $C_{21}H_{27}N_3O_4S_3$ (molecular mass 481). The yersiniabactin also found in human and animal pathogenic enterobacteria such as *Yersinia* spp., *E. coli*, *Citrobacter* spp., *Klebsiella* spp., *Salmonella enterica* and *Enterobacter* spp.

2.6.5 Pyridine-2,6-bis(monothiocarboxylic acid) (PDTC)

Pyridine-2,6-bis(monothiocarboxylic acid) or PDTC (molecular mass 198) is siderophore which contained several ability such as convert the pollutant CCl_4 to CO_2 in iron-limiting conditions, form complexes with metals and involve in the defense mechanism of bacteria against heavy metal toxicity. PDTC is repressed by the pyoverdine production. PDTC forms 2:1 complexes with iron stability ($\sim 10^{33}$), nickel and cobalt (Stolworthy et al. 2001). Different metal-PDTC complexes have been found to have antimicrobial activities (Sebat et al. 2001).

2.6.6 Quinolobactin

Quinolobactin (QB) (8-hydroxy-4-methoxy-2-quinoline carboxylic acid) is a secondary siderophore with a low affinity constant for Fe(III). It is produced in

the first 16 hours of iron stress before suppressed by pyoverdine production. Quinolobactin can detect by IEF and CAS (Cornelis and Matthijs 2007).

2.7 Siderophore extraction and characterization

Once the universal siderophore detection method was developed by Schwyn and Neilands (1987). New siderophores have been increasingly discovered because a large diversity of its structure and their chemical and physical properties. The several techniques for siderophore detection, extraction and purification have been improved. Solvent extraction is widely used in many studies for long time because it is easy to extract and concentrate.

New techniques of Chromatography have been developed and published. Sayyed and Chincholkar (2006) purified the siderophores of *Alcaligenes faecalis* BCCMID2374 by using Amberlite XAD-4 column and absorbed on Sep-PakC₁₈ column. TLC techniques on polyamide TLC and silica TLC could separate the siderophores of *Erwinia* sp., but polyamide TLC gave the better separation of catechol-type siderophores (Xie et al. 2006). Eghbali et al. (2009) developed siderophore separation in biological samples were by a complexed biomixture in pressure-driven mode using perfectly ordered pillar array columns.

Siderophore characterization and structure elucidation have been investigated. Boopathi and Rao (1999) purified the siderophore of *P. putida* type A1 and determined the structure and characterization of siderophore by amino acid analysis, MS, absorption and fluorescence measurements and EPR. Zane and Butler (2013) isolated siderophore of marine *Pseudoalteromonas* sp. and structural analyzed as lystabactins by MS, amino acid analysis, and NMR. Several techniques have been conducted to study and characterize of siderophores such as FTIR (Patel et al. 2009; Ahire et al. 2011; Upritchard et al. 2011), XAFS (Harrington et al. 2012b; Kruff et al. 2013), UV-Vis spectroscopy (Enyedy et al. 2004; Tseng et al. 2006; Harrington et al. 2011), TLC (Xie et al. 2006; Rashmi et al. 2013). The literature reviews of several techniques used in siderophore characterization are shown in Table 1.

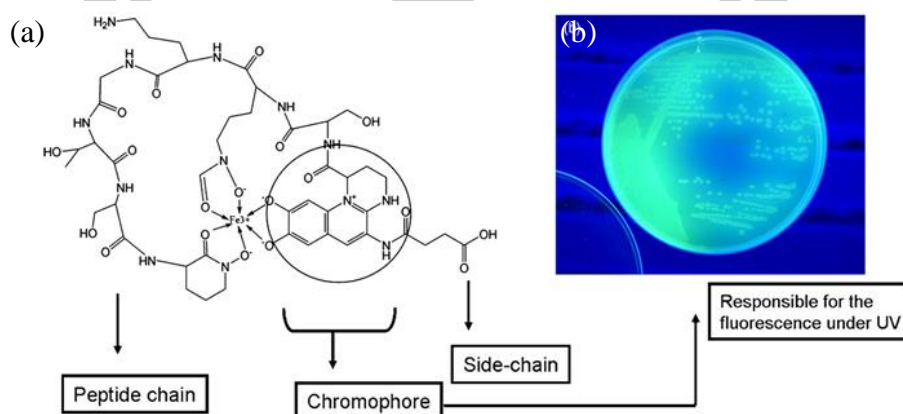
Table 1 The literature review of several techniques used in siderophore characterization.

Techniques	Organism	Siderophores	References
UV spectroscopy, FTIR and HPLC	<i>Arthrobacter luteolus</i>	catechol-type siderophores	Emmanuel et al. (2012) Journal of Biosciences. 37: 25-37
ATR-IR Spectroscopy	<i>E. coli</i>	Enterobactin	Upritchard et al. (2011) Langmuir. 27: 10587–10596
UV-Vis spectroscopy, TLC and HPLC	<i>Alcaligenes faecalis</i>	*Not identified	Sayed and Chincholkar (2006) Biorresource Technology. 97: 1026-1029
UV-Vis spectroscopy, HPLC and MS	<i>Streptomyces</i> sp.	Catechol derivative siderophore	Liermann et al. (2000) Geochimica et Cosmo chimica Acta. 64(4): 587–602
HPLC and LC-MS analysis	<i>Laccaria laccata</i> and <i>Laccaria bicolor</i>	Hydroxamate siderophore	Haselwandter et al. (2013) Biometals. 26:969–979
TLC	<i>Erwinia</i> sp.	Catechol-type siderophores	Xie et al. (2006) Journal of Microbiological Methods. 67: 390-393
TLC	<i>Synechococcus elongates</i> BDU130911	Hydroxamate siderophore	Rashmi et al. (2013) Biorresource Technology. 130: 204–210
UV-Vis analysis, ES-MS, Amino acid content analysis, and NMR	<i>Rhizobium leguminosarum</i> ATCC14479bv. trifolii	Trihydroxamate siderophore viciobactin	Wright et al. (2013) Biometals. 26:271–283
UV-Vis measurements, EPR, and XAS	<i>P. aeruginosa</i>	Pyochelin	Tseng et al. (2006) Journal of Biological Inorganic Chemistry. 11:419–432
UV-Vis measurements	<i>Penicillium chrysogenum</i> and <i>Neurospora crassa</i>	Desferricoprogen (DFC)	Enyedy et al. (2004) Journal of inorganic biochemistry 98: 1957–1966
UV-Vis spectroscopy	<i>Ceratobasidium papillatum</i>	Trishydroxamate siderophore basidiochrome	Harrington et al. (2011) Journal of inorganic biochemistry. 105: 1670–1674
UV-Vis spectroscopy and spectrofluorimeter	<i>P. aeruginosa</i> 4EA	Pyochelin and pyoverdine	Naik and Dubey (2011) Current Microbiology. 62:409–414
EXAFS and infrared spectroscopy	-	DFOB were purchased from Sigma-Aldrich	Kruft et al. (2013) Journal of Inorganic Biochemistry. 129: 150–161
X-ray spectroscopy	-	Pyoverdin-CFML90-51, Pyoverdin PaA and rhizoferrin	Harrington et al. (2012) Geochimica et Cosmo chimica Acta. 88: 106–119
UV-Vis spectroscopy, MS and XAS	<i>Azotobacter vinelandii</i>	Protochelin, Desferrioxamine B	Harrington et al. (2012) Biometals. 25:393–412

2.7.1 *Pseudomonas* siderophore detection

2.7.1.1 Pyoverdine

Yellowish-green pyoverdines are detectable under UV light (365 nm) by their bluish-green fluorescence. Maximum absorbance of free-pyoverdines in visible are 365 nm and 380 nm (pH<5), 402 nm (pH 7) and 410 nm (pH 10). The maximum absorbance of Fe(III)-chelated typical pyoverdines is near 400 nm (pH 3–8), with broad charge transfer bands at 470 and 550 nm. The siderotyping technique is a powerful tool for characterize pyoverdine (Meyer 2000). Figure 11 show pyoverdine complex with Fe³⁺ and the emission of fluorescence after exposed under UV light.



Reference: Eghbali et al. (2009)

Figure 11 Pyoverdine structure (a) Molecular structure of a pyoverdine, (b) Petri dish exposed under UV-light.

2.7.1.2 Pyochelin

Pyochelin is light yellow with a yellowish-green fluorescent, it is confused to pyoverdine. In methanol, it forms a wine-red (pH 2.5) to orange (pH 7.0), non-fluorescent when complex with iron. Iron free pyochelin have maximum absorbances are 218, 248 and 310 nm and iron-pyochelin complexes are 237, 255, 325, 425 and 520 (pH 2.5) or 488 (pH 7.0) nm. TLC and HPLC are the popular method to detect pyochelin. IEF and CAS overlay also detect this siderophores. In TLC, salicylic acid and pyochelin are detected in concentrated chloroform or dichloromethane extracts of acidified culture supernatants. In HPLC, ethyl acetate extracts of acidified culture supernatants are concentrated before injection. Salicylic

acid, dihydroaeruginic acid and pyochelin I and II are identified by their retention times and UV spectra (Bultreys 2007).

2.7.1.3 Pseudomonine

Pseudomonine emit blue fluorescent under UV light. Pseudomonine have the maximum absorbances at 298, 237 and 203 nm and detectable by HPLC (Anthoni et al. 1995).

2.7.1.4 Yersiniabactin

Yersiniabactin is nearly colorless and orange when chelated to iron. Ferri-yersiniabactin is detected in the culture medium by HPLC and identified by its spectral characteristics. The maximum absorbances are near 227, 255, 305, at pH 5.3 and 386 nm at pH 7.0 (Bultreys et al. 2006).

2.7.1.5 Pyridine-2,6-bis(monothiocarboxylic acid) (PDTC)

PDTC emits a blue Fe(II)-complex and a brown Fe(III)-complex; the maximum absorbances of Fe(III)-(PDTC)₂ are 345, 468, 604 and 740 nm, and of Fe(II)-(PDTC)₂ are 314 and 687 nm. PDTC concentration is usually determined by measuring the absorbance of Fe(II)-(PDTC)₂ at 687 nm.

2.8 Marigold for heavy metal phytoremediation

2.8.1 Marigold

Marigold or Tagetes is an annual or perennial plant that popular around the world. There are various sizes among 0.1 to 2.2 m tall and their leave are pinnate. Their flowers are golden, orange, yellow and white colors, the floral head are averagely 4–6 cm diameter with both ray florets and disc florets.

The scientific classification is following;

Kingdom: Plantae

Order: Asterales

Family: Asteraceae

Subfamily: Asteroideae

Tribe: Tageteae

Genus: Tagetes

Marigolds grow well in any sort of soil with good drainage. The advantages of marigold are used as food coloring, perfume oil, and cut-flower marketing. The orange pigments in flower called carotenoid and lutein are mixed in chicken feed to improve egg yolk coloration. The marigold cut flowers in Thailand are usually apply in various ways including religious worship such as Hindu, Buddhist, and other ceremonies. Planting of marigolds for cutting flowers are mainly in the North and North East of Thailand.

There are 56 species of marigolds including *T. erecta* L. (African marigold, Aztec marigold), *T. lucida* Cav. (Mexican mint marigold, Texas tarragon), *T. minuta* L. (wild marigold, black mint), *T. patula* L. (French marigold), *T. tenuifolia* Cav. (signet marigold) and any hybrid species. In Thailand, *T. erecta*, *T. patula* and hybrid marigold such as mule marigolds, nugget marigold, fireworks marigold, red seven-star marigold and showboat marigold are popular for cut-flower market. Figure 12 shows the flowers of *T. erecta* and *T. patula*.



Figure 12 Some species of marigolds in Thailand, *T. erecta* (a) and *T. patula* (b).

2.8.2 Marigold planting

The general steps for marigold planting are sowing marigold seed in plug tray or container and watering well for seed germination. This stage may be take a several days (12-20 days) for true 2-4 leaves occurred. Then the young marigolds are transplanted to growing pot or planting area, watering once a day, fertilizers are needed. It was various fertilizers following farmer and most is secret for their

commercial. After 45-60 days, the marigold flowers will be flowering and ready to cut for sale.

2.8.3 Application of marigold in phytoremediation

For sustainable phytoremediation in agricultural area, an economic plant such as marigold is a good choice. They contain appropriate properties including; (1) economic ornamental flower in Thailand and (2) good hyperaccumulator of heavy metals such as Cd which contaminates in agricultural area in Mae Sot, Tak province, Thailand. These reasons could motivate the people who live in the contaminated area to go along with phytoremediation process. Marigolds have been reported and studied in phytoremediation. Microbial inoculation or bioaugmentation has been reported for improving the heavy metal accumulation in marigold. There are no reports about the application of SPB or siderophores to assist heavy metal accumulation in marigolds. Nevertheless, the marigold study for phytoremediation in Thailand has reported. Chintakovid et al. (2008) reported the application of marigold in phytoremediation for sustainable development in As contaminated area, Ron Phibun, Nakorn Si Thammarat, Thailand. The literature reviews of marigold in phytoremediation are shown in Table 2.

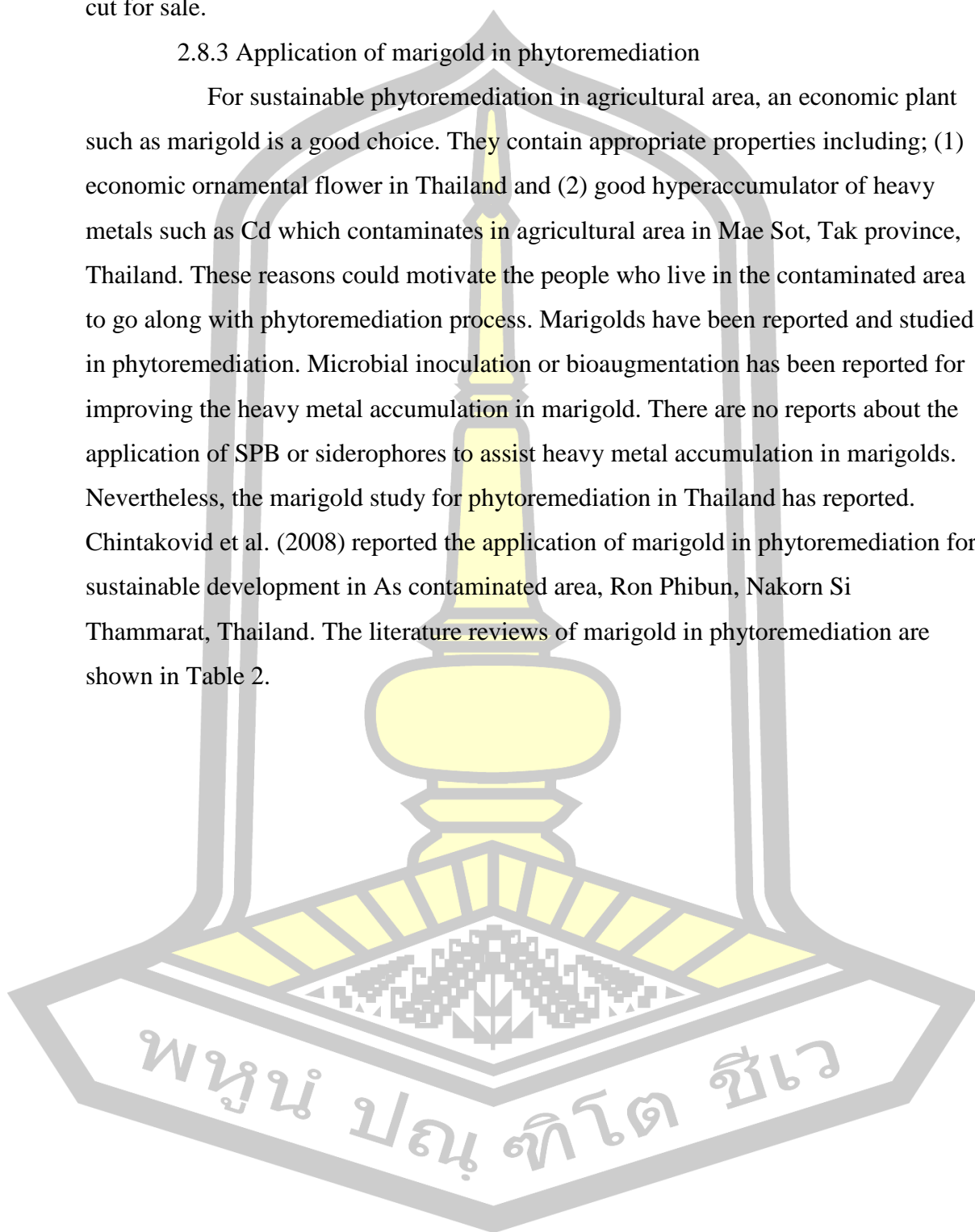


Table 2 Literature review of marigold in phytoremediation.

Marigold species	Results	References
Nugget marigold	Field experiment of nugget marigold was examined in As contaminated area of Ron Phibon, Thailand. As was found in largely leaves (46.2%) but the flower (5.8%) was less than in leaves. Nugget marigold in experimental plots accumulated high As and grew better in As contaminated area. Addition of phosphate fertilizer improved the uptake of As in flowering stage.	Chintakovid et al. (2008) <i>Chemosphere</i> . 70: 1532-1537
<i>T. erecta</i> , <i>Chrysanthemum indicum</i> and <i>Gladiolus grandiflorus</i>	Marigold, chrysanthemum and gladiolus were examined the potential of Cd phytoextraction. they concluded that gladiolus was highest potential for Cd phytoremediation	Lal et al. (2008) <i>Bioresource Technology</i> . 99: 1006-1011
Marigold (<i>T. erecta</i>)	The effects of mycorrhiza <i>Glomus intraradices</i> on Cu uptake in marigold were examined. Their results indicated that <i>G. intraradices</i> could enhance the Cu tolerance in marigold by accumulate Cu in vesicles but not increase the Cu in marigold biomass.	Castillo et al. (2011) <i>New Biotechnology</i> . 29(1): 156-164
Marigold (<i>T. erecta</i>)	They studied the effects of mycorrhiza on growth, cadmium accumulation and physiology of marigold in growth chamber. The results showed the mycorrhiza decreased Cd accumulation in marigold.	Liu et al. (2011) <i>Pedosphere</i> 21(3):319–327
French marigold (<i>T. patula</i>)	The effects of Cd on growth, enzymatic activities and accumulation in French marigold were examined in hydroponic experiment. <i>T. patula</i> highly accumulated Cd 450 mg Cd kg ⁻¹ dry weight in shoot and 3500 mg Cd kg ⁻¹ dry weight in root after 14 days' exposure at 10 and 50 μM CdCl ₂ , respectively. The translocation factors of Cd were greater than 1 in plants exposed to 10 μM CdCl ₂ . They concluded that <i>T. patula</i> is a Cd accumulator and its tolerate Cd by antioxidative defense system.	Liu et al. (2011) <i>Journal of Hazardous Materials</i> . 189: 724–731
French marigold (<i>T. patula</i>) and impatiens (<i>Impatiens walleriana</i>)	The exponential decay model was conducted to predict the maximum Cd removal by EDTA in French marigold and impatiens. The bioconcentration (BCF) and translocation (TF) factors of the two species when exposed with EDTA was four replicates.	Wei et al. (2012) <i>Ecotoxicology and Environmental Safety</i> . 84: 173–178
<i>T. patula</i>	<i>T. patula</i> was decolorized about 90% of the dye Reactive Blue 160 within 4 days.	Patil and Jadhav. (2013) <i>Chemosphere</i> . 92: 225–232
<i>T. erecta</i> L.	This study showed the distribution of ¹⁰⁸ Cd in <i>T. erecta</i> split root-seedling. Their results indicated that Cd is translocation via phloem.	Qin et al. (2013) <i>Chemosphere</i> . 93: 2284–2288

CHAPTER 3

RESEARCH METHODOLOGY

This research investigated the effects of Zn, Cd and Zn plus Cd on siderophore production and characterized the siderophore induced by Zn, Cd and Zn plus Cd (Figure 13) and the application of crude siderophore extracts on Zn and Cd accumulations in *T. erecta* L. for improving the phytoextraction (Figure 14). Each experiment was completed in triplicate. Chemicals used in this study were of analytical grade, and all glasswares were soaked in 5% (w/w) HNO₃ for 24 hours and then rinsed with deionized water to remove cohesive ions on their surface.

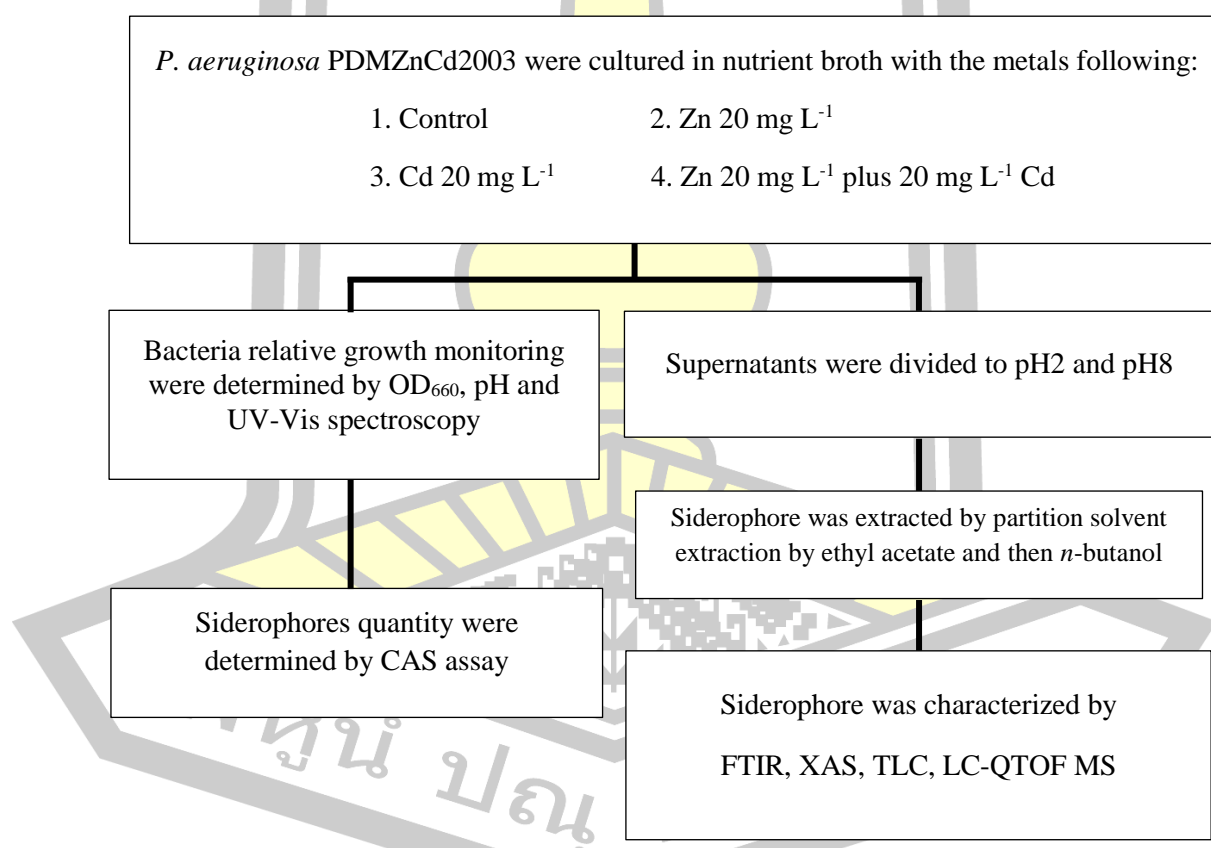


Figure 13 Research diagram for studying the effects of Zn and/or Cd on siderophore production by *P. aeruginosa* PDMZnCd2003

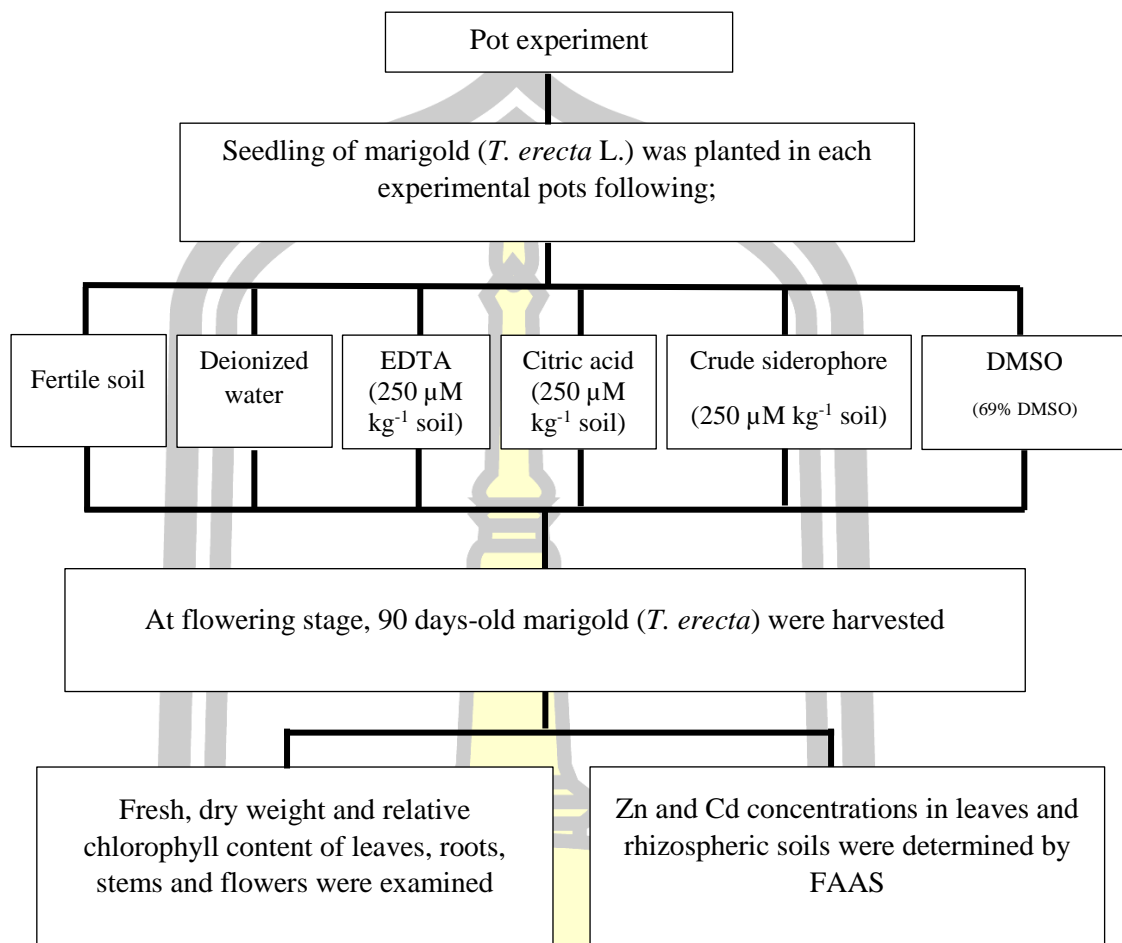


Figure 14 Research diagram for pot experiments to study the application of siderophores and other chelating agents on Zn and Cd accumulation in marigold (*T. erecta*).

3.1 Siderophores production, extraction and characterization

3.1.1 Bacterial cultivation under Zn and/or Cd treatments

Due to a high range of Fe concentration (9-20 g kg⁻¹) in soil of a crop field in Mae Sot, the effect of Fe-free media was not investigated. It was sufficient for bacterial growth in the Fe concentration at 10⁻⁸-10⁻⁵ M (Andrews et al. 2003). *P. aeruginosa* PDMZnCd2003 (accession number JX193586) in a culture starter of OD₆₆₀ = 0.8 was inoculated as a ratio of 2%_(v/v) inoculum size into nutrient broth (NB) containing each of Zn 20 mg L⁻¹ (code: Zn), Cd 20 mg L⁻¹ (Code: Cd) and Zn plus Cd 20 mg L⁻¹ Zn and 20 mg L⁻¹ Cd (code: Zn+Cd) by following (Meesungnoen et al.

2012). The Zn and Cd stock solutions (pH 5) were prepared from $\text{ZnSO}_4 \cdot 7\text{H}_2\text{O}$ and $3\text{CdSO}_4 \cdot 8\text{H}_2\text{O}$, respectively. The bacterial cultures were incubated at $30 \pm 2^\circ\text{C}$ and collected every 3 hours at 0-24 hours and 6 hours at 30-72 hours. Optical density (OD) at 660 nm and pH of bacterial cultures were investigated. Supernatants were separated from the bacterial cells by centrifugation at 8,000 rpm for 3 minutes, and the samples were stored in a refrigerator (4°C). The siderophore concentration were examined by Chrome Azurol Sulfonate (CAS) assay, and the UV-Visible absorption spectra were scanned by a UV-Vis spectroscopy.

3.1.2 Supernatant scanning by UV-Vis spectroscopy

Supernatants were scanned by UV-Vis spectrophotometry (Beckman Coulter, California) in a wavelength range of 200-800 nm. In case of absorbance value over than a detection limit of the instrument, the supernatants were diluted before rescanning and measurement.

3.1.3 Quantification of siderophore by CAS assay

Siderophores in the supernatants were quantitative examined by the CAS assay (Schwyn and Neilands 1987). Every step to prepare CAS assay solution has to prepare under a stirring system. A 6 ml of 10 mM Hexadecyltrimethylammonium bromide (HDTMA) was added to 20 ml deionized water. A 1.5 ml of iron (III) solution (1 mM $\text{FeCl}_3 \cdot 6\text{H}_2\text{O}$, 10 mM HCl) was slowly added into a beaker containing 7.5 ml of 0.2 mM CAS solution, then the mixed solution was slowly added into the HDTMA solution. Buffer solution was prepared by dissolving 4.307 g of piperazine-N,N'-bis(2-ethanesulfonic acid) (PIPES) in deionized water and slowly added 6.25 ml of 12 M HCl and adjusted the pH to 5.6-6 by 0.5 M NaOH. Then, the buffer solution was added to the mixed HDTMA flask under stirring and adjusted the volume to 100 ml to obtain the CAS assay solution (blue color solution). To examine the siderophore, 0.5 ml of a supernatant sample was mixed with 0.5 ml of CAS assay solution. The reactants were incubated for 2 hours. The reduction of the absorbance of blue color was detected at wavelength 630 nm. Deionized water was used as blank solution. The product of siderophore were quantified as an EDTA equivalent at a concentration between 0-0.03 mM EDTA.

3.1.4 Siderophore extraction

The siderophore extraction was modified from Payne (1994). The supernatants were divided into two portions. One part of the supernatant was adjusted to pH 2 by added 12 M HCl for releasing metal in siderophores (Payne 1994). The other part was not adjusted the pH to obtain metal-siderophore complexes. The scheme of the solvent partition extraction is shown in Figure 15. The 100 ml of supernatants were extracted twice with 50 ml of ethyl acetate by separation funnel at a 1:0.5 ratio of supernatant: solvent. The ethyl acetate (EtOAc) fractions were pooled together. Then, the partial supernatant fractions were continuously extracted twice with a 50 ml of *n*-butanol. The *n*-butanol (BuOH) fractions were pooled together. The ethyl acetate and *n*-butanol fractions were concentrated by rotary vacuum evaporator (Büchi, Switzerland) at 50 °C. Crude extracts were rinsed by 99.9% methanol and collected in 1.5 ml brown vial to prevent light. The remaining methanol in the vial were purged by nitrogen gas and stored at -20 °C.

3.1.5 Analytical methods

3.1.5.1 Zn and Cd concentration in crude siderophore extracts

The sample digestive method was modified from Pages et al. (2008). Crude siderophore extracts were digested with concentrated HNO₃ at 150 °C and filtrated by acid resistant filter paper (No.50, Whatman® GE Healthcare) before measured the Zn and Cd concentrations by Flame atomic absorption spectroscopy (FAAS) (Shimadzu AA 680, Japan). Zn and Cd reference standard solutions (AAS standard, AVS Titrinorm, Belgium) at the concentrations of 1000 ppm were used for constructed standard curves at 0.125-3.000 mg L⁻¹.

3.1.5.2 Thin layer chromatography (TLC)

The TLC condition was modified from Sayyed and Chincholkar (2006). Crude siderophore extracts were spotted on 20×20 cm TLC silica gel 60 F₂₅₄ on aluminium sheets (Merck, Germany) and suddenly dried with hair dryer. The TLC plates were moved to chromatographic chamber saturated with *n*-butanol: acetic acid: distilled water (12:3:5) as a mobile phase. The TLC plates was detected under UV lamp at wavelength 254 and 366 nm.

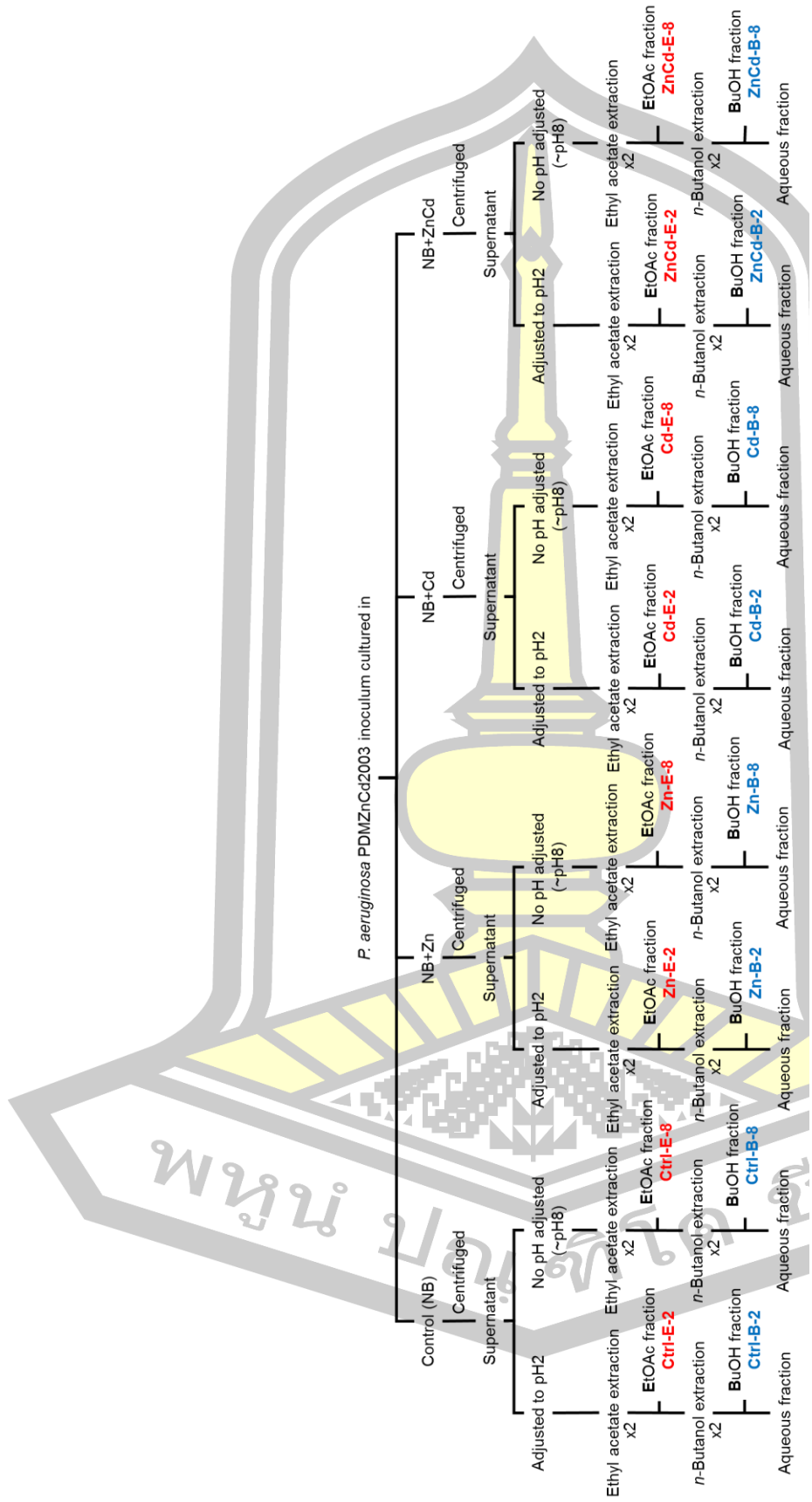


Figure 15 The steps of partition solvent extraction in this study and code name of crude siderophore extracts obtained in each steps.

3.1.5.3 Liquid chromatography-quadrupole time-of-flight mass spectrometry (LC-QTOF MS)

A 10 μl of each crude siderophore extract was dissolved in 99% methanol and filtrated before analyzed with LC-QTOF MS. The 10 mM sodium formate (HCOONa) was used as internal standard. The LC-QTOF MS analysis was performed on DIONEX-UltiMate 3000 HPLC (Thermo Scientific, USA) coupled with micrOTOF-Q II mass spectrometers (Bruker, USA). The separation of the sample solution was performed on Poroshell 120 EC- C_{18} reverse phase column (size 4.6x150 mm, particle size 2.7 μm , Agilent Technologies, USA). The solvent flow rate was 0.3 ml min^{-1} and 2 μl of the sample solution was injected into the LC system. The binary gradient elution system was composed of deionized water as a solvent A and acetonitrile as a solvent B, both contained 0.1%_(v/v) formic acid. The linear gradient elution was started from 10% of the solvent B, and started to increase at 5 minutes and reached 80% of the solvent B at 50 minutes. The conditions for the positive electrospray ionization (ESI) source were as follows: syringe pump flow rate 60 $\mu\text{l min}^{-1}$, the mass scanning from 50-1,500 m/z at positive ion polarity, capillary voltage 4.5 kV, the collision cell radio frequency (RF) 150 peak-to-peak voltage (Vpp), nebulizer 2 bar, dry heater 180 $^{\circ}\text{C}$, and nitrogen drying gas 8 L min^{-1} . The LC-QTOF MS data were collected and processed by Compass 1.3 software (Bruker, USA).

Relative peak area of each siderophore chromatogram peaks were calculated by the equation below

$$\text{Relative peak area} = \frac{\text{Peak area} \times \text{Density}}{\text{Peak area of internal standard}}$$

3.1.5.4 Fourier transform infrared microspectroscopy (FTIR)

Crude siderophore extracts were smeared to be a thin film on IR Reflected Kevley low-electron microscope slide (Kevley technologies, USA) and vacuum dried. The sample slides were analyzed by IR spectrometer (Tensor 27, Bruker Optic) connected to an IR microscope (Hyperion 2000, Bruker Optic) with Mercury Cadmium Tellride (MCT) detector ($4,000\text{-}700\text{ cm}^{-1}$), the system were flew with nitrogen gas and cooled with liquid nitrogen in IR microscope. Spectra were analyzed by IR reflection mode at a resolution of 4 cm^{-1} , 32 scan and replicated 150 spectra per sample. The obtained spectrum was analyzed by OPUS 6.5 (Bruker Optic,

German). The FTIR spectra were transformed by baseline offset and linear baseline correction, and Extended Multiplicative Signal Correction (EMSC). The transformed spectra were statistical analyzed by Principle Component Analysis (PCA) using the Unscrambler X 10.5 software package (CAMO, Norway). The peaks were identified by referring to IR Mentor Pro 6.5 (Bio-Rad 1999).

3.1.5.5 X-ray absorption spectroscopy (XAS)

Crude siderophore extracts were loaded into polypropylene film pockets (Chemplex® industries, Inc, USA). While the reference chemicals were prepared by grounded and smeared on Kapton tape (Dupont, USA) for analyze in transmission mode. Reference chemicals of S K-edge were FeSO₄, CdS, ZnS, Zn-cysteine complex, Cd-cysteine complex, Zn-glutathione complex, Cd-glutathione complex, ZnCd-glutathione complex, Zn-methionine complex, Cd-methionine complex and ZnCd-methionine complex. Reference chemicals of Zn K-edge were Zn(CH₃COO)₂, ZnCO₃, ZnO, ZnS, ZnSO₄, Zn(NO₃)₂, Zn-cysteine complex, ZnCd-cysteine complex and Zn-glutathione complex. Reference chemicals of Cd K-edge used in this study were Cd(CH₃COO)₂, Cd(NO₃)₂, CdO, CdS, CdSO₄ and Cd-cysteine complex. The S, Zn and Cd K-edge were evaluated by XAS. The parameter of each experiments showed in Table 3.

Table 3 Experimental conditions for XAFS analysis of S, Zn and Cd K-edge.

Parameters	S	Zn	Cd
Beamline	BL-8, Synchrotron Light Research Institute (Public Organization) (SLRI) (Nakhonratchsima, Thailand)	BL-8, Synchrotron Light Research Institute (Public Organization) (SLRI) (Nakhonratchsima, Thailand)	NW10A, Photon Factory Advanced Ring (PF-AR), High Energy Accelerator Research Organisation (KEK) (Tsukuba, Japan)
Operation energy	1.2 GeV	1.2 GeV	6.5 GeV
Monochromator	Double crystal InSb(111) monochromator	Double crystal Si(111) monochromator	Double crystal Si(311) monochromator
Fluorescence X-ray detector	13-channel Germanium detector	13-channel Germanium detector	19-channel Germanium detector
Gas filled in sample chamber	Helium	Nitrogen	-
Temperature	Room temperature	Room temperature	Room temperature
Calibrated Material/chemical	FeSO ₄	Zn foil	Cd foil

All spectra were processed by Athena under IEFIT version 1.2.11d (Ravel and Newville 2005). The replicated spectra were aligned before merged, and then calibrated and normalized. The S K-edge XANES spectra as flattened $\mu(E)$ were analyzed by Peak Fitting of 7 Gaussian and Lorentzian peaks including sulfide, thiol, disulfide, sulfoxide, sulfone, sulfonate and sulfate and one arctangent step at range 2.456-2.486 keV. The normalized Zn and Cd K-edge XANES spectra as flattened $\mu(E)$ were performed Linear Combination Fit (LCF) from 9.638 to 9.717 and 26.669 to 26.774 keV, respectively, weighted sum to 1 and forced between 0 and 1. All reference chemicals were included to evaluate and chosen the best fit model. The normalized Zn and Cd K-edge EXAFS data of $\chi(R)$ at 1-2.5 \AA° and $\chi(k)$ at 3-10 \AA^{-1} were fitted by Athemis version 1.2.11d. The single scattering paths of electron were generated by Atom package under IEFIT. The cif files were obtained from www.crystallography.net including 1101051.cif and 2014019.cif for Zn and 1011054.cif and 4324771.cif for Cd. The parameters of EXAFS fitting equation including the coordination number (N), the inter-atomic distance (ΔR), Debye–Waller factor (σ^2) and energy shift of the data and the theory of E_0 (ΔE_0) were adjusted to obtain the best fit while amplitude reduction factor (S_0^2) was fixed at 1 for all fittings.

3.2 The effect of crude siderophore extract on Zn and Cd accumulation in marigold (*T. erecta* L.).

3.2.1 Plant pathogenicity test

The plant pathogenic test was modified following Blakney and Patten (2011). Vegetative stage of healthy and closely height marigold plants were prepared to test bacterial infection by spraying water and covered in transparent plastic bag for 24 hours. The bacterial solution was prepared by using twice washed 24 hours-old bacterial cells by 0.85% NaCl and adjusted the bacterial cell to 10^4 CFU ml^{-1} . A 5 ml of the bacterial suspension was sprayed on marigold leave and applied on soil. Plastic bag was covered to the infected marigold and incubated for 7 days. The appearances of symptom including wilt, soft rot, lesion, blight, necrosis and tumor was observed every day. Leaves and soil samples were taken to detect the bacteria on NA agar plate.

3.2.2 Pot experiment of *T. erecta* L.

Pot experiments were performed in two times upon including (i) from siderophore-metal complexes and free-siderophores.

The treatments in this experiment were non-contaminated soil (code: Fertile soil), contaminated soil supplement with deionized water (code: control), contaminated soil supplement with EDTA (code: EDTA), contaminated soil supplement with citric acid (code: citric acid), contaminated soil supplement with crude siderophore extract dissolved with DMSO (code: siderophore) and contaminated soil supplement with DMSO as the same ratio as crude siderophore (code: DMSO). The contaminated soil in this study was obtained from agricultural field nearby zinc mining in Mea Sot, Tak (N 16° 40'26" E 98° 37'46"). The non-contaminated soil was obtained from agriculture field in Chainghain village, Maha Sarakham. Both soil were dried by sun light and sieved through 2 mm nylon sieve.

Seeds was sown in trays with the mixes of peat moss and fertile soil in a ratio of 1:1, watering every day. One-month old, healthy and closely height seedlings were transplanted to each experimental pots contained 1 kg of soil. The marigold was watered by 100 ml tap water per pot. The marigolds were acclimatized for 30 days before started to treat by any treatments. Each treatments were added near root every week for 4 weeks.

Crude siderophore extracts from Zn+Cd were chosen for the pot experiment, because the crude extracts contained Zn and Cd siderophores complexes. Dimethyl sulfoxide (DMSO) was used to dissolve the crude siderophore extracts and de-ionized water was also added to the crude siderophore solution to dilute the DMSO concentration. The dissolved crude siderophore was quantitatively evaluated the siderophore concentration by CAS assay. The concentration of siderophore was modified following Cornu et al. (2014) at 250 $\mu\text{mol kg}^{-1}$ soil. Other chelators such as EDTA and citric acid were compared the effect of crude siderophore and DMSO solution. The equal ratio of crude siderophore solution was used to compare the self-effect of DMSO in the crude siderophore solution.

Three month olds marigold was harvested at flowering stage. The rhizosphere soil were kept and each parts of plant were separated. The leaves and roots were washed by tap water for 2-3 times and wiped the plants by wiped paper

before collected the wet weight. Root washing process was modified following Zhang et al. (2015). The roots were washed in tap water for 2-3 times and soaked in the 0.85% NaCl solution with 0.01 M EDTA for 1 minute and washed in 0.85% NaCl solution for 2-3 times. The washed roots were wiped by wiped paper before collected the wet weight. All samples were dried at 60 °C until the weight stable to obtained dry weight.

3.2.3 Zn and Cd analysis

3.2.3.1 Total Zn and Cd extractions in shoot

The dry samples were grounded before the extraction. The plant extraction procedure was modified following Miller (1998). A 0.1 g of the sample were added into an acid-tolerant glass tube. The 3 ml of 70% HNO₃ were added to the sample tube and left overnight. The sample tubes were heated at 150 °C for 1 hour. The 1 ml of 70% HClO₄ were added slowly into the sample tubes and heat at 215 °C for 2 hours. A 3 ml of deionized water were added into the sample tube and incubated in water bath at 90 °C for 1 hour. The digestion samples were filtrated by Whatman filter paper No.50 and adjusted the volume in 10 ml-volumetric flask.

3.2.3.2 Total Zn and Cd extractions in soil

This procedure were modified following ASTM (2004). A 0.1 g of dry soil were added into an acid-tolerant glass tube. A 5 ml of aqua regia (conc. HCl mixed with conc. HNO₃ in a ratio as 3:1) were added into the sample tube and left overnight. After that, the sample tube were heated at 150 °C for 1 hour and heated again in water bath at 90 °C for 1 hour, leave it cool. Then filtrated by Whatman paper (No.50, Whatman® GE Healthcare) and adjusted the volume by 10 ml-volumetric flask.

3.2.3.3 Water extractable Zn and Cd in soil

The metal extractable method was modified from (Cajuste et al. 2000). A 0.5 g of dry soil were added into a 15 ml-centrifuge tubes. 10 ml of deionized water were added into the soil tubes, mixed and shaken at 150 rpm for 2 hours. The sample tubes were then centrifuged at 6,000 rpm for 5 minutes. The supernatants were filtrated with Whatman paper No.2 and adjusted the volume to 10 ml by deionized water.

3.2.4 Method validation

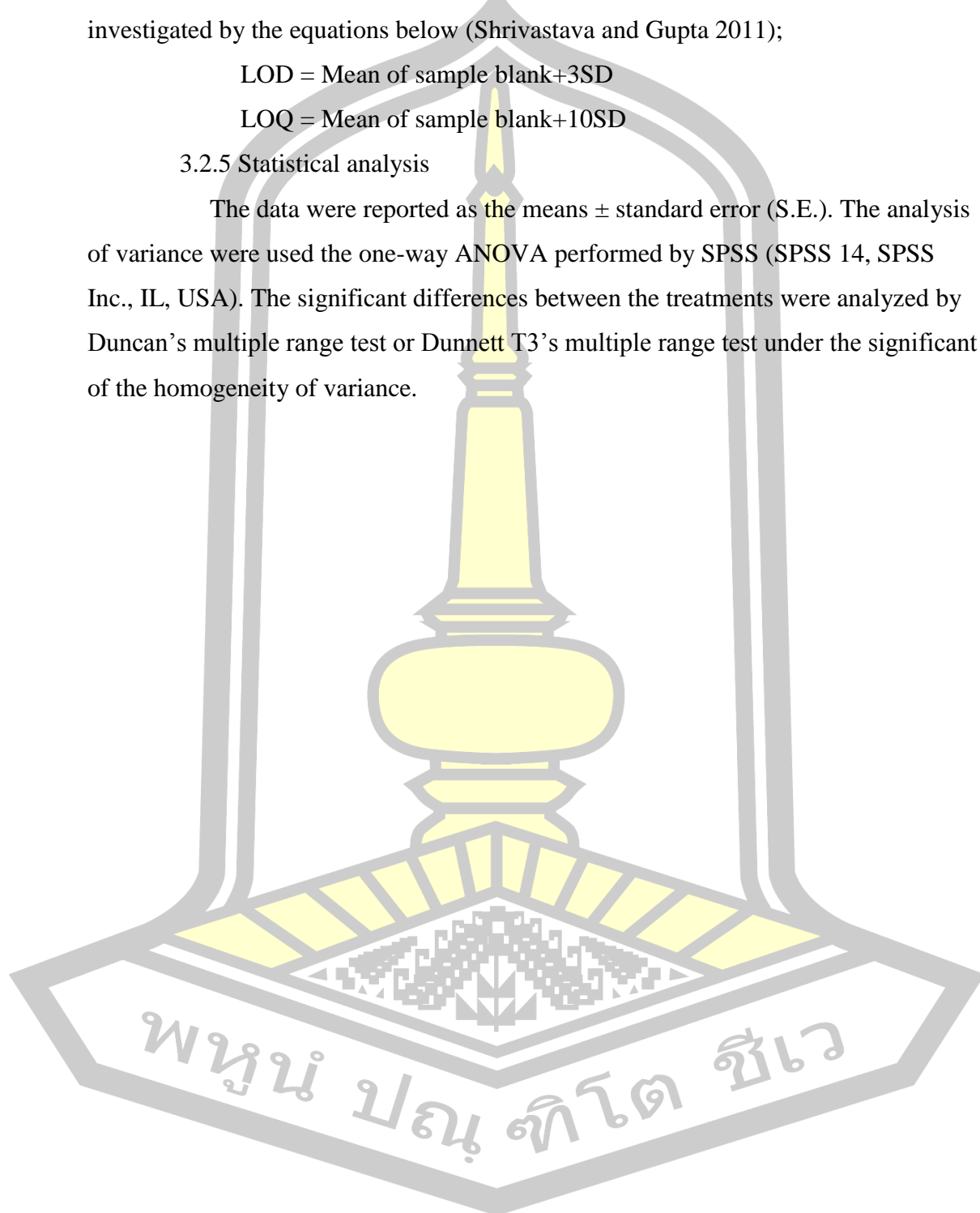
The limit of detection (LOD) and the limit of quantitation (LOQ) were investigated by the equations below (Shrivastava and Gupta 2011);

$$\text{LOD} = \text{Mean of sample blank} + 3\text{SD}$$

$$\text{LOQ} = \text{Mean of sample blank} + 10\text{SD}$$

3.2.5 Statistical analysis

The data were reported as the means \pm standard error (S.E.). The analysis of variance were used the one-way ANOVA performed by SPSS (SPSS 14, SPSS Inc., IL, USA). The significant differences between the treatments were analyzed by Duncan's multiple range test or Dunnett T3's multiple range test under the significant of the homogeneity of variance.



CHAPTER 4

RESULTS

According to the methodology in Chapter 3, the results obtained was separated into 2 parts of (i) the effects of siderophore production and analysis of the productive siderophore induced by Zn, Cd and Zn plus Cd and (ii) the application of crude siderophore extracts on Zn and Cd accumulations in *T. erecta* L. for phytoextraction.

4.1 Siderophore production and analysis of the productive siderophore induced by Zn, Cd, and Zn plus Cd

4.1.1 Bacterial growth curve and siderophore production

Bacterial growth curve was done for understand the bacterial physiology and characteristic of the siderophore production. The bacterial growth curves in each treatment including Zn (code: Zn), Cd (code: Cd), Zn plus Cd (code: Zn+Cd) and control (code: Ctrl) show in Figure 16(a). Lag phase did not presented in all treatments and control. Log phase occurred in 3-21 hours in all treatments. Stationary phase in all treatments were short period, then the bacterial growth entered to death phase. However, the absorbance (OD₆₆₀) of Cd and Zn+Cd were lower than Ctrl and Zn. The bacterial growth curve was similar pattern to the previous report of (Meesungnoen et al. 2012) that also examined dry weight and protein content. Therefore, these results could refer to the previous results.

The pH of bacteria during the growth increased along the relative bacterial growth and was rather stable after entered the death phase as well as the siderophore concentration (Figure 16(b, c)). The increasing of pH may be due to the oxidative deamination of amino acid in the peptone, which is a composition of NB media, and occurring ammonia as a by-product of the process.

Figure 16(c) shows siderophore productions of the bacteria in each treatments. The siderophore concentrations increased at hour 6-15 in Ctrl and at hour

6-21 in Cd and Zn+Cd. Siderophore concentration in all treatments were hardly change after entering hour 24. The siderophore concentration of Zn was lowest because Zn is essential element and it was sufficient available in this treatment than the others, therefore, it was not activated the siderophore production. While both Cd and Zn+Cd were the highest in siderophore concentrations.

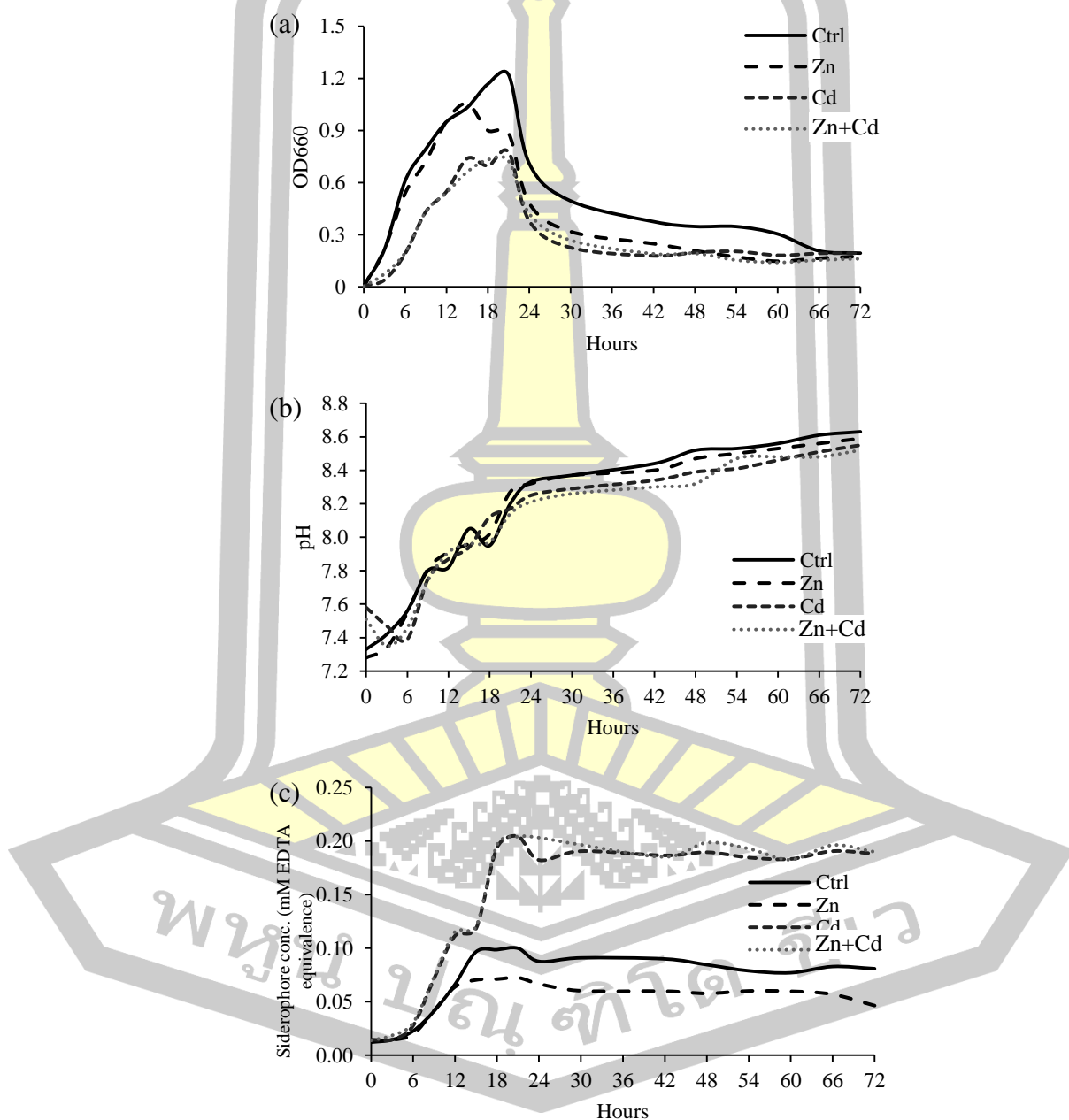


Figure 16 Relative growth (a), pH (b) and siderophore concentration (c) during *P. aeruginosa* PDMZnCd2003 cultivation in Ctrl (solid line), Zn (long dash line), Cd (dash line) and Zn+Cd (dot line) at 0-72 hours.

The supernatant colors are shown in Figure 17. The supernatants of Zn and Ctrl were parrot-green and light-yellow, respectively. While, the Cd and Zn+Cd color were yellow-green. The yellow-green color was defined to be a pyoverdine. The parrot green color could contained pyocyanin in the culture media. However, there are colorless siderophore such as pyridine-2,6-bis(monothiocarboxylic acid) (PDTC) and pseudomonine. Therefore, other analytical methods were investigated. The supernatants of all treatments were preliminary analyzed the siderophores by UV-Vis spectroscopy.

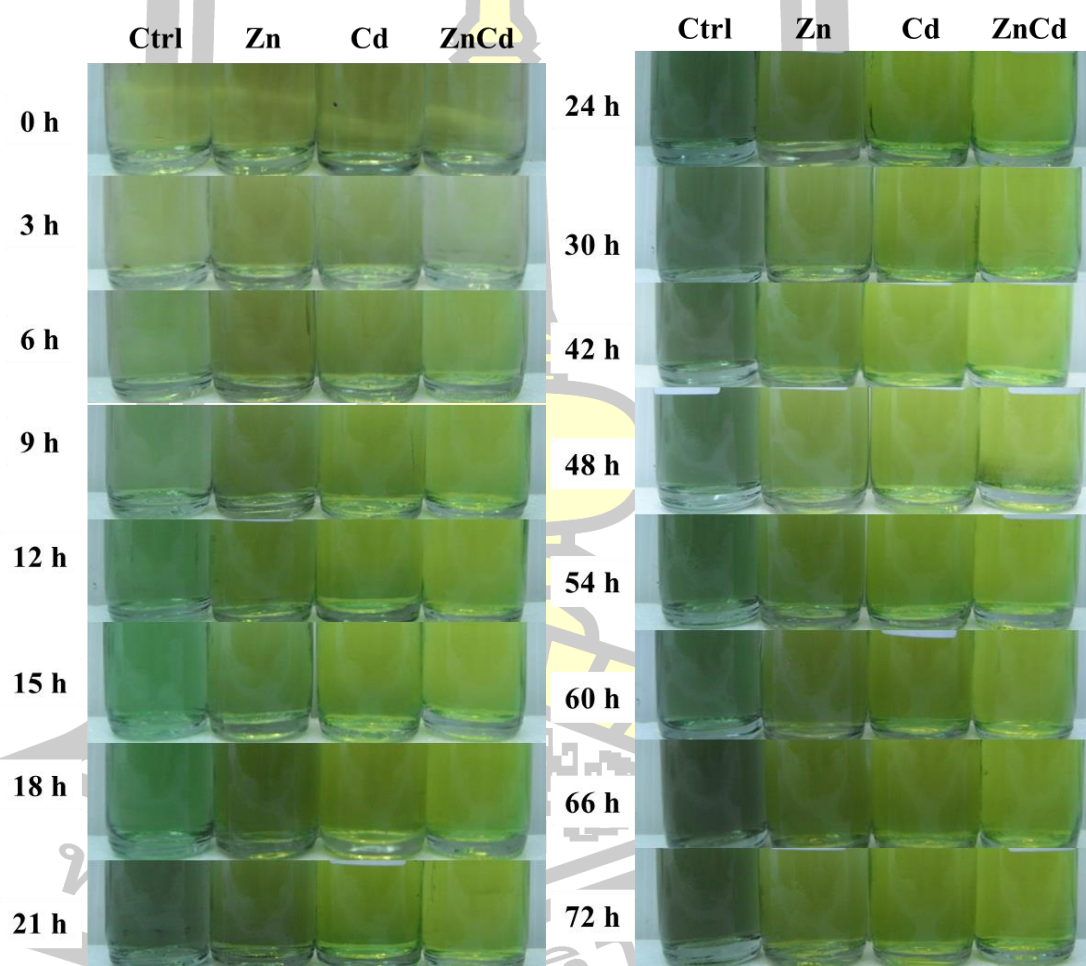


Figure 17 Supernatant colors of *P. aeruginosa* PDMZnCd2003 in the Ctrl, Zn, Cd and Zn+Cd at 0-72 hours show that Zn and Ctrl were parrot-green and light-yellow, respectively, while the Cd and Zn+Cd color were yellow-green.

4.1.2 UV-Vis spectra of all supernatants

The UV spectra of *Pseudomonas* supernatants were reported including pyoverdine at 300-400 nm and pyochelin at 200 and 300 nm. In addition, pyochelin is light yellow with a yellowish-green fluorescent, it is confused to pyoverdine. Iron free pyochelin have maximum absorbance at 218, 248 and 310 nm and iron-pyochelin complexes at 237, 255, 325, 425 and 520 (pH 2.5) or 488 (pH 7.0) nm. Pyoverdines are detectable under UV light (365 nm) by their bluish-green fluorescence. Maximum absorbance of free-pyoverdines in visible are 365 nm and 380 nm (pH<5), 402 nm (pH 7) and 410 nm (pH 10). The maximum absorbance of Fe(III)-chelated typical pyoverdines is near 400 nm (pH 3–8), with broad charge transfer bands at 470 and 550 nm.

The UV-Vis analysis were done in non-diluted supernatants for preliminary screening of siderophores. The UV-Vis spectra of supernatants (Figure 18) show the peaks at 250 and 330 nm in all treatments and control and at 420 nm in Cd and Zn+Cd. The hidden peak of 250 nm was clearly presented in the diluted supernatants of 24 hours at 100-fold (Figure 18). Therefore, the UV-Vis spectra of supernatants at 250 and 330 nm assume to be a peak of pyochelin (Cox and Graham 1979) and the peak at 420 nm was pyoverdine (Naik and Dubey 2011). The peak at 420 nm was detected only the yellow-green color supernatants. Moreover, pyochelin in Ctrl (Figure 18(a)) was higher than the others because the pyochelin biosynthesis involve to iron than other metals (Schalk et al. 2011). While pyoverdine increased along the time until almost stable at entering dead phase (Appendix A) because the metal (Cd) stimulate the biosynthesis of pyoverdine (Schalk et al. 2011).



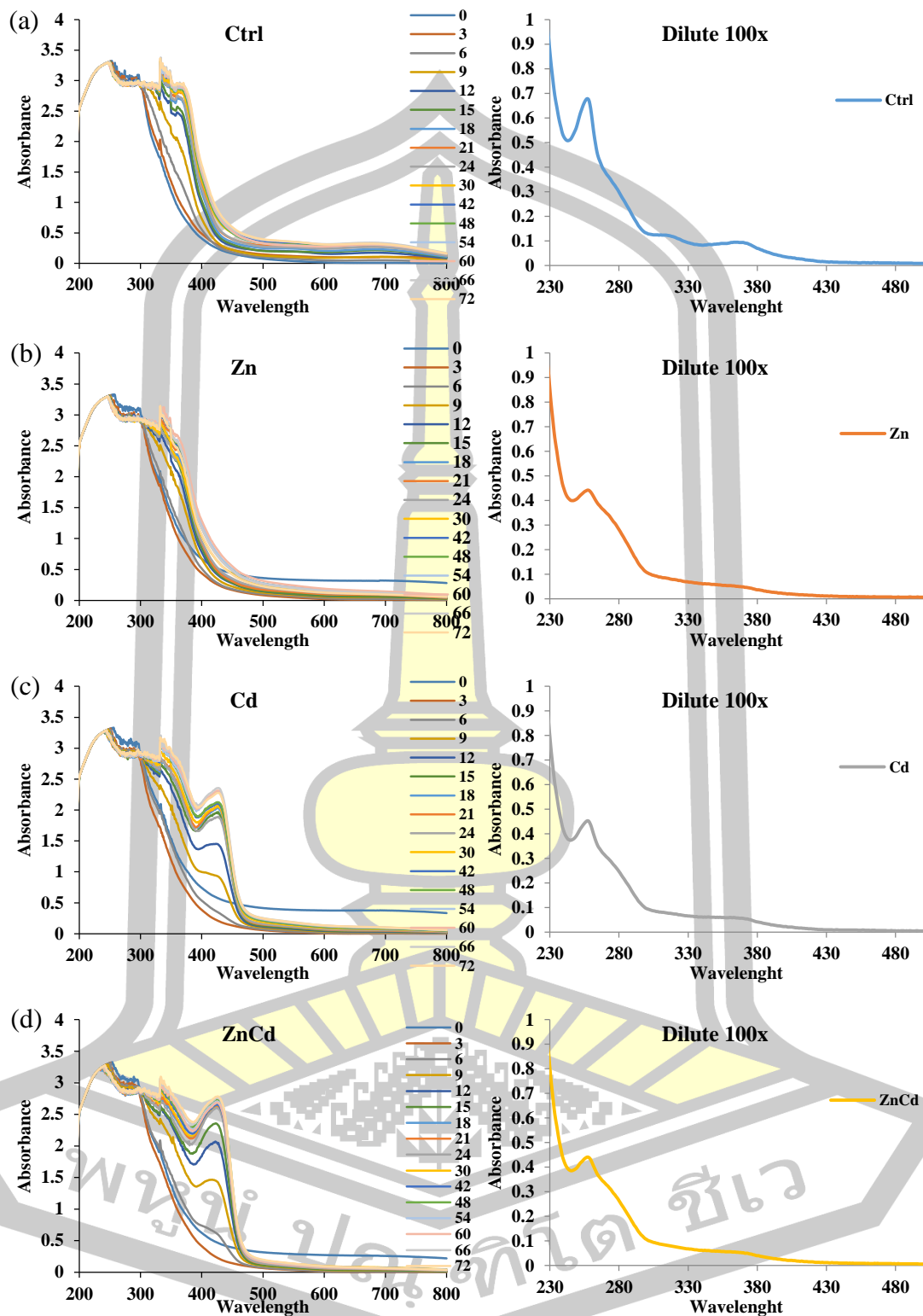


Figure 18 UV-Vis spectra of *P. aeruginosa* PDMZnCd2003's supernatants at 0-72 hours and 100x diluted supernatants at 24 hours in the Ctrl (a), Zn (b), Cd (c) and Zn+Cd (d) show the peaks at 330 nm in all treatments and control, and at 420 nm in Cd and Zn+Cd. The hidden peak of 250 nm was clearly presented in the 100x diluted supernatants of 24 hours.

4.1.3 Analysis of crude siderophore extracts

4.1.3.1 Zn and Cd concentrations in crude siderophore extracts

Before the step of partition solvent extraction, each supernatants from the four treatments were divided into two portions. Siderophores in supernatants without pH adjustment (pH 8) contained Zn and/or Cd whereas the other portion of each supernatants were adjusted the pH to pH 2 for releasing the metal ions in the siderophore complexes and obtained the free-siderophores (Payne 1994). The crude siderophores from the pH 2 supernatants were called the pH-2 extracts. While the crude siderophores from the no pH adjusted supernatants were called the pH-8 extracts. Then it was partitionally extracted by two solvents, ethyl acetate (EtOAc) and *n*-butanol (BuOH). Therefore, the crude siderophore extracts from ethyl acetate and *n*-butanol fractions were called the EtOAc fraction and the BuOH fraction, respectively. The crude siderophore extracts and solvent fraction color were separated to 16 samples following to Table 4.

The solvent fraction color (Table 4, Appendix B) of each fractions were correspond to pyochelin and pyoverdine in the fractions. Pyochelin is light yellow with a yellowish-green fluorescent. In methanol, it forms a wine-red (pH 2.5) to orange (pH 7.0), non-fluorescent when complex with iron (Cornelis and Matthijs 2007). Whereas, pyoverdine show yellow-green fluorescent. The fraction colors indicated that the pyochelin and pyoverdine from supernatants were extracted into the solvent fractions.

Table 4 Crude siderophore extract's code names and the colors of solvent fractions.

Treatments	Fraction	Siderophore fraction		Color of solvent fraction	
		pH-2 extract	pH-8 extract	pH-2 extract	pH-8 extract
Ctrl	EtOAc	Ctrl-E-2	Ctrl-E-8	Yellow-orange	Yellow-orange
	BuOH	Ctrl-B-2	Ctrl-B-8	Red-orange	Blue
Zn	EtOAc	Zn-E-2	Zn-E-8	Yellow-orange	Yellow-orange
	BuOH	Zn-B-2	Zn-B-8	Red-orange	Blue
Cd	EtOAc	Cd-E-2	Cd-E-8	Yellow-orange	Yellow-orange
	BuOH	Cd-B-2	Cd-B-8	Red-orange	Fluorescent green
Zn+Cd	EtOAc	ZnCd-E-2	ZnCd-E-8	Yellow-orange	Yellow-orange
	BuOH	ZnCd-B-2	ZnCd-B-8	Red-orange	Fluorescent green

For further quantitative or comparative study, crude siderophore extracts were examined the density by grams of crude siderophore extract per volume (Table 5). Zn and Cd concentrations in the crude siderophore extracts were examined. The crude siderophore extract density of the EtOAc fractions were lower than the BuOH fractions, however, in case of Zn+Cd, it was not different. The FAAS results in Table 5 show that the Zn and Cd concentrations in the pH-2 extracts were lower than the pH-8 extracts. It indicated that the metal ions in the pH-2 extracts was released from the siderophores. While the siderophores in the pH-8 extracts was mainly in the siderophore-metal complex form. Ethyl acetate is polar aprotic solvent which do not dissolved the metal ions into its fraction while *n*-butanol is polar protic solvent which can dissolve the metal ions. Hence, the rest metal ions in the partial supernatant from ethyl acetate extraction could be transferred and dissolved in the *n*-butanol fraction. It was the one factors caused the higher Zn and Cd concentrations in the BuOH fractions than the EtOAc fractions. Therefore, the pH-2 extracts and the pH-8 extracts were used to study the different between free-siderophore and siderophore-metal complex, respectively.

Table 5 Crude siderophore extract density and Zn and Cd concentrations (mg g^{-1}) in all crude siderophore extracts.

Sample	Crude siderophore density ^b				Zn (mg g^{-1}) ^c				Cd (mg g^{-1}) ^c			
	pH-2 extract		pH-8 extract		pH-2 extract		pH-8 extract		pH-2 extract		pH-8 extract	
	EtOAc	BuOH	EtOAc	BuOH	EtOAc	BuOH	EtOAc	BuOH	EtOAc	BuOH	EtOAc	BuOH
Ctrl	0.734	1.040	0.786	1.055	0.009	0.038	0.059	0.198	-	-	-	-
Zn	0.838	0.950	0.793	1.068	0.037	0.157	0.281	2.055	-	-	-	-
Cd	0.784	0.858	0.814	0.947	0.007	0.012	0.018	0.355	-	0.350	0.672	11.396
Zn+Cd	0.908	0.920	0.882	0.956	0.030	0.108	0.516	3.506	-	0.430	0.254	2.122

^a < LOQ and LOD (LOQ = 0.022 and LOD = 0.009)

^b Crude siderophore extracts density were examined by grams of crude siderophore extract per volume

^c Unit of mg g^{-1} obtained by the metal concentration (mg ml^{-1}) divided by crude siderophore extract

4.1.3.2 Thin layer chromatography (TLC)

TLC was carried out to primarily determine the approximate number and characteristic of siderophores in the crude siderophore extracts. A 1 μ l of each crude siderophore extracts were spotted on TLC plate to semi-quantitative comparison among crude siderophore extracts. Figure 19(a) shows the TLC chromatogram detected under UV light at 360 nm. The TLC figure was adjusted for sharpen the chromatogram by PhotoScape program. There are some TLC chromatograms emitted blue and green fluorescent. The pyoverdine and pyochelin emit yellowish-green and pseudomonine emit blue fluorescence under UV light. Therefore, the pyochelin, pyoverdine and pseudomonine were detected by TLC.

Retention factor (R_f) is the distance migrated of each chromatograms divided by the total distance of the solvent. Each groups have the similar R_f and number of chromatogram (Figure 19(b)). The crude siderophore extracts were represented into 4 groups including EtOAc-pH-2, EtOAc-pH-8, BuOH-pH-2 and BuOH-pH-8 (Figure 19). The pattern of the R_f and TLC chromatogram in each groups was corresponded to the solvent fractions and pH in the extraction. The polar, charge, or free- or metal complex forms of siderophores in each crude siderophore extracts caused the differences of TLC band characteristics. The crude siderophore extracts from the Zn+Cd supernatants were completely entire bands than the others. Moreover, the Zn+Cd supernatant was contained pyochelin and pyoverdine. Therefore, the four crude siderophore extracts from the Zn+Cd supernatant including ZnCd-E-2, ZnCd-E-8, ZnCd-B-2 and ZnCd-B-8 were selected to indicate the siderophore molecules by LC-MS.

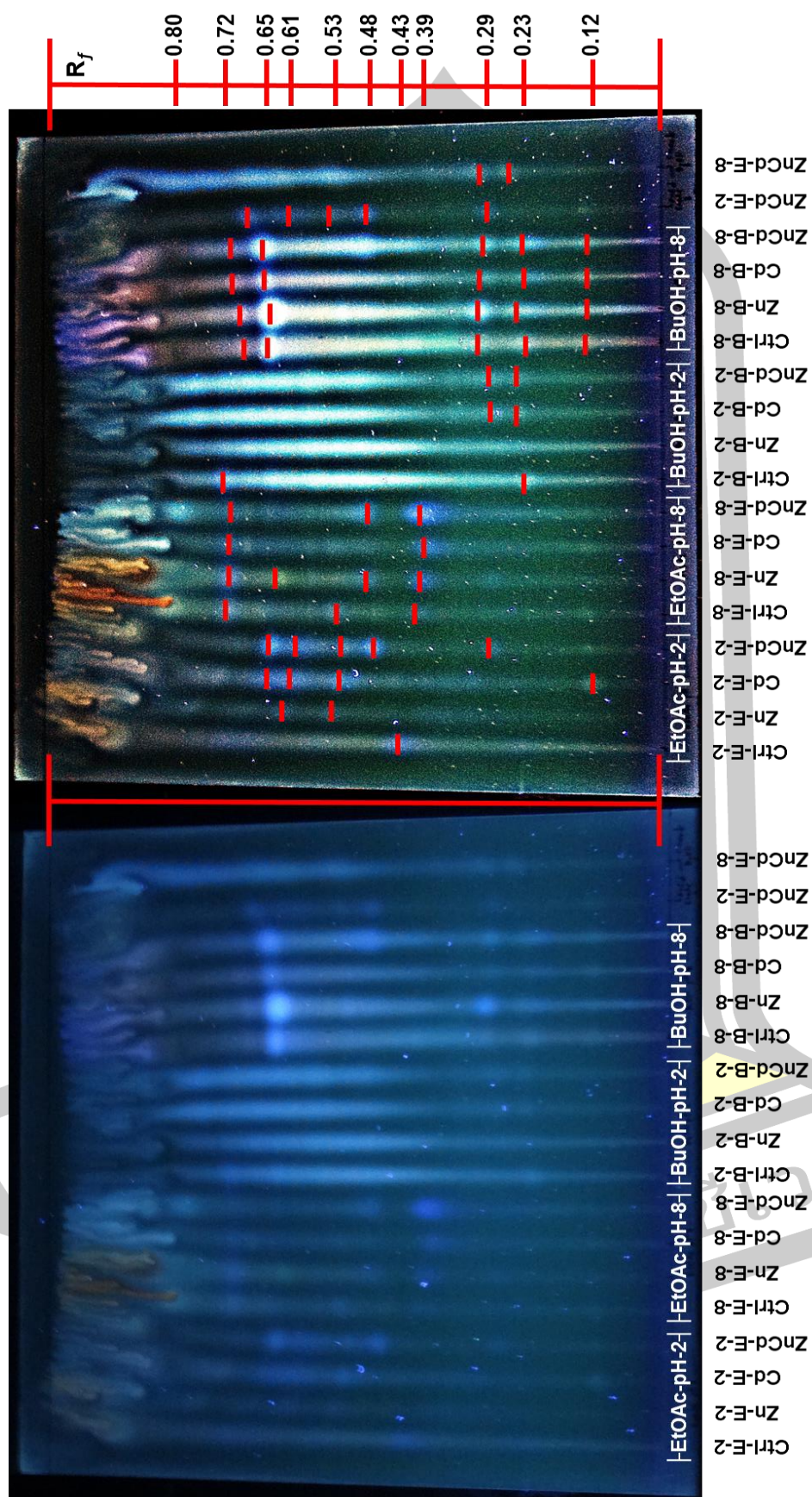


Figure 19 TLC chromatogram detected under UV 360 nm (a) and TLC figure was adjustment process in photoscape program (b). All crude siderophore extracts were represented related to the solvent fractions and pH in the extraction including EtOAc-pH-2, EtOAc-pH-8, BuOH-pH-2 and BuOH-pH-8. Retention factor (R_f) is the distance migrated of each chromatograms divided by the total distance of the solvent.

4.1.3.3 Liquid chromatography-mass spectrometry (LC-MS)

LC-MS was carried out to search and confirm the siderophores in the crude siderophore extracts. A 10 μ l of crude siderophore extracts were dissolved by methanol and 10 mM sodium formate was used as internal standard. Based on the data of crude siderophore density (Table 7), the quantitative analysis of peak area could be compared. The LC chromatograms (Figure 20) show the difference between the EtOAc fractions (ZnCd-E-2 and ZnCd-E-8) and the BuOH fractions (ZnCd-B-2 and ZnCd-B-8) because the characteristics of siderophores obtained by each solvent extraction, charge, free- or metal siderophore complex form of the crude siderophore extracts. Some peaks in the LC chromatograms were presented in all four crude siderophore extracts while the other peaks were found in its groups (Figure 20).

There are 6 peaks of siderophores, PDTC (peak 1), pyoverdine chromophore (peak 2), pyocyanin (peak 3), pyochelin (peak 4) and pseudomonine fragments (peak 5-6), were identified (Figure 20) including [PDTC]⁺ in de-hydrogen of thiol form (197.12 m/z at RT 6.6 mins) and [pyocyanin]⁺ (211.14 m/z at RT 13 mins) (El-Fouly et al. 2015) in all samples, [pyochelin]⁺ (325.07 m/z at RT 28.2 mins) in ZnCd-E-2, ZnCd-E-8 and ZnCd-B-8, the [chromophore]⁺ of pyoverdine (261.12 m/z at RT 11.1 mins) (Ruangviriyachai et al. 2004) in ZnCd-E-2, ZnCd-B-2 and ZnCd-B-8 and pseudomonine fragments (286.21 and 314.21 m/z at RT 35.3 and 39.2 mins, respectively) in ZnCd-E-2 and ZnCd-E-8. Table 6 shows the m/z in each peak and its fragments found in MS data to support the peak identification. The data of MS of peak 1-6 in each sample were shown (Appendix C). Most distinctive peaks in each crude siderophore extracts were not clearly identify.

The concentrations of each siderophores were quantitatively examined to compare the obtained siderophores in each crude siderophore extracts. Table 7 shows relative peak area of 6 siderophore peaks including PDTC, pyoverdine chromophore, pyocyanin, pyochelin and two pseudomonine fragments. The extracted solvent affected the concentrations of obtained siderophores. Two pseudomonine fragments found in the EtOAc fractions corresponding to the pseudomonine blue emission of the EtOAc fractions in TLC chromatograms. Moreover, the pseudomonine in ZnCd-E-8 was higher than ZnCd-E-2. The pyochelin concentration in ZnCd-B-8 was extremely higher than the others. While the PDTC, pyoverdine

chromophore and pyocyanin concentrations were not much different. In addition, the concentrations of PDTC, pyoverdine chromophore and pyochelin were higher in ZnCd-B-8 than the others. It suggested that these siderophores were highly obtained when extracted from no pH adjustment supernatants by used n-butanol.

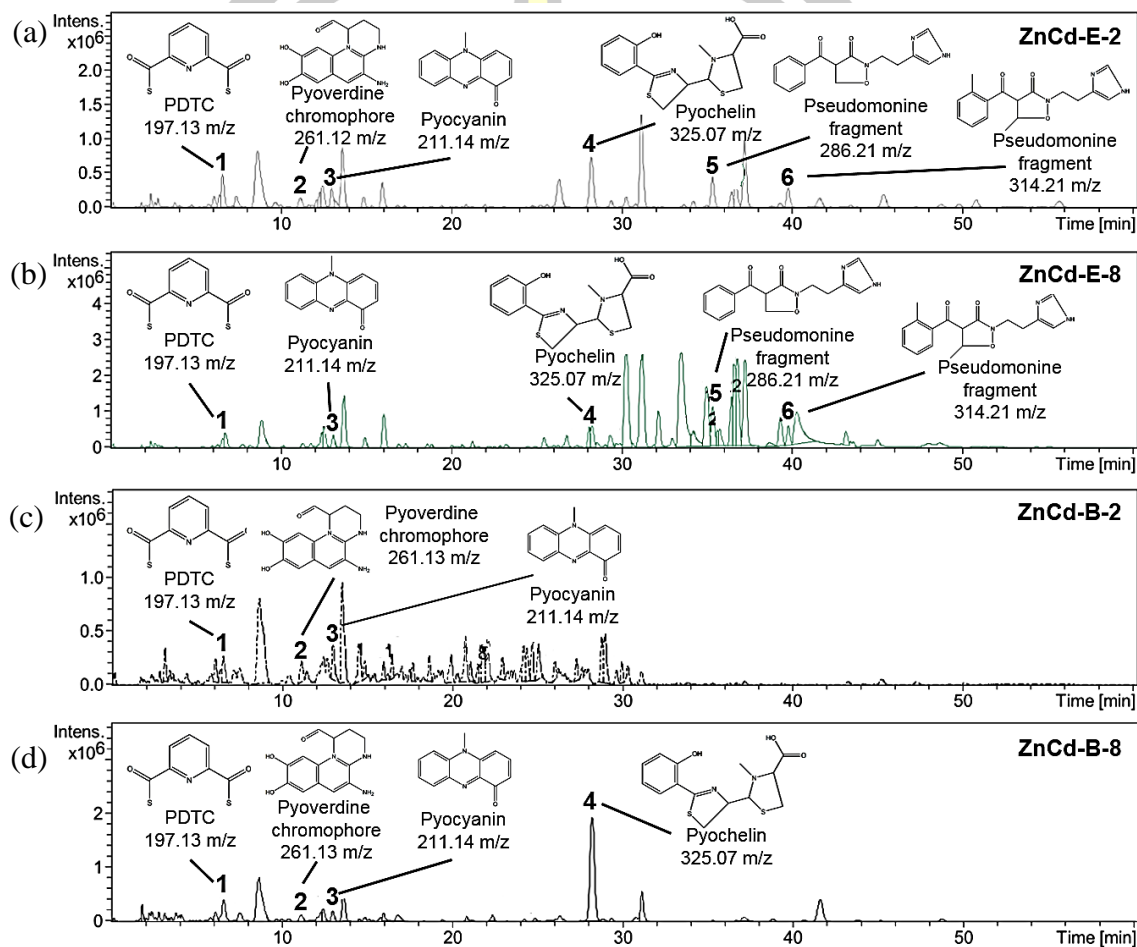


Figure 20 LC chromatogram of the crude siderophore extracts including ZnCd-E-2 (a), ZnCd-E-8 (b), ZnCd-B-2 (c) and ZnCd-B-8 (d) show their siderophore identity peaks in each crude siderophores. Peak identification; PDTC (peak 1), pyoverdine chromophore (peak 2), pyocyanin (peak 3), pyochelin (peak 4), pseudomonine fragments (peak 5-6).

Table 6 LC-MS peak evaluation which consisted of molecular formula, $[M+H]^+$ m/z and $[M+H]^+$ m/z fragments.

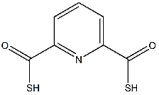
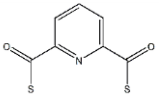
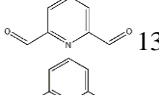
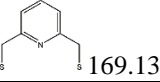
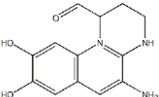
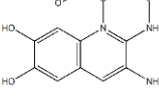
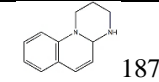
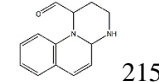
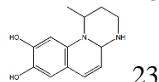
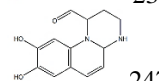
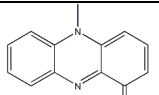
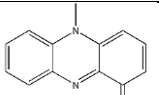
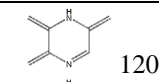
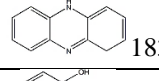
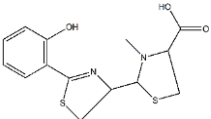
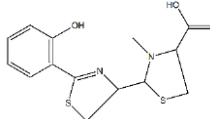
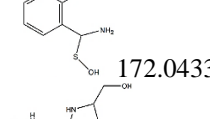
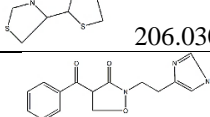
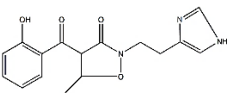
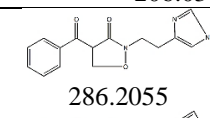
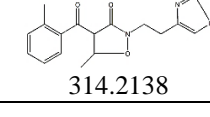
Peak	RT (min)	Siderophore	Molecular formula	$[M+H]^+$ m/z	$[M+H]^+$ m/z Fragment
1	6.6	PDTC	 $C_7H_5NO_2S_2$	 197.13	 136.0762  169.1333
2	11.1	PVD chromophore	 $C_{13}H_{14}N_3O_3$	 261.12	 187.1229  215.1177  233.1293  247.1648
3	13.0	Pyocyanin	 $C_{13}H_{10}N_2O$	 211.14	 120.0815  183.1488
4	28.2	Pyochelin	 $C_{14}H_{16}N_2O_3S_2$	 325.07	 172.0433  206.0307
5, 6	35.3, 39.7	Pseudomonine	 $C_{16}H_{17}N_3O_4$	315.1219 (Not found)	 286.2055  314.2138

Table 7 The relative siderophore peak area of the LC chromatogram.

Sample	Relative siderophore peak area ¹					
	PDTC	Pyoverdine chromophore	Pyocyanin	Pyochelin	Pseudomonine fragment ²	Pseudomonine fragment ³
ZnCd-E-2	10.87	3.75	5.57	20.49	10.42	7.24
ZnCd-E-8	6.88	0.00	5.20	9.47	17.88	8.76
ZnCd-B-2	3.90	3.20	4.06	0.00	0.00	0.00
ZnCd-B-8	15.11	4.54	5.62	85.06	0.00	0.00

¹ Relative peak area were calculated by the LC peak area obtained in the experiment multiply by crude siderophore density in each samples and divided by the peak area of internal standard sodium formate

² Pseudomonine fragment from peak 5

³ Pseudomonine fragment from peak 6

4.1.3.4 X-ray absorption near edge structure (XANES)

Crude siderophore extracts of the pH-2 extracts and the pH-8 extracts was studied by X-ray absorption fine structure (XAFS). XAFS can detail the different between the pH-2 extracts and the pH-8 extracts at atom level. XAFS was analyzed at two regions including; (i) pre-edge and absorption edge of element, this structure called X-ray absorption near edge structure (XANES). XANES indicate the oxidation state of each elements in crude siderophore extracts, and (ii) post absorption edge called extended X-ray absorption fine structure (EXAFS) indicate the ligands of Zn and Cd in crude siderophore extracts, All XAFS spectra were normalized to quantitatively compare the peak position and peak height in case of XANES spectra. While Zn and Cd can analyse EXAFS in case of clear spectra, the high signal-to-noise ratio spectra were analysed in XANES.

The LC-MS indicated the PDTC, pyoverdine, pyocyanin, pyochelin and pseudomonine contained in the crude siderophore extracts. PDTC and pyochelin have thiol and sulfur in their structures, respectively. Sulfur is potential to be a metal ligands. Therefore, the crude siderophore extracts were analyzed the S, Zn and Cd elements.

The sulfur concentration in the crude siderophore extracts was relative examined by the count of X-ray fluorescence (XRF) spectra (Figure 21). The sulfur concentration in the crude siderophore extracts was sufficient for the S XANES measurement. The sulfur signal in the BuOH fraction were higher than the EtOAc fractions.

4.1.3.4.1 Sulfur K-edge XANES

The S K-edge XANES spectra of all crude siderophore extracts show in Figure 22. It shows the multi-oxidation at 2472, 2475 and 2480 eV. The S XANES spectra of the pH-2 extracts and the pH-8 extracts were different by comparing the height of each peaks in each metal treatments. The S XANES spectra of Cd and Zn+Cd were similarly in the pattern of each peaks while the control and Zn treatment spectra were not related to each other. However, three peaks of S XANES consisted of the hidden oxidation peak inside the main peak. The organic sulfur oxidations were reported including sulfide, thiol, disulfide, sulfoxide, sulfone, sulfonate and sulfate. These organic sulfur oxidations were -2, -1/-0.5, -1/0, +2, +4,

+5 and +6, respectively (Schmalenberger et al. 2011). Therefore peak fitting was used to analyse the oxidations of sulfur in S XANES data.

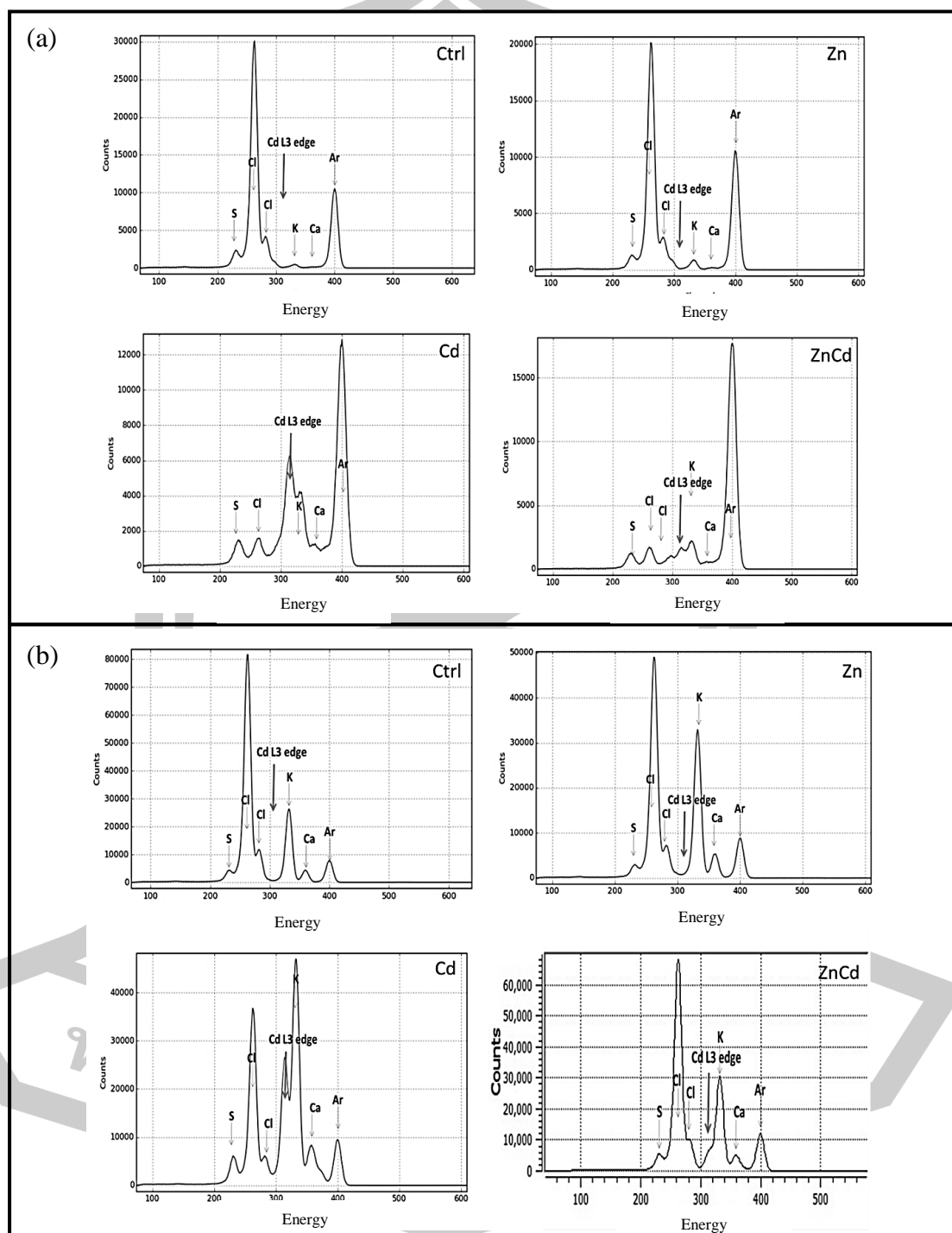
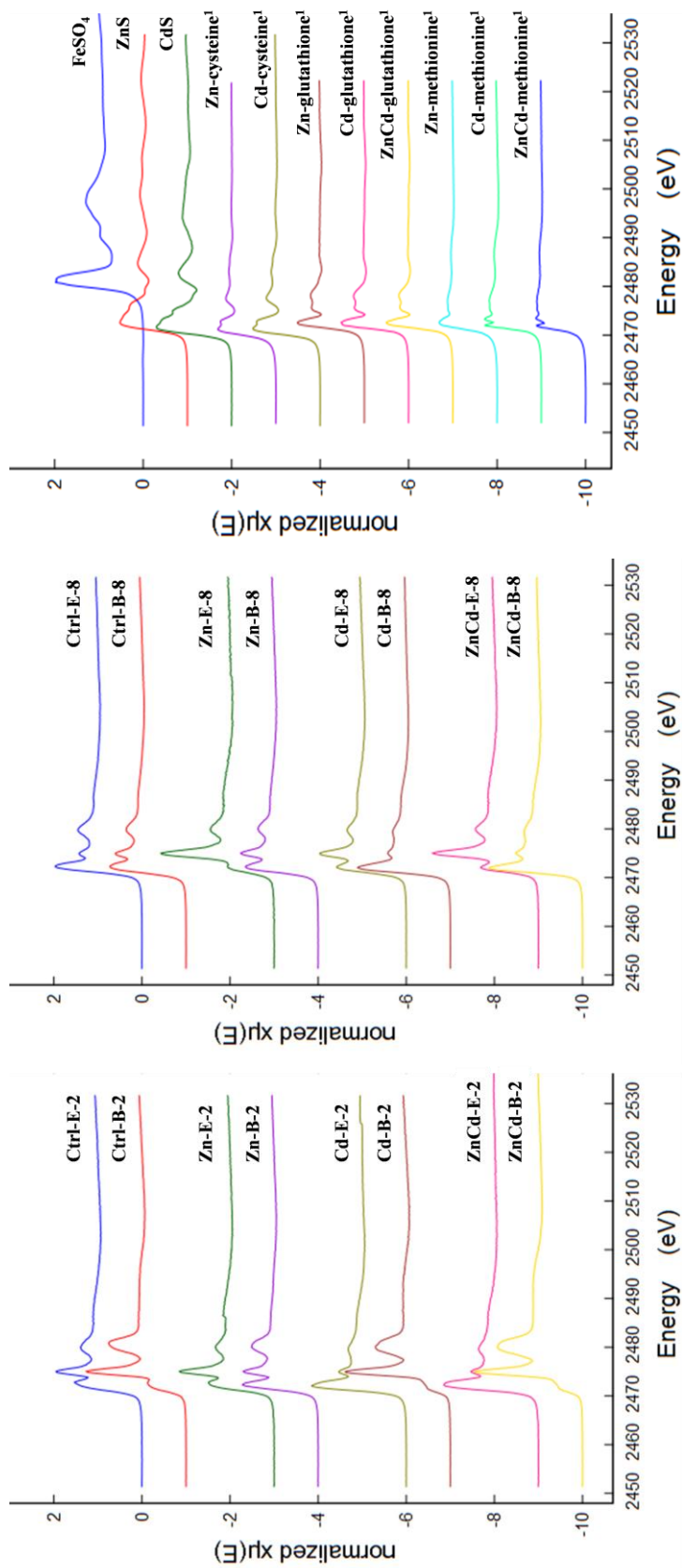


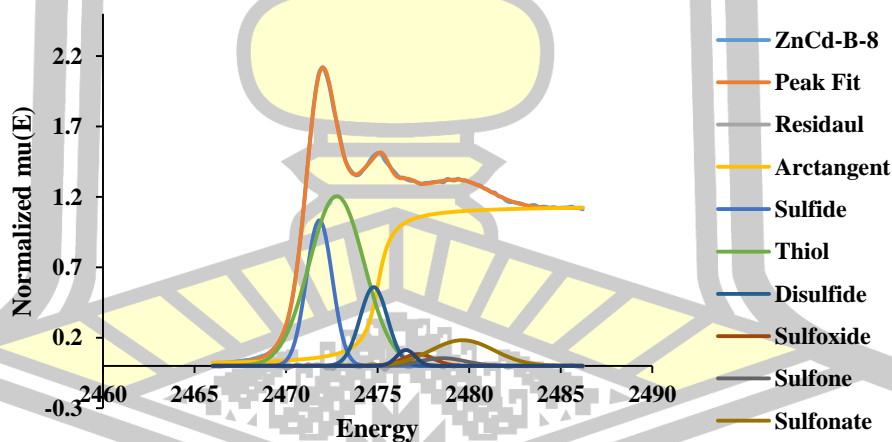
Figure 21 X-ray fluorescent (XRF) spectra of the EtOAc-pH-8 (a) and BuOH-pH-8 (b) extracts including Ctrl, Zn, Cd and Zn+Cd show the elements such as S, Cl, Cd, K and Ca.



¹ The reference compounds were in the complex form

Figure 22 Normalized S K-edge XANES absorption spectra of the pH-2 extracts (a), the pH-8 extracts (b) and the reference compounds (c).

The S XANES spectra of all crude siderophore extracts were fitted the analytical line shapes of sulfide, thiol, disulfide, sulfoxide, sulfone, sulfonate and sulfate to S XANES data (Figure 23). The results obtained from peak fitting were photon energy and area of each analytical line shapes. The photon energy of each analytical line shapes indicate the oxidation and position of each sulfur. The area of each analytical line shapes corresponded to the concentration of each line shapes. Configurations of each sulfur were showed in Figure 23. The Gaussian peaks used in this calculations were referred by following Rompel et al. (1998), Schmalenberger et al. (2011) and Lin et al. (2014). The percentages of S XANES peak fitting area were show in Table 8. The sulfur species in the reduced form (sulfide, thiol and disulfide) were larger than the sulfur species in the intermediate form (sulfoxide) and oxidized form (sulfone, sulfonate and sulfate). The reduced form of sulfur indicated that the sulfur in siderophores can donate electron to metal ions. The thiol groups were related to disulfide by the thiol increased and disulfide decreased. The present of thiol supported the presenting of PDTTC in the crude siderophore extracts.



Sulfur functional group	Sulfide	Thiol	Disulfide	Sulfoxide	Sulfone	Sulfonate	Sulfate
Oxidation	-2	-1/-0.5	-1/0	+2	+4	+5	+6
Photon energy (eV)	2471	2472	2474	2476	2477	2478	2479
Configuration	R-S-R	R-S-H	R-S-S-R	R-(S=O)-R	R-C-SO ₃	R-O-SO ₃	SO ₄

Figure 23 Normalized S K-edge XANES peak fitting by the 7 Gaussian and Lorentzian peaks including position of sulfide, thiol, disulfide, sulfoxide, sulfone, sulfonate and sulfate peaks. The oxidation, photo energy and configuration of each peaks were showed in table below.

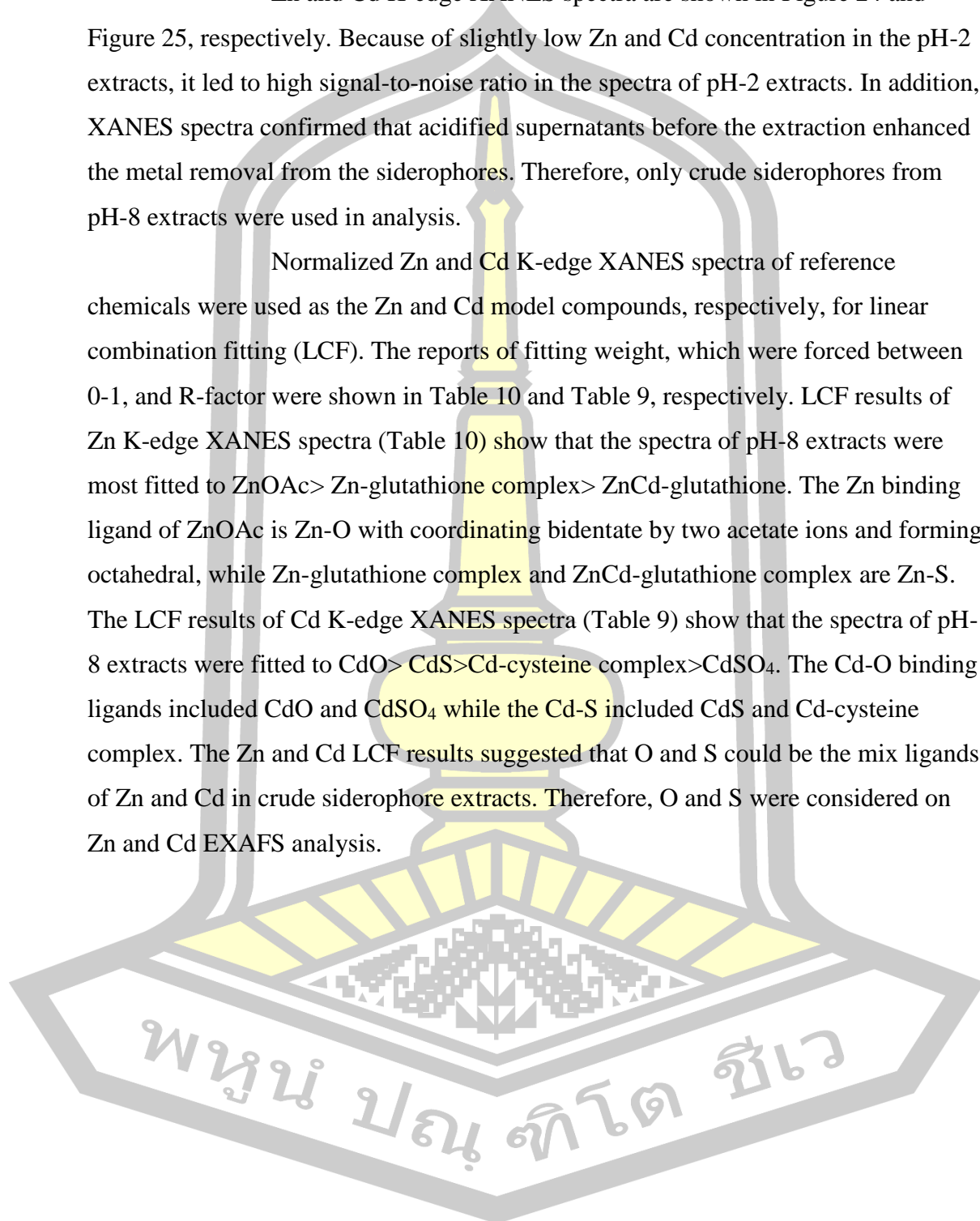
Table 8 The percentages of S XANES peak fitting area of all crude siderophore extracts.

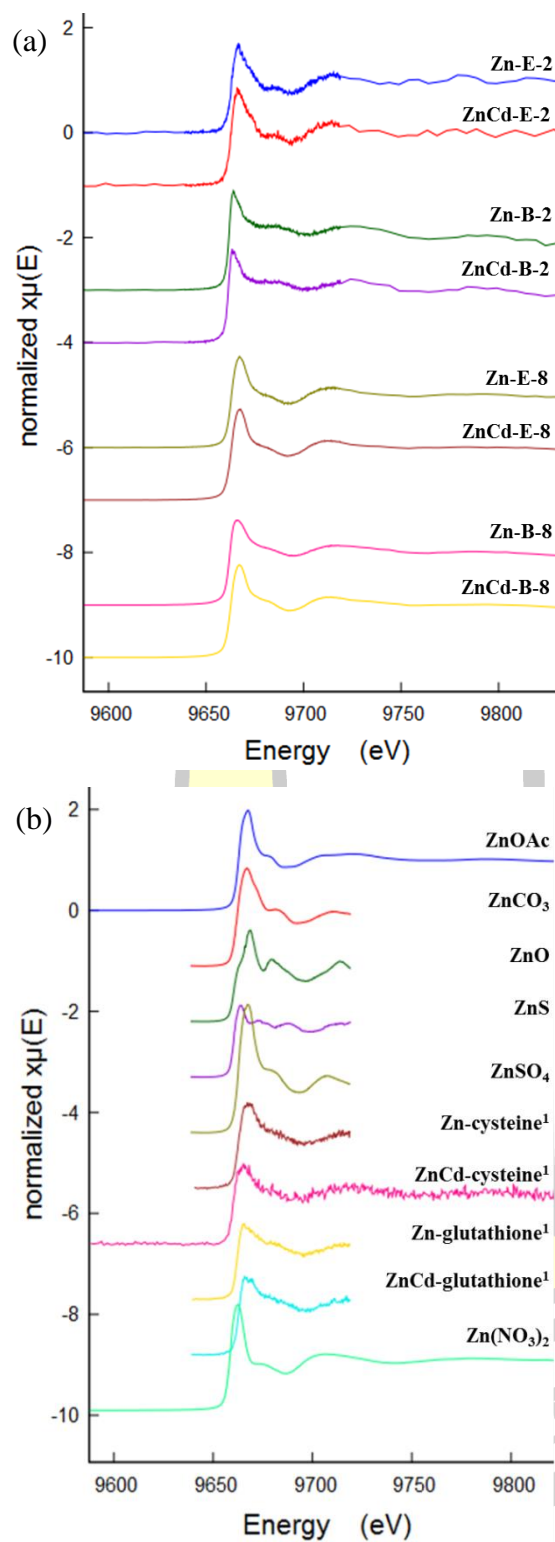
Sample	Sulfide (%)		Thiol (%)		Disulfide (%)		Sulfoxide (%)		Sulfonate (%)		Sulfate (%)		R-factor		
	pH-2	pH-8	pH-2	pH-8	pH-2	pH-8	pH-2	pH-8	pH-2	pH-8	pH-2	pH-8	pH-2	pH-8	
Ctrl	EtOAc	22.55	22.08	2.12	12.05	13.75	6.49	1.77	5.67	5.25	3.56	1.74	2.97	0.0003	0.0002
	BuOH	15.99	9.33	0.00	31.04	16.15	2.94	1.44	1.80	7.97	2.76	5.41	5.17	0.0002	0.0001
Zn	EtOAc	1.58	14.96	26.10	1.52	13.55	25.65	3.34	1.91	2.27	3.86	1.86	3.42	0.0002	0.0003
	BuOH	15.95	22.52	9.40	4.70	11.10	12.94	2.73	4.78	8.63	2.86	0.21	4.17	0.0002	0.0002
Cd	EtOAc	18.58	17.58	16.70	8.41	5.03	16.72	4.40	2.49	5.55	1.02	0.00	3.52	0.0003	0.0002
	BuOH	5.09	16.82	5.23	30.37	19.19	0.95	1.41	0.83	7.63	5.91	6.58	0.00	0.0001	0.0002
Zn+Cd	EtOAc	18.29	12.58	21.02	7.32	6.27	19.80	1.49	2.47	2.80	1.15	2.83	3.97	0.0002	0.0002
	BuOH	7.08	11.08	2.83	27.38	19.58	6.41	1.45	0.86	10.48	1.02	7.04	4.77	0.0002	0.0001

4.1.3.4.2 Zinc and cadmium K-edge XANES

Zn and Cd K-edge XANES spectra are shown in Figure 24 and Figure 25, respectively. Because of slightly low Zn and Cd concentration in the pH-2 extracts, it led to high signal-to-noise ratio in the spectra of pH-2 extracts. In addition, XANES spectra confirmed that acidified supernatants before the extraction enhanced the metal removal from the siderophores. Therefore, only crude siderophores from pH-8 extracts were used in analysis.

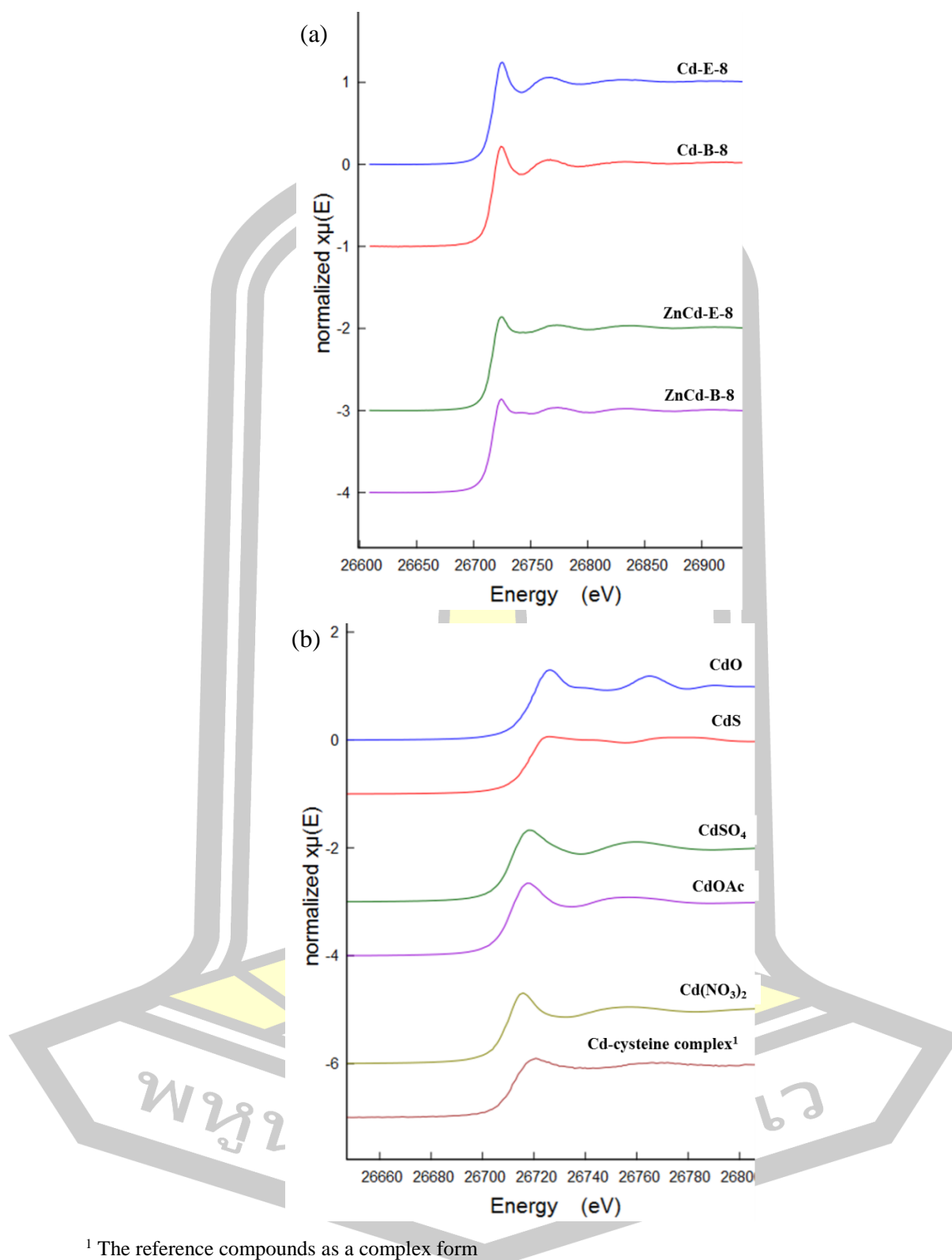
Normalized Zn and Cd K-edge XANES spectra of reference chemicals were used as the Zn and Cd model compounds, respectively, for linear combination fitting (LCF). The reports of fitting weight, which were forced between 0-1, and R-factor were shown in Table 10 and Table 9, respectively. LCF results of Zn K-edge XANES spectra (Table 10) show that the spectra of pH-8 extracts were most fitted to ZnOAc > Zn-glutathione complex > ZnCd-glutathione. The Zn binding ligand of ZnOAc is Zn-O with coordinating bidentate by two acetate ions and forming octahedral, while Zn-glutathione complex and ZnCd-glutathione complex are Zn-S. The LCF results of Cd K-edge XANES spectra (Table 9) show that the spectra of pH-8 extracts were fitted to CdO > CdS > Cd-cysteine complex > CdSO₄. The Cd-O binding ligands included CdO and CdSO₄ while the Cd-S included CdS and Cd-cysteine complex. The Zn and Cd LCF results suggested that O and S could be the mix ligands of Zn and Cd in crude siderophore extracts. Therefore, O and S were considered on Zn and Cd EXAFS analysis.





¹ The reference compounds as a complex form

Figure 24 Zn K-edge XANES absorption spectra of (a) crude siderophore extracts and (b) the reference compounds in the complexes form.



¹ The reference compounds as a complex form

Figure 25 Cd K-edge XANES absorption spectra of (a) crude siderophore extracts and (b) the reference chemicals in the complexes form.

Table 10 Linear Combination Fit (LCF) of normalized Zn K-edge spectra from 9638 to 9717 eV, Weights sum to 1 and forced between 0 and 1.

Sample	ZnOAc	ZnCO ₃	ZnO	ZnS	ZnSO ₄	Zn(NO ₃) ₂	Zn ₂ Cysteine	ZnCd ₂ Cysteine	Zn ₂ Glutathione	ZnCd ₂ Glutathione	R-factor
Zn-E-8	0.509 ±0.05	- ^a	0.123 ±0.02	- ^a	- ^a	- ^a	0.052 ±0.04	- ^a	0.316 ±0.03	- ^a	0.0063
ZnCd-E-8	0.484 ±0.02	- ^a	0.109 ±0.03	- ^a	0.046 ±0.02	- ^a	- ^a	- ^a	- ^a	0.360 ±0.02	0.0044
Zn-B-8	0.202 ±0.03	0.046 ±0.07	- ^a	0.266 ±0.04	0.110 ±0.04	0.015 ±0.01	0.036 ±0.04	- ^a	0.325 ±0.11	- ^a	0.0049
ZnCd-B-8	0.378 ±0.01	0.157 ±0.01	0.111 ±0.01	- ^a	0.003 ±0.01	0.036 ±0.01	0.067 ±0.01	- ^a	0.087 ±0.01	0.160 ±0.02	0.0043

^a = Not match spectra in the best fit of LCF

Table 9 Linear Combination Fit (LCF) of normalized Cd K-edge spectra from 26669 to 26774 eV, weights sum to 1 and forced between 0 and 1.

Sample	CdOAc	Cd(NO ₃) ₂	CdO	CdS	CdSO ₄	Cd ⁺ Cysteine	R-factor
Cd-E-8	- ^a	- ^a	0.667 ±0.11			0.333 ±0.02	0.0049
ZnCd-E-8	- ^a	- ^a	0.581 ±0.04	0.025 ±0.05		0.394 ±0.06	0.0054
Cd-B-8	- ^a	- ^a	0.261 ±0.09	0.402 ±0.05	0.039 ±0.04	0.298 ±0.06	0.0019
ZnCd-B-8	- ^a	- ^a	0.179 ±0.02	0.533 ±0.08	0.107 ±0.03	0.181 ±0.06	0.0018

^a = Not match spectra in the best fit of LCF

4.1.3.5 Fourier transform infrared spectroscopy (FTIR) analysis

From the results of XANES indicated that O and S were coordinating ligands for Zn and Cd ions. The S XANES was clearly demonstrated the difference between the pH-2 and pH-8 extracts. For study the alteration of O and S ligands between the pH-2 and pH-8 extracts, FTIR is suitable because it detailed the changes of metal bonding or chelating to metal ions. The alteration of FTIR peaks indicate the metal bonding or chelating by the shift of wavenumber (D'Souza et al. 2008; Sutton et al. 2015), peak increasing or decreasing and new peak appearances. Little alteration of FTIR spectra in metafile of FTIR data were indicated by multivariate analysis PCA. Before analysis by PCA, all FTIR spectra were normalized to be compared the altered peaks such as shift and/or change in absorption.

The FTIR spectra of all crude siderophore extracts show in Figure 26. There are the same peaks in each crude siderophore extracts spectra but different in the absorbance or wavenumber shift. Therefore, these FTIR spectra supported the alteration among crude siderophore extracts. All FTIR spectra were analysed by PCA. The PCA consist of two information including the clustering of sample sets (each FTIR spectra) reporting as score plot and the identification of the variables (wavenumber, cm^{-1}) showing as loading plot. The principal component (PC) value inform the important of the variable.

The possible ligands in the functional groups of the FTIR spectra were C=O ($1600\text{-}1800\text{ cm}^{-1}$), C-O ($1050\text{-}1150\text{ cm}^{-1}$), S=O ($1060\text{-}1110\text{ cm}^{-1}$) and S-O ($810\text{-}870\text{ cm}^{-1}$). These functional groups can donate lone pair electrons to metal ions. Thiol was a weak peak near 2400 cm^{-1} and it was not presented in the FTIR spectra. The FTIR and PCA analysis was supported the difference in the O and S ligands between the pH-2 extracts and the pH-8 extracts by the separation as shown in the score plots. The alteration of wavenumber and absorption of C=O, C-O, S=O and S-O were shown in Table 11 and this results were determined couple to the results of PCA.

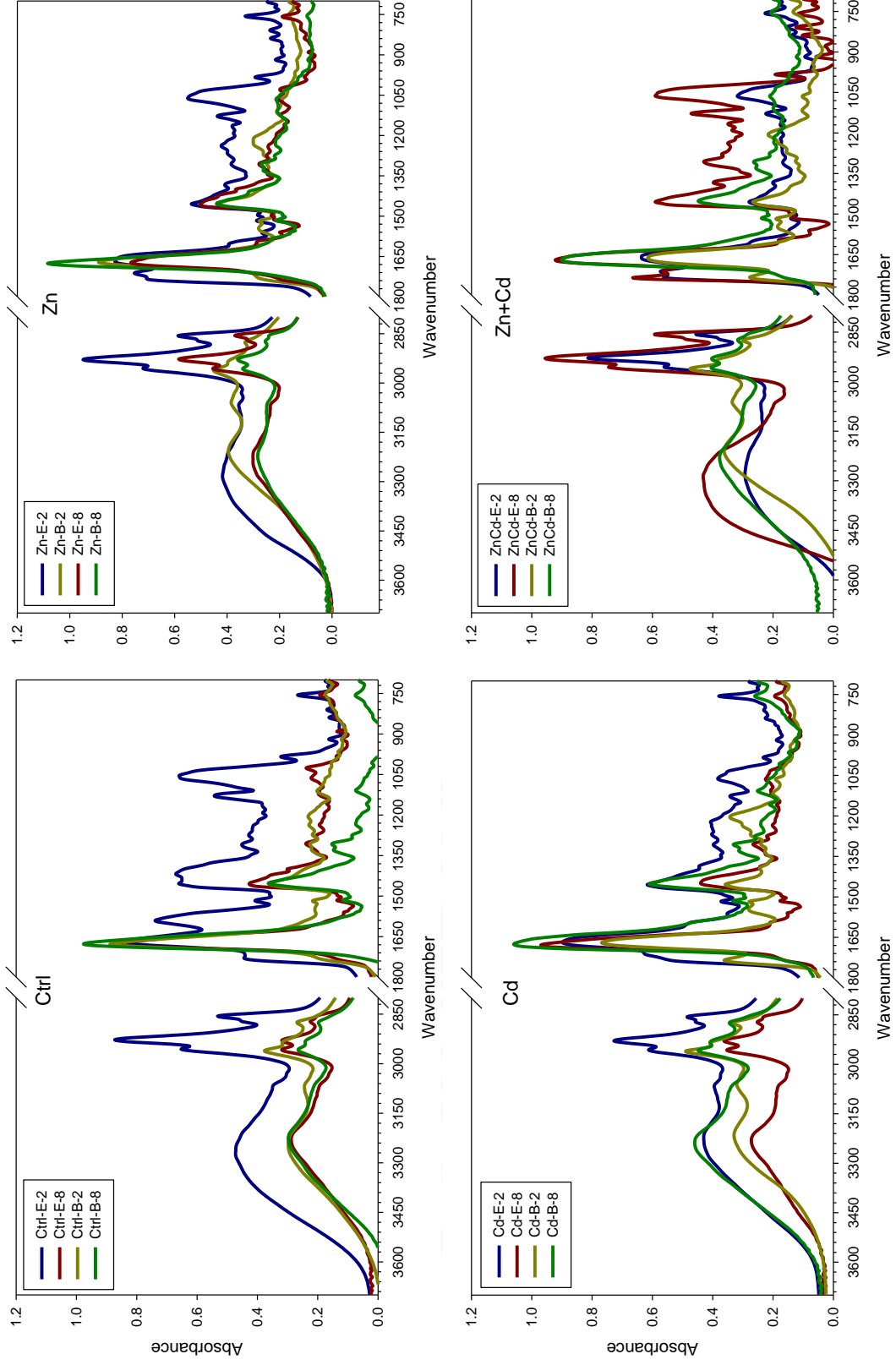


Figure 26 The FTIR spectra of Ctrl (a), Zn (b), Cd (c) and Zn+Cd (d).

Table 11 Alteration of the functional groups related to O and S metal binding ligands found in the siderophore crude extracts.

Functional group	Wavenumber (cm ⁻¹)		Wavenumber (cm ⁻¹)/ absorbance change ¹	Wavenumber (cm ⁻¹)		Wavenumber (cm ⁻¹)/ absorbance change ¹
	pH-2	EtOAc pH-8		pH-2	BuOH pH-8	
Control						
C=O	1681	1681	-▼	1681	1675	-6/▼
C-O	1120	1124	+4/▲	1135	1133	-2/▲
S=O	1077	1077	-▲	1076	1068	-8/▲
S-O	773	773	-▲	765	760	-5/▲
Zn						
C=O	1675	1677	+2/▼	1675	1677	+2/▲
C-O	1133	1135	+2/▼	1128	1128	-/▼
S=O	1066	1077	+11/▼	1083	1083	-/▼
S-O	759	763	+4/▼	767	771	+4/▼
Cd						
C=O	1675	1683	+8/▲	1675	1681	+6/▲
C-O	1137	1137	-/▼	1135	1118	-17/▲
S=O	1070	1079	+9/▼	1081	1081	-/▲
S-O	757	767	+10/▼	769	765	-4/▲
Zn+Cd						
C=O	1669	1675	+6/▲	1671	1675	+4/▲
C-O	1133	1131	-2/▲	1133	1124	-9/▲
S=O	1070	1066	-4/▲	1081	1079	-2/▲
S-O	761	763	+2/▼	763	765	+2/▲

¹ Key to symbol; ▲ increase, ▼ decrease

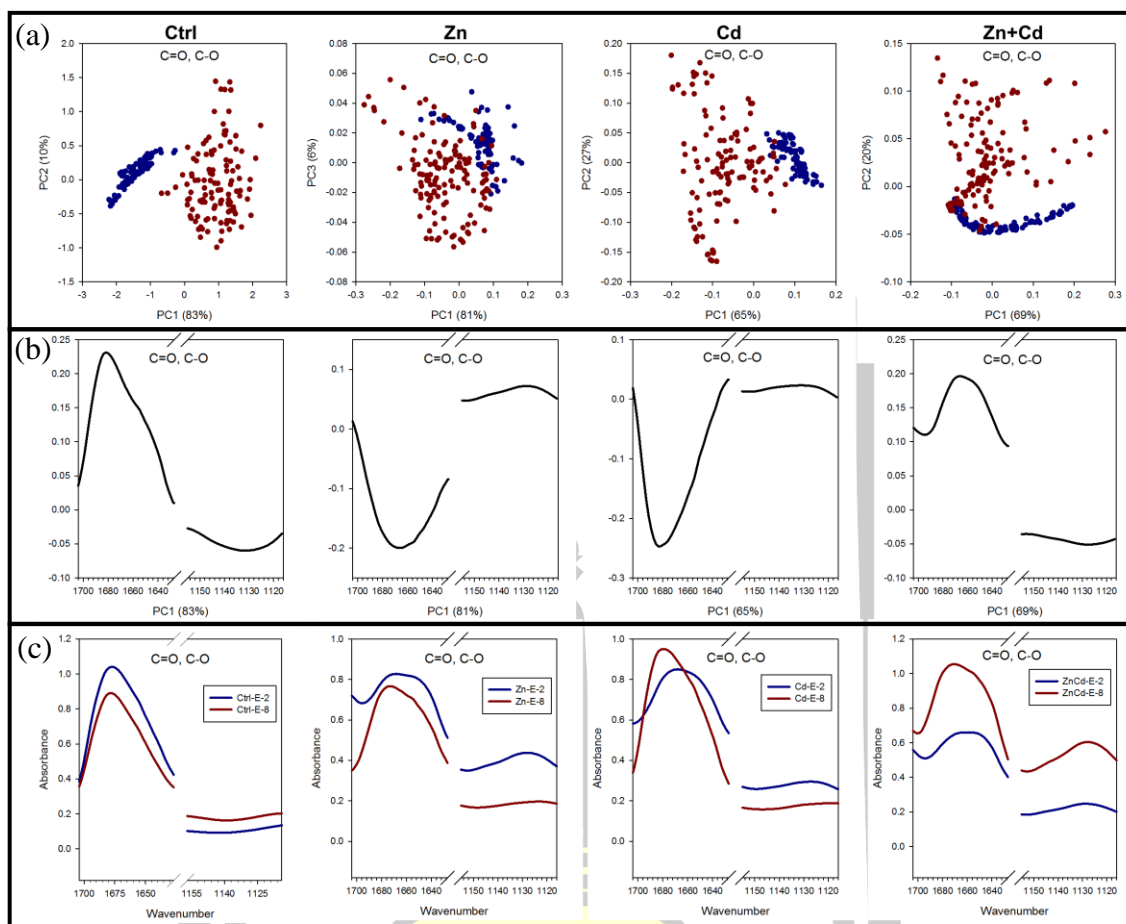


Figure 27 The C=O and C-O peaks of the EtOAc (Ctrl, Zn, Cd and Zn+Cd) consisted of score plot (a), loading plot (b) and the average of normalized FTIR spectra (c).

Figure 27 shows that C=O ($1600-1800\text{ cm}^{-1}$) and C-O ($1050-1150\text{ cm}^{-1}$) functional groups of the pH-2 extracts and pH-8 extracts were different. All crude siderophores found the shift of C=O in the pH-8 extracts only except the Ctrl-E-8. The shift of C=O indicated to metal ion binding (Mizuguchi et al. 1997). The shift of wavenumber at 1675 cm^{-1} in the control sample was found only in Ctrl-B-8. Moreover, the C-O absorbances of Zn, Cd and Zn+Cd were higher than Ctrl.

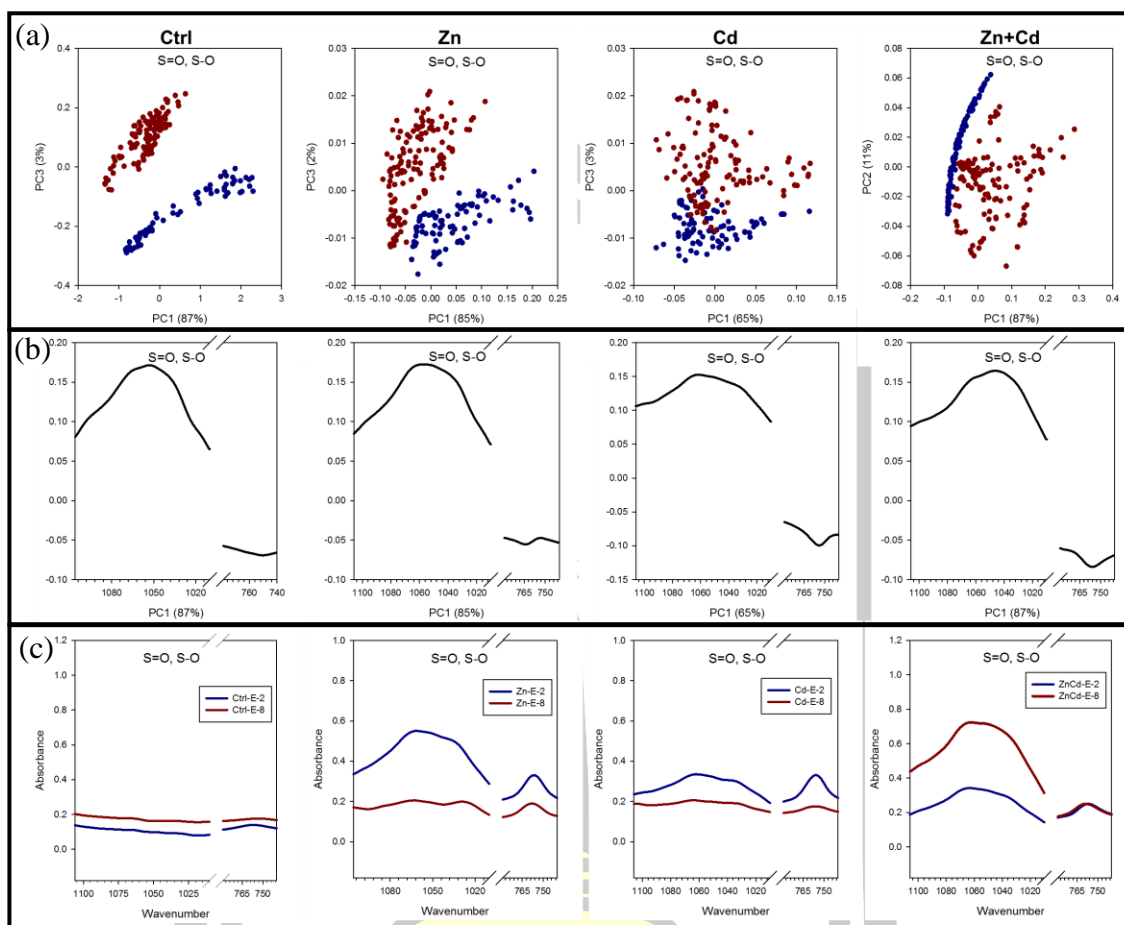


Figure 28 The S=O and S-O peaks of the EtOAc (Ctrl, Zn, Cd and Zn+Cd) consisted of score plot (a), loading plot (b) and the average of normalized FTIR spectra (c).

Figure 28 shows that S=O ($1060-1110\text{ cm}^{-1}$) and S-O ($810-870\text{ cm}^{-1}$) functional groups of the pH-2 extracts and the pH-8 extracts were different. However, the S=O and S-O were shifted to higher wavenumber in the Zn and Cd. These functional groups could chelate the metal ions. However, no reports supported of the S=O and S-O shifted by metal chelation. Moreover, the absorbance of the Zn and Cd were higher than control and Zn+Cd.

พหุ ประถมศึกษา

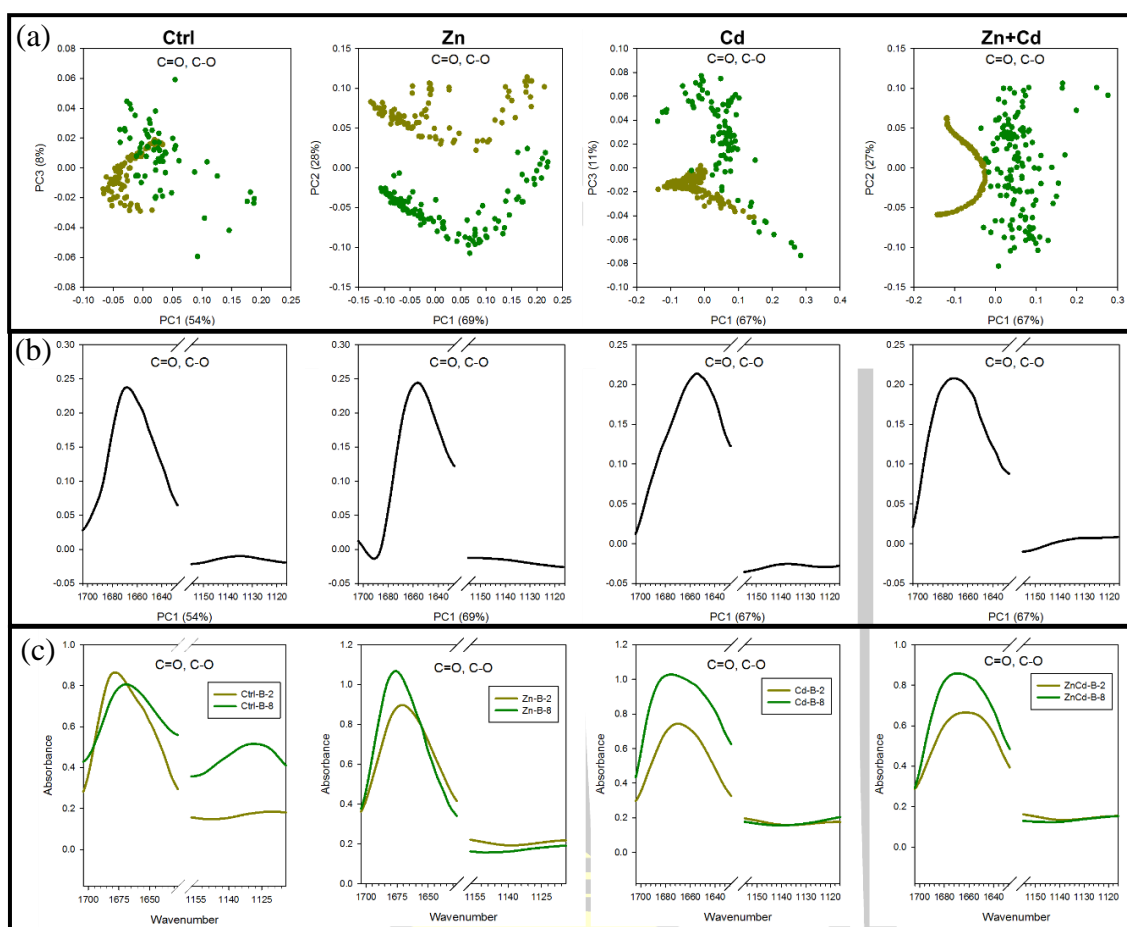


Figure 29 The C=O and C-O peaks of the BuOH fractions (Ctrl, Zn, Cd and Zn+Cd) consisted of score plot (a), loading plot (b) and the average of normalized FTIR spectra (c).

Figure 29 indicates that C=O ($1600\text{--}1800\text{ cm}^{-1}$) and C-O ($1050\text{--}1150\text{ cm}^{-1}$) functional groups of the pH-2 extracts and the pH-8 extracts were distinct. All crude siderophores had the shift peak of C=O. The C=O peak in the samples of Zn, Cd and Zn+Cd were shifted to higher absorbance whereas the peak in control samples was shifted to lower absorbance. The C-O of control, Cd and Zn+Cd were shifted to lower absorbance. The shift to lower wavenumber indicated the functional group bond to metal ion (D'Souza et al. 2008; Sutton et al. 2015). Moreover, the C=O absorbance of Zn, Cd and Zn+Cd was higher than control and the C-O of control was higher than Zn, Cd and Zn+Cd.

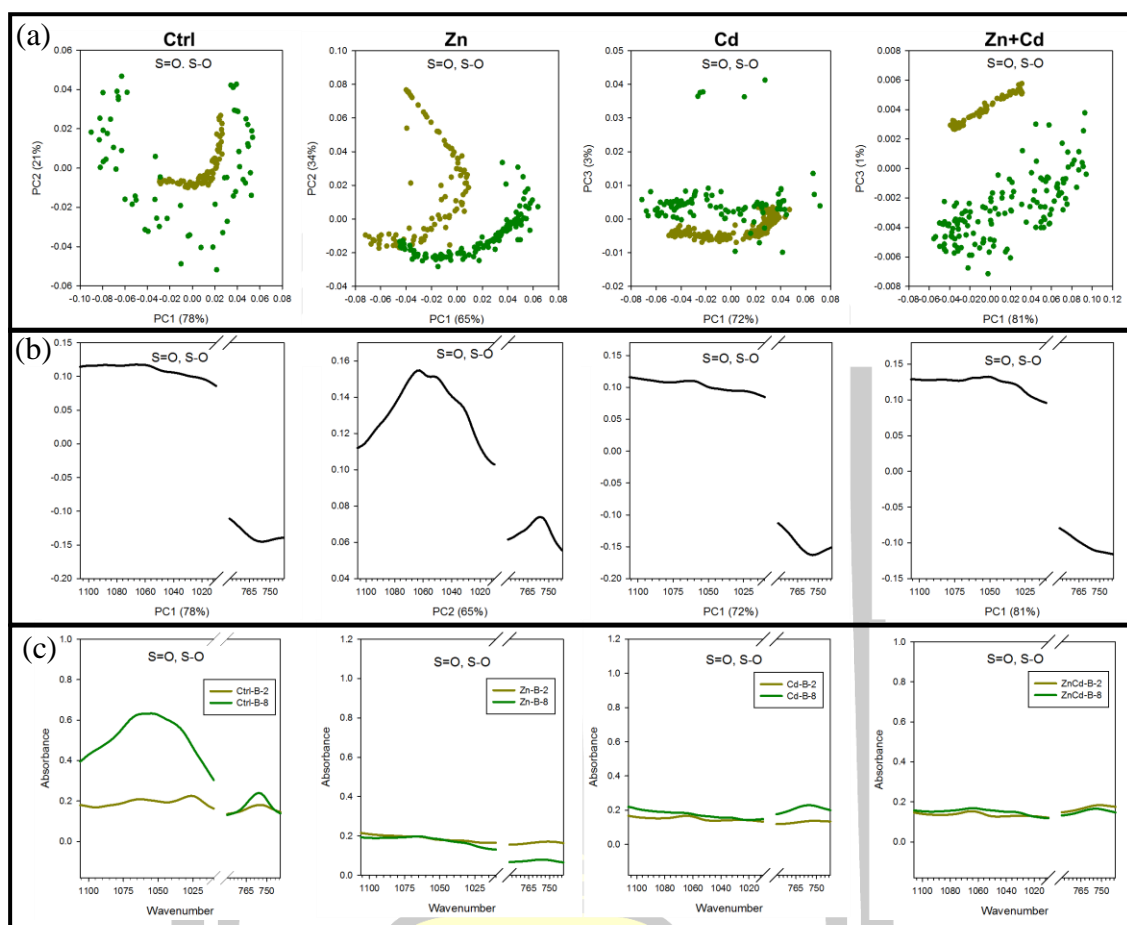


Figure 30 The S=O and S-O peaks of the BuOH fractions (Ctrl, Zn, Cd and Zn+Cd) consisted of score plot (a), loading plot (b) and the average of normalized FTIR spectra (c).

Figure 30 indicates that S=O ($1060-1110\text{ cm}^{-1}$) and S-O ($810-870\text{ cm}^{-1}$) functional groups of the pH-2 extracts and the pH-8 extracts were distinct. The S-O demonstrated the shift in all treatments and control. While the S=O was shifted to lower wavenumber in control and Zn+Cd. The shift to lower wavenumber indicated the functional group bond to metal ion (D'Souza et al. 2008; Sutton et al. 2015). Moreover, the S=O absorbance of control was higher than Zn, Cd and Zn+Cd.

4.1.3.6 EXAFS analysis of Zn and Cd

Zn and Cd XANES LCF results indicated the Zn and Cd coordinated with O and S ligands. Moreover, PCA analysis of the FTIR spectra supported that O and S ligands chelated with metal ions. Crude siderophore extracts from the pH-8 extracts were analyzed by EXAFS. Almost Zn and Cd coordinating with ligands were demonstrated by EXAFS. The EXAFS fitting plot results of $\chi(k)$ and the magnitude $\chi(R)$ of Fourier transformed data of the first shell show in Appendix D. The EXAFS spectra can detail the coordination number (N), Debye–Waller factor (σ^2) and bond distance (R). The shape of $\chi(R)$ in the crude siderophore extracts were asymmetry, hence, more than one electron scattering paths were investigated to fit in EXAFS. Table 12 shows the two electron scattering paths in the first shell. Zn in the EtOAc fraction and the BuOH fraction were coordinated with Zn-O at bond distance 1.8-2.0 Å and Zn-O/S at bond distance 1.6-2.2 Å, respectively. The Cd in Cd-E-8 only was Cd-O coordination in the first shell at bond distance 2.2-2.4 Å whereas the others were Cd-O/S at bond distance 2.2-2.6 Å. In addition, the ligands in the BuOH fractions were O and S while the EtOAc fractions were O, except ZnCd-E-8. The number of coordination of Zn and Cd were 4-8 and 3-5, respectively. The number of bonding indicated that Zn and Cd were chelated by the crude siderophore extracts.

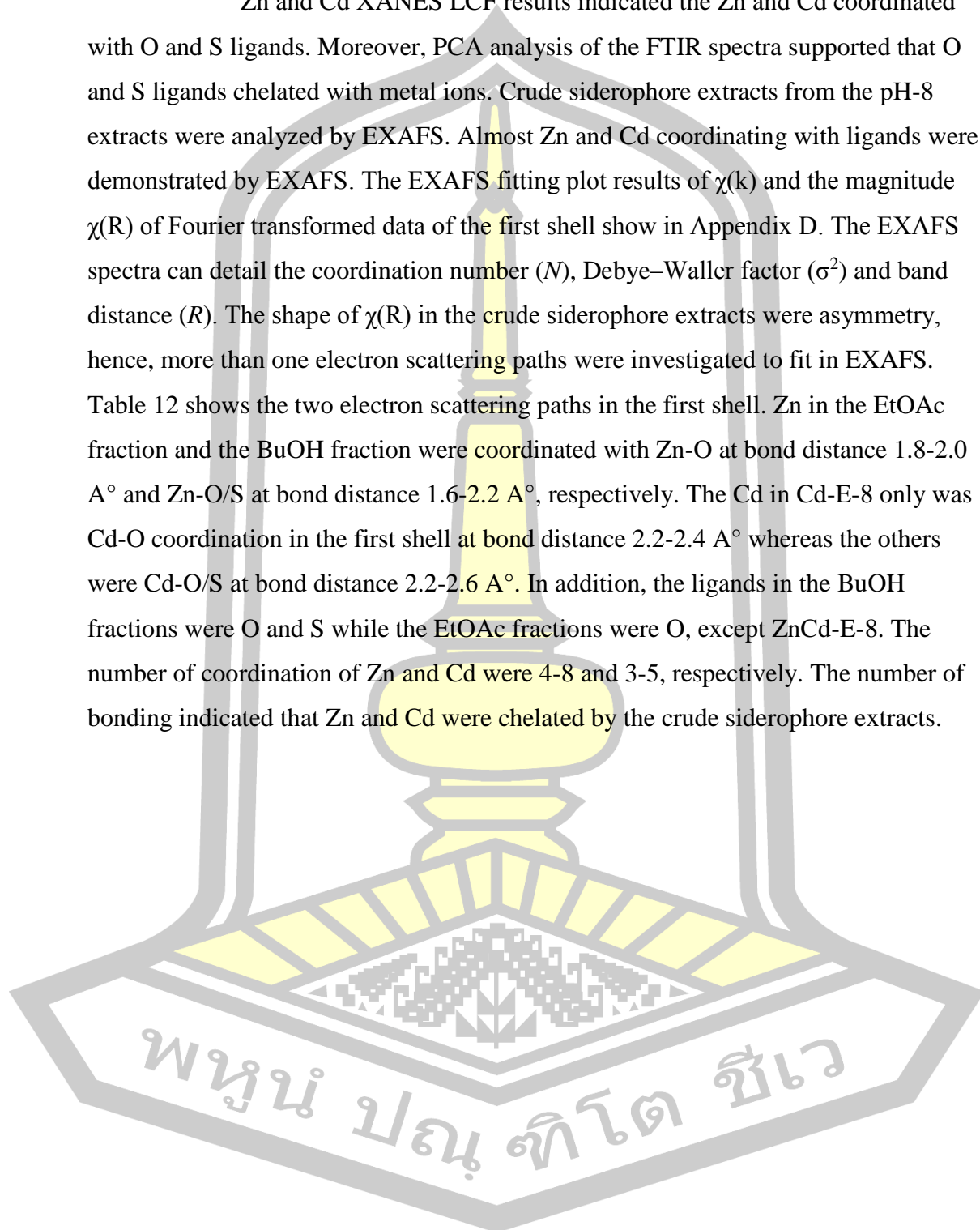


Table 12 Zn and Cd EXAFS results.

	First shell				R-factor
	Path	N	σ^2	R (Å ^o)	
Zn EXAFS Fitting					
Zn-E-8	Zn-O	4	0.0015	2.010±0.05	0.034
	Zn-O	2	0.0016	1.833±0.06	
Zn-B-8	Zn-O	2	0.0017	1.837±0.02	0.012
	Zn-S	2	0.0038	2.211±0.04	
ZnCd-E-8	Zn-O	4	0.0050	1.858±0.03	0.012
	Zn-O	4	0.0029	2.047±0.03	
ZnCd-B-8	Zn-O	1	0.0048	1.680±0.04	0.025
	Zn-S	4	0.0097	2.106±0.06	
Cd EXAFS Fitting					
Cd-E-8	Cd-O	4	0.0035	2.276±0.06	0.057
	Cd-O	1	0.0022	2.468±0.19	
Cd-B-8	Cd-O	2	0.0016	2.254±0.05	0.020
	Cd-S	1	0.0004	2.544±0.05	
ZnCd-E-8	Cd-O	2	0.0057	2.082±0.07	0.020
	Cd-S	2	0.0040	2.418±0.04	
ZnCd-B-8	Cd-O	3	0.0021	2.319±0.06	0.062
	Cd-S	1	0.0096	2.593±0.12	

Fitting in $\chi(R) = 1-2.5 \text{ \AA}^o$ and $\chi(k) = 3-10 \text{ \AA}^o^{-1}$ and showed the coordination number (N), Debye-Waller factor (σ^2) and bond distance ($R (\text{Å}^o)$)



4.2 The application of crude siderophores on Zn and Cd uptake in marigold.

4.2.1 Plant pathogenicity test

Before applied the crude siderophore extracts on marigold, it need to evaluate the possibility of the pathogenicity of *P. aeruginosa* PDMZnCd2003 on marigold. The pathogenicity test was carried out in two inoculation ways, by spraying on leave and soil and injecting in shoot. Even if leaving the inoculated marigold for 7 days, it was no any symptoms appeared (Appendix E). The leaves and soils were taken for the bacterial detection on NA agar plates to confirm that the bacteria were in/on the plant and soil. It found that the bacteria were in the leaf and soil samples (Figure 31). Although the bacteria was found in the plants and soils, it had no symptom or adverse effects on marigold.

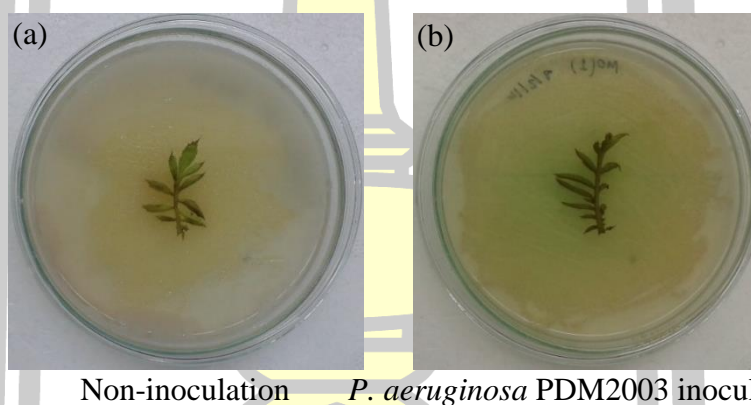


Figure 31 Bacterial detection on shoot from non-inoculation (a) had no green color secreted while the *P. aeruginosa* PDM2003 inoculation showed the secretion of green chemical.

4.2.2 Pot experiment

Pot experiments were performed in two times upon type of crude siderophore treatments including (i) from siderophore-metal complexes that aimed to improve Zn and Cd uptake in marigold and (ii) from free-siderophores that concerned the metal scavenging in soil and uptake into marigold. Other chelators including EDTA and citric acid were investigated for comparing the effects to crude siderophore extracts. EDTA is widely used as chelators in plants but it had side effects. While citric acid is a plant root exudate that also contained chelator property.

In the first pot experiment, bud stage of two month-old marigold plants were treated with crude siderophore extracts from ZnCd-E-8 and ZnCd-B-8, which were in siderophore-metal complex form, as a Zn and Cd supplements for improving Zn and Cd accumulation in marigold. Flowering stage of three month-old marigold plants were harvested. Flowers, leaves, roots, stems and rhizosphere soil were collected.

No significantly different of fresh and dry weights between control and other treatments (Figure 32 and Figure 33) of leaf, root, stem and flower. The results indicated that the chelator treatments were not improved the marigold growth when compare to the control. The chlorophyll contents in the plants treated with siderophore were significantly higher than the control plants and the plants treated by EDTA, citric acid and DMSO (Figure 34). The chlorophyll contents of plants treated with DMSO were the lowest, because DMSO had adverse effect on marigold by its toxicity. However, the chlorophyll in the siderophore treatments was not affected by DMSO toxicity.

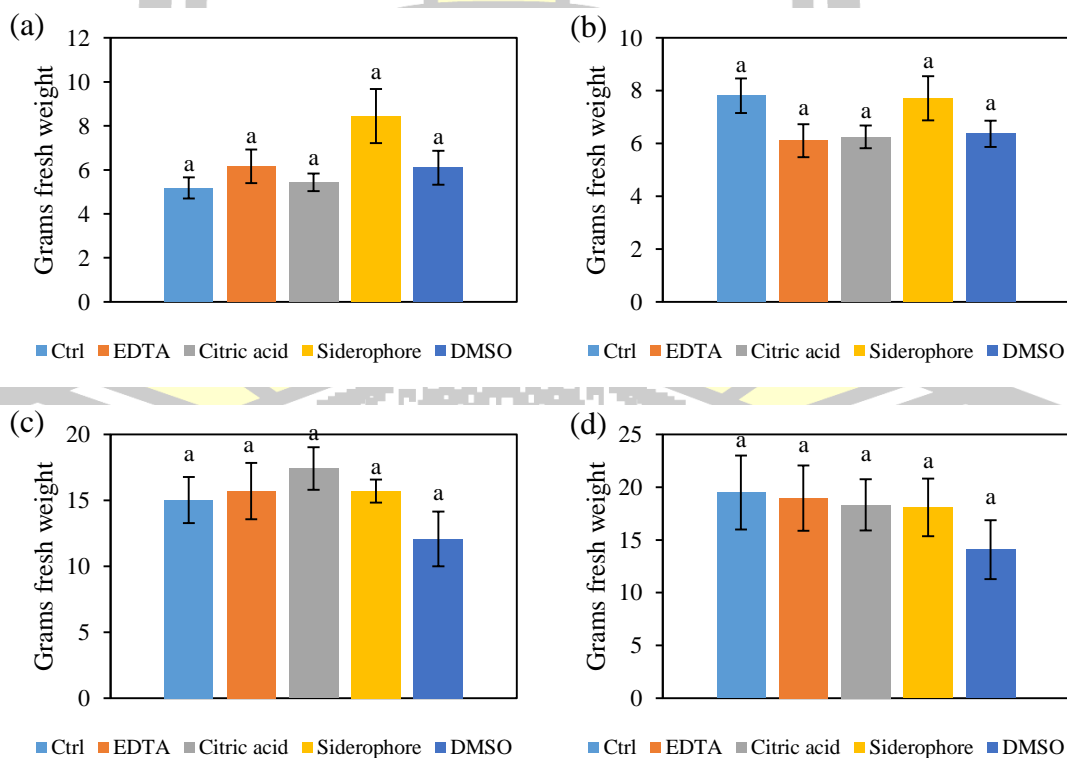


Figure 32 Fresh weight (g) of leaf (a), flower (b), stem (c) and root (d) in each treatments.

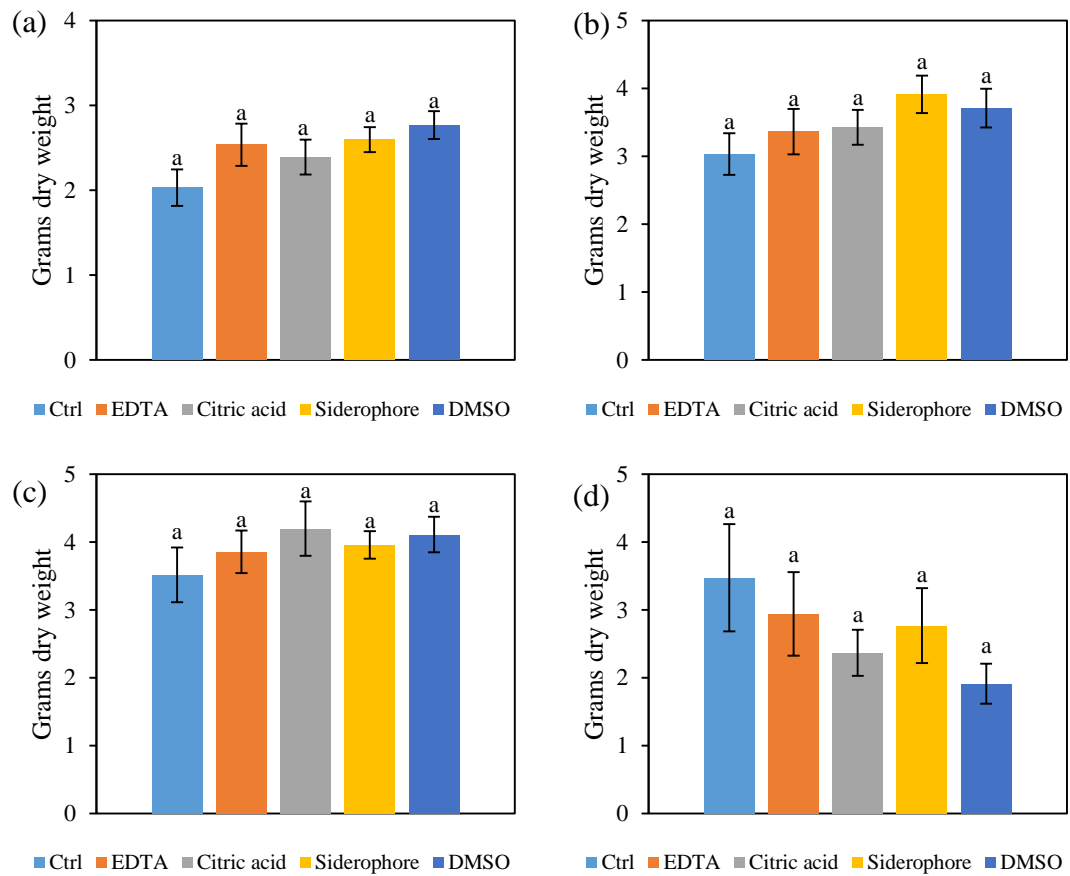


Figure 33 Dry weight (g) of leaf (a), flower (b), stem (c) and root (d) in each treatments.

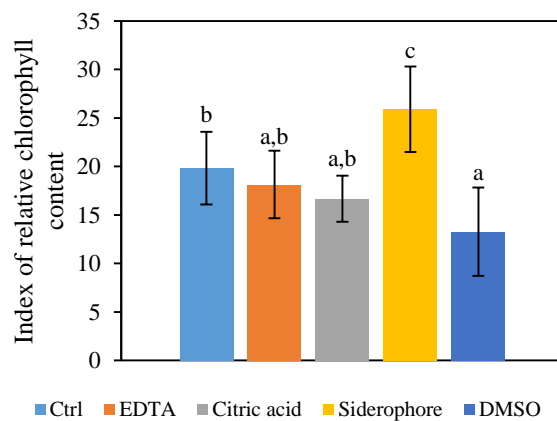


Figure 34 Index of relative chlorophyll content in each treatments.

Zn and Cd concentration in leaves were no significantly different between control and treatments (Figure 35). It indicated that these chelators had no effect on Zn and Cd accumulation in leaves. Zn concentration in the rhizosphere soil of the DMSO treatment was lower than the soil from control and the treatments of EDTA, citric acid and siderophore (Figure 36(a)). In addition, the Cd concentration in rhizosphere soil in control and treatments were not significantly different.

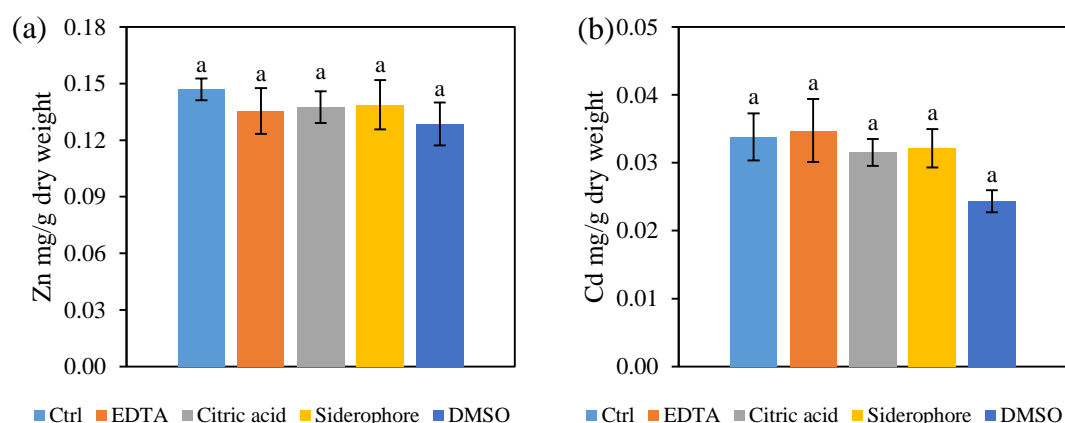


Figure 35 Total Zn (a) and Cd (a) concentrations (mg g^{-1} dry weight) in leave of marigold in each treatments.

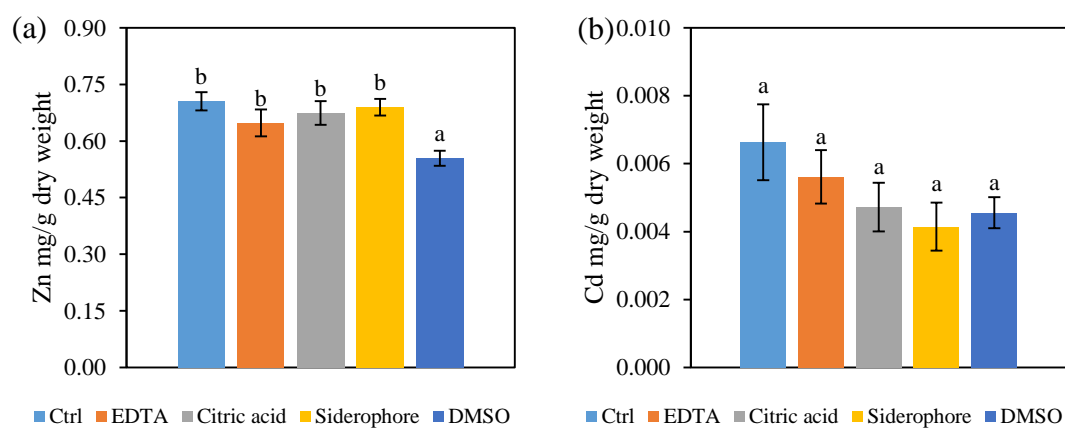


Figure 36 Total Zn (a) and Cd (b) concentrations (mg g^{-1} dry weight) in rhizosphere soil of marigold in each treatments.

The second experiment for the marigold pot experiment was carried out. Fertile soil and no planting soil were added in this second experiment to study the fertile and contaminated soil and metal mobility without the effect of plants, respectively. In addition, vegetative stage of one month-old marigolds were treated by crude siderophore extracts from ZnCd-E-2 and ZnCd-B-2, which were used as free-siderophore for enhancing metal chelated in soil. After 2 weeks of treating, marigold in vegetative stage were harvested. All shoots and soils were collected to examine wet and dry weight and Zn and Cd concentrations.

The fresh weight of the fertile soil was significantly highest than the contaminated soil (Figure 37(a)). It indicated that the heavy metals in the contaminated soil had effected the growth of marigold. In the treatments, the fresh weight of the control, EDTA and citric acid were significantly higher than the crude siderophores and DMSO (Figure 37(a)). The dry weight of the fertile soil was significantly not different from the EDTA, citric acid and crude siderophores. While the DMSO were significantly lower than the others (Figure 37(b)). The DMSO toxicity caused the siderophore and DMSO marigolds withered that caused the loss of fresh weight. However, the dry weights of plants obtained from the crude siderophore treatments were not significantly different from the plants growing in the fertile soil. Therefore, it indicated that the treatments of EDTA, citric acid and crude siderophores alleviated the marigolds from the adverse effects of contaminated soil when compared with the control.

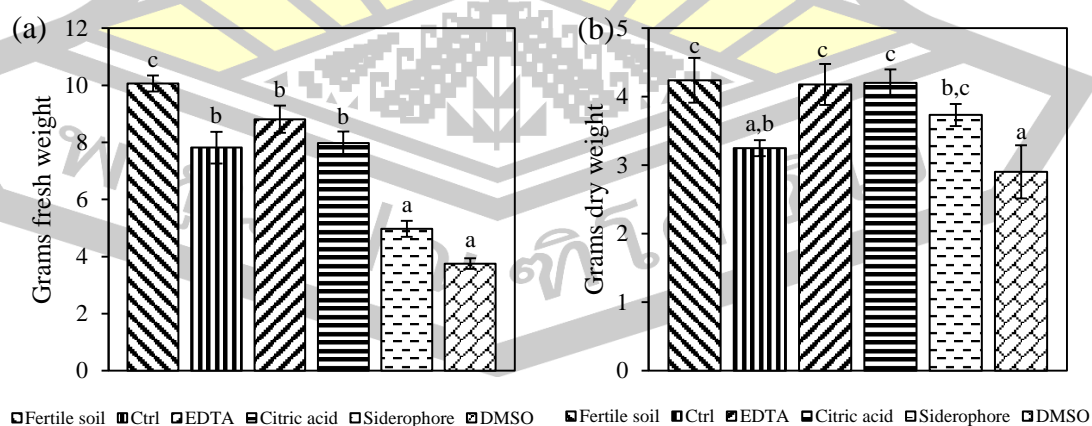


Figure 37 Shoot fresh weight (a) and dry weight (b) of marigold in each treatments.

The Zn concentrations in shoot of all treatments were not significantly different (Figure 38(a)). While the Cd concentration in shoot of the EDTA was significantly higher than the others (Figure 38(b)). Added citric acid and siderophore were not improved the Zn and Cd accumulated in shoot of marigold except the EDTA when compared to the control.

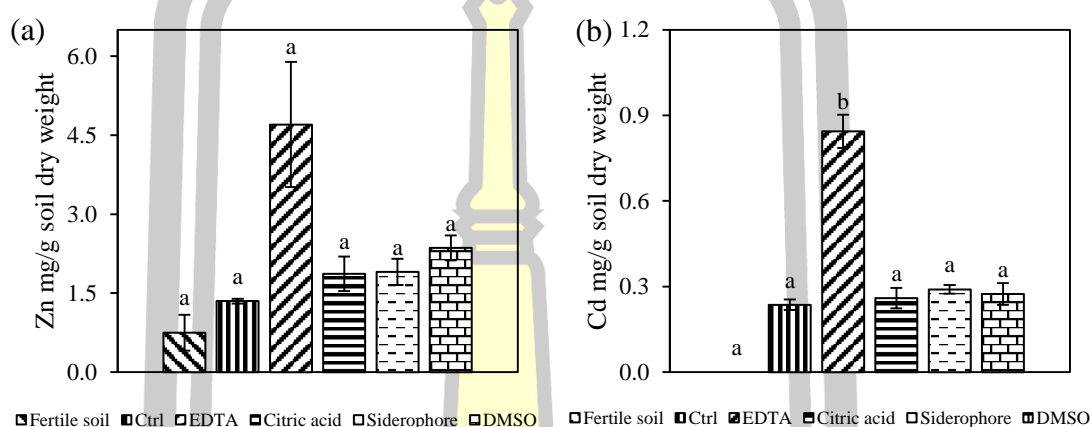


Figure 38 Total Zn (a) and Cd (b) concentrations (mg g^{-1} dry weight) in shoot of marigold in each treatments.

The rhizosphere soil of marigold were extracted the Zn and Cd by water extraction method to obtain the soluble Zn and Cd. The Zn and Cd concentrations of all experimental groups were under the LOD and LOQ except the EDTA (Table 13). The EDTA was significantly higher than the others when compared to the control.

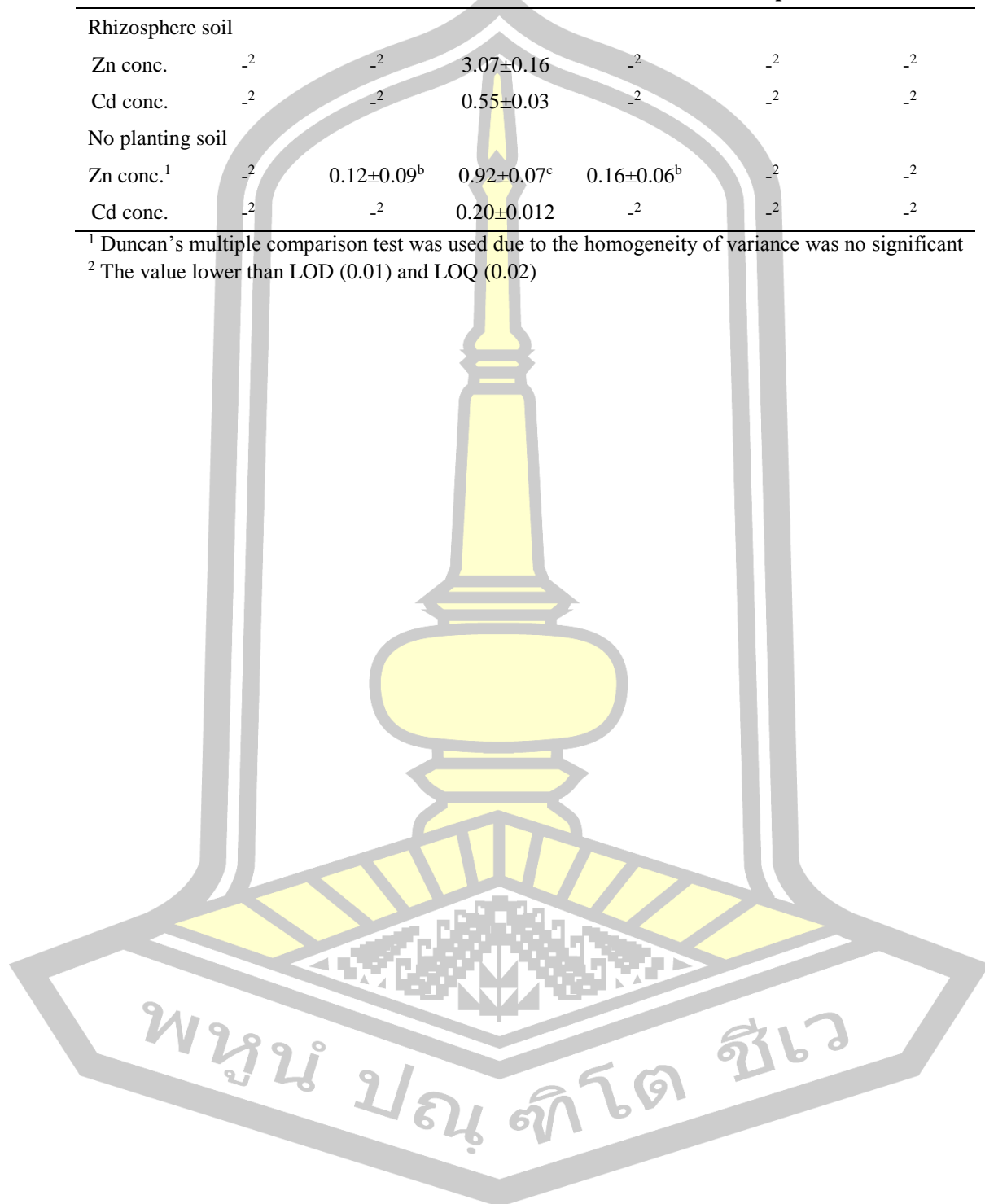
The no planting pots in each experiments was set to determine the effect of the treatments on Zn and Cd solubility in soil without the effects of plant in each experimental treatment set. The Zn concentrations in fertile soil, crude siderophores and DMSO (Table 13) were under the LOD and LOQ. While the EDTA was significantly higher than the control and citric acid. The Cd concentrations in the soil of control, citric acid, siderophore and DMSO were under the LOD and LOQ (Table 13). The EDTA affected the Zn and Cd solubility in soil. Whereas, the soil applied with citric acid, siderophore and DMSO were not affected the Zn and Cd solubility, when compared with the untreated Zn/Cd contaminated soil (control).

Table 13 Water extractable Zn and Cd concentrations (mg g^{-1} soil dry weight) of rhizosphere and no planting soils.

	Fertile soil	Control	EDTA	Citric acid	Siderophore	DMSO
Rhizosphere soil						
Zn conc.	-. ²	-. ²	3.07±0.16	-. ²	-. ²	-. ²
Cd conc.	-. ²	-. ²	0.55±0.03	-. ²	-. ²	-. ²
No planting soil						
Zn conc. ¹	-. ²	0.12±0.09 ^b	0.92±0.07 ^c	0.16±0.06 ^b	-. ²	-. ²
Cd conc.	-. ²	-. ²	0.20±0.012	-. ²	-. ²	-. ²

¹ Duncan's multiple comparison test was used due to the homogeneity of variance was no significant

² The value lower than LOD (0.01) and LOQ (0.02)



CHAPTER 5

DISCUSSION, CONCLUSION AND SUGGESTIONS

5.1 Discussion

Siderophores is accepted as one of key factors for improving heavy metal phytoremediation by enhancing metal mobilization (Karimzadeh et al. 2013), phytoextraction, and decrease oxidation stress in plants (Dimkpa et al. 2008; Rajkumar et al. 2010). Bacteria adapt to environmental changing such as the presence of heavy metals. The iron or metal ions concentrations induce the regulation or biosynthesis of siderophores (Raymond and Dertz 2004; Meyer 2007; Visca et al. 2007). Heavy metals are divided into biotic/essential and abiotic metals such as Zn and Cd, respectively. Gaonkar and Bhosle (2013) found that biotic metals increased siderophore concentration while abiotic metals decreased siderophore concentration.

The growth curves of *P. aeruginosa* PDMZnCd2003 were corresponded to Meesungnoen et al. (2012). The CAS assay indicated that the siderophores contained in all Zn and/or Cd treatments and control. The production of siderophores along the growth curve was similar to the siderophore production of *Bacillus* spp. (Patel et al. 2009). Dao et al. (1999) also indicated that Cd stimulated pyoverdine production. The stable of high siderophore concentration after 24 hours indicated that siderophores production was activated by the metal toxicity of Cd. The bacterium produced siderophores to reduce the available of metal ions in the culture media by chelating and accumulated the metals in the culture media (Schalk et al. 2011). Siderophore gene located in bacterial chromosome (Sasirekha and Srividya 2016). Ferric uptake regulator (Fur) associates in many metabolic pathways of iron homeostasis (Kaushik et al. 2016). In pyoverdine biosynthesis, Fe binds to Fur and forms Fe-Fur complex that results to repress *pvdS* promotor, which is a promotor of pyoverdine biosynthesis transcription genes (Nadal-Jimenez et al. 2014). Cd could interact with Fur instead of Fe, then Fur is released from the *pvdS* promotor (Dao et al. 1999; Izrael-Živković et al. 2018). However, Sasirekha and Srividya (2016) reported that siderophore

produced from *P. aeruginosa* FP6 decreased when the bacterium was cultured in a media contaminated with 10 μ M Cd. In case of Zn treatment, (Rossbach et al. 2000) found that Zn induced pyoverdine production.

The yellow-green color of supernatant indicates to be a pyoverdine (Elliott 1958; Carrillo-Castañeda et al. 2005). The parrot green color could be a *Pseudomonas* blue pigment pyocyanin (Hassan and Fridovich 1980). The UV spectra of *Pseudomonas* supernatants have been reported. Parker et al. (2007) measured pyoverdine of *P. putida* BG-1 and MnB1 by UV absorption spectra in the range 300-500 nm. Naik and Dubey (2011) reported the UV absorption spectra of *P. aeruginosa* 4EA. They found the peaks of pyochelin (247 nm and 310 nm) and pyoverdine (370 nm). Izrael-Živković et al. (2018) observed pyochelin at 310 nm and pyoverdine at 400 nm. Radzki et al. (2013) and Carrillo-Castañeda et al. (2005) also showed the UV absorption spectra at a dominant peak about 400 nm. The UV-Vis spectra in this study indicated that there are pyochelin (peaks at 250 and 310 nm) in all Zn and/or Cd treatments and control. Pyoverdine (peak at 420 nm) was in Cd and Zn+Cd treatments. The results indicated that Cd affected the pyoverdine synthesis. Złoch et al. (2016) also found that siderophores biosynthesis increased when increase the Cd concentration. In addition, pyoverdine and pyochelin siderophores could be synthesized in the same condition (Gasser et al. 2015).

The siderophores in the bacterial supernatants obtained from each treatments were extracted by the partition solvent extraction. Ethyl acetate and *n*-butanol were carried out to extract more siderophores form the supernatants. Ethyl acetate was applied to extract pyochelin from the acidified supernatant of *P. aeruginosa* PAO-1 and 10145 (Cox and Graham 1979). However, the obtained pyochelin in this study was the highest in the BuOH-pH-8 fraction. More than one siderophores were found in the crude siderophore extracts. The Zn and Cd concentrations in the crude siderophore extracts obtained from the pH-2 extracts and the pH-8 extracts were examined by FAAS. The Zn and Cd concentrations in the pH-2 extracts were lower than the pH-8 extracts, because the pH adjustment from pH 8 to pH 2 before the extraction could release both Zn and Cd from the metal-siderophore complexes (Payne 1994).

The TLC bands of the crude siderophore extracts demonstrated bands of pyochelin, pyoverdine and pseudomonine. Pyoverdine and pyochelin emit yellowish-green color (Cox and Graham 1979), and pseudomonine emits blue fluorescence under UV light (Cornelis and Matthijs 2007). The LC-MS confirmed that pyochelin and pyoverdine in the supernatants contained in the crude siderophore extracts. In addition to pyochelin and pyoverdine, the LC-MS spectra clearly indicate to pyoverdine, pyocyanin, PDTC and pseudomonine fragments. They are the *Pseudomonas* siderophores, which have been reported. Ruangviriyachai et al. (2004) elucidated the pyoverdine from *P. putida*, and the pyoverdine chromophore mass (m/z) was referred in this study. Yasmin et al. (2017) extracted the siderophores from acidified supernatants of *P. aeruginosa* BRp3 by ethyl acetate. They used LC-MS/MS to determine the crude extracts and found the siderophores 1-hydroxy-phenazine, pyocyanin and pyochelin.

The differences of metal binding ligands between the pH-2 extracts and the pH-8 extracts were determined by XAFS and FTIR. Siderophore ligands consist of carboxylic acid, hydroxamate, catecholate, hydroxy-carboxylic acid (Springer and Butler 2016) and also the thiol. The PDTC have thiol group in the structure. The S K-edge XANES spectra demonstrated the three peaks at 2472, 2475 and 2480 eV. These multi-oxidation in S K-edge XANES were reported (Morra et al. 1997; Schmalenberger et al. 2011; Shakeri Yekta et al. 2012; Zhu et al. 2016). Comparisons between the pH-2 extracts and the pH-8 extracts in each peak height showed some difference following the treatments. The Cd and Zn+Cd treatments had the similar pattern of the peaks whereas control and Zn treatment were not related to each other. This results suggested that Cd and Zn+Cd treatments had similar sulfur species in their crude siderophore extracts. The percentages of S K-edge XANES peak fitting area indicated that the most of sulfur species in the crude siderophore extracts were in the reduced form. It suggested that the siderophores could donate electron to metal ions. The present of thiol also supported that the PDTC was in the crude siderophore extracts.

The Zn and Cd binding ligands were determined by EXAFS. Crude siderophore extracts were liquid form. Therefore, the R-space shape of the EXAFS spectra were asymmetry and the bonding in first shell are varied. It indicated that the

Zn and Cd binding ligands in the EtOAc fractions were O and O/S (except Ctrl-E-8 was O), respectively while the BuOH fractions were mix ligands O/S. This results related to the O/S ligands in the *Pseudomonas* siderophores detected by LC-MS. More than four coordination number in the first shell indicated that Zn and Cd were chelated by the siderophore structure. The coordination number of the siderophores were more than 5 (Edwards and Myneni 2005; Duckworth et al. 2009; Harrington et al. 2012b, a). In addition, the bond lengths of Cd were longer than of Zn (Duckworth et al. 2009). The FTIR statistical analysed by PCA indicated that the O and S functional groups between the pH-2 extracts and the pH-8 extracts were different. The shift of C=O to higher wavenumber in the pH-8 extracts from Zn, Cd and Zn+Cd treatments showed the metals chelating with C=O of siderophores. Mizuguchi et al. (1997) showed the FTIR spectra of Ca^{2+} -EDTA complex shifted to higher wavenumber. The shift of wavenumber related to the geometry of metal bonding (Sutton et al. 2015). Conversely, showed the shift to lower wavenumber of FTIR peaks (hydroxyl, amino, carbonyl and phosphoryl) was caused by Cd ions bound to the peaks (D'Souza et al. 2008).

The *P. aeruginosa* PDMZnCd2003 siderophores obtained in this study was assessed the possibility for applying in phytoextraction. The bio-chelators could assist the metal bioavailable instead of synthetic chelators such as EDTA. It was overcome the adverse effects of synthetic chelators including degradable, green-compound and hardly leachate as the results of marigold pot experiment. In the first marigold pot experiment, there are no different between control and the treatments on growth and Zn and Cd accumulation. Siderophore enhanced the chlorophyll content. Treatment at vegetative stage by DMSO had more extreme adversity on marigold than the bud stage when compared with the results obtained from the second pot experiment. Siderophores had reports to improve chlorophyll concentration (Dimkpa et al. 2009a, b; Nagata et al. 2013; Radzki et al. 2013). Plant growth in heavy metal contaminating area was affected by oxidative stress and interfering Fe uptake, which adversely resulted from the heavy metals. Siderophores reduced the stress and increased the Fe uptake to plant even if in the presence of heavy metals (Dimkpa et al. 2009b).

Cd reduced biomass, chlorophyll content, cell viability and antioxidant enzymes in the marigold (Liu et al. 2011a). The crude siderophore and DMSO

treatments caused the plants to lowering fresh weight than the other treatments, because DMSO had affected on protein denature in cell membrane leading to loss control of osmosis or homeostasis (Singh et al. 1977). Nevertheless, EDTA, citric acid and crude siderophore significantly improved the growth of marigold in heavy metal contaminated soil when compared to the fertile soil. The citric acid and the siderophore were not enhanced the Zn and Cd accumulated in the plant shoots, except the EDTA, when compared to the control. The concentrations of water extractable Zn and Cd from the rhizospheric soils treated with the EDTA was the highest. It indicated that EDTA was better solubilizing Zn and Cd in the contaminated soil than the other chelates. Due to the highest water soluble Zn and Cd concentrations, the Zn and Cd concentrations in the plant shoots growing from the EDTA treatment were the highest. In comparison with the control soil, EDTA affected the Zn and Cd solubility from no-planting soil, while citric acid, siderophore and DMSO did not have any effects. The siderophore has advantages than the EDTA such as friendly to environments and not allowed soluble metals to leachate widespread. A limitation of crude siderophore extract dissolving in water was the serious factor affecting to the results of siderophore application. DMSO was applied to increase the solubility of the crude siderophore extract. However, a high amount of DMSO applied might cause the cell damage. In addition, DMSO has S=O group that can bind with metal ions. Therefore, the effect of crude siderophore extracts on Zn and Cd accumulated by marigold was still unclear.

Siderophore improved the plant growth by preventing heavy metal uptake to root leading to lower adverse effect from heavy metals toxicity (Dimkpa et al. 2009b). Siderophore containing culture filtrates (SCF) enhanced sunflower (*Helianthus annuus*) growth and Cd uptake in the sunflower shoot (Dimkpa et al. 2009a). Karimzadeh et al. (2012) found that DFOB enhanced Cd accumulation in shoot and root of *Thlaspi caerulescens* when presented with zeolite. Chelators such as EDTA was reported the potential of improving the Cd accumulation (at 200-2,000 mg kg⁻¹) in impatient and French marigold (Wei et al. 2012). Citric acid, a chelator, was also reported to the alleviation of Cd toxicity on *Brassica napus* L by increasing biomass and photosynthesis, reducing oxidative stresses and improving Cd accumulated in root, stem and leaves (Ehsan et al. 2014). Marigold is a suitable plant in sustainable

development in contaminated area. The economic part such as marigold cut-flower could accumulate a high Cd of 6.5 mg kg^{-1} (Lal et al. 2008). Marigold has advantages in income by selling flower, elemental recovery by phytomining and helping to clean up contaminated area (Nakbanpote et al. 2016).

5.2 Conclusion

P. aeuginosa PDMZnCd2003 produced siderophores under the Zn, Cd and Zn+Cd treatments as well as control. Each Zn and/or Cd treatment and control showed the different green color in the culture media. The UV-Vis spectra indicated that pyochelin was found in all treatments and control, while only Cd and Zn+Cd treatments contained pyoverdine. The siderophores from each supernatants were extracted by partition solvent extraction. Before the extraction, the supernatants were divided into no pH adjustment (pH 8) and pH adjustment to pH 2 for releasing the metals from the siderophores. Then the supernatants were extracted by the partition solvent extraction with ethyl acetate and *n*-butanol, respectively. Extraction with the two solvents could gain more siderophores and observe the characteristics of each siderophore obtained from each solvent fractions. The charge molecules or ions were extracted by *n*-butanol. The LC-MS confirmed that pyochelin and pyoverdine were in the crude siderophore extracts. The LC-MS spectra demonstrated the mass of pyochelin, chromophore of pyoverdine, PDTC, pyocyanin and pseudomonine.

The differences of metal binding ligands between the pH-2 and the pH-8 crude siderophore extracts were determined by XAFS and FTIR. The S K-edge XANES spectra demonstrated the multi-oxidation in the crude siderophore extracts by three peaks at 2472, 2475 and 2480 eV. The S K-edge XANES spectra were evaluated the relative sulfur species by peak fitting. The percentages of S K-edge XANES peak fitting area demonstrated that the reduced sulfur were the most sulfur species found in the crude siderophore extracts. Therefore, the siderophores could donate electron to metal ions. The containing of thiol also denoted the PDTC containing in the crude siderophore extracts. The Zn K-edge and Cd K-edge EXAFS spectra indicated that the binding ligands of Zn and Cd in the EtOAc-pH-8 were O and O/S (except Ctrl-E-8 was O), respectively. Whereas, the binding ligands of Zn and Cd in the BuOH

fractions were O/S and O/S, respectively. The coordination number of Zn and Cd indicated that the metals were chelated with the siderophores. The FTIR and PCA analysis showed that the O and S ligands between the pH-2 extracts and the pH-8 extracts were different. The shifting to higher wavenumber of C=O groups in the pH-8 extracts obtained from Zn, Cd and Zn+Cd treatments indicated that the C=O was involved with the metal chelation. This study suggested that more than one siderophores were induced by Zn and Cd. Pyoverdine could involve in metal detoxification, and it was induced by the Cd toxicity. The overall metal binding ligands of the siderophore consisted of O/S ligands.

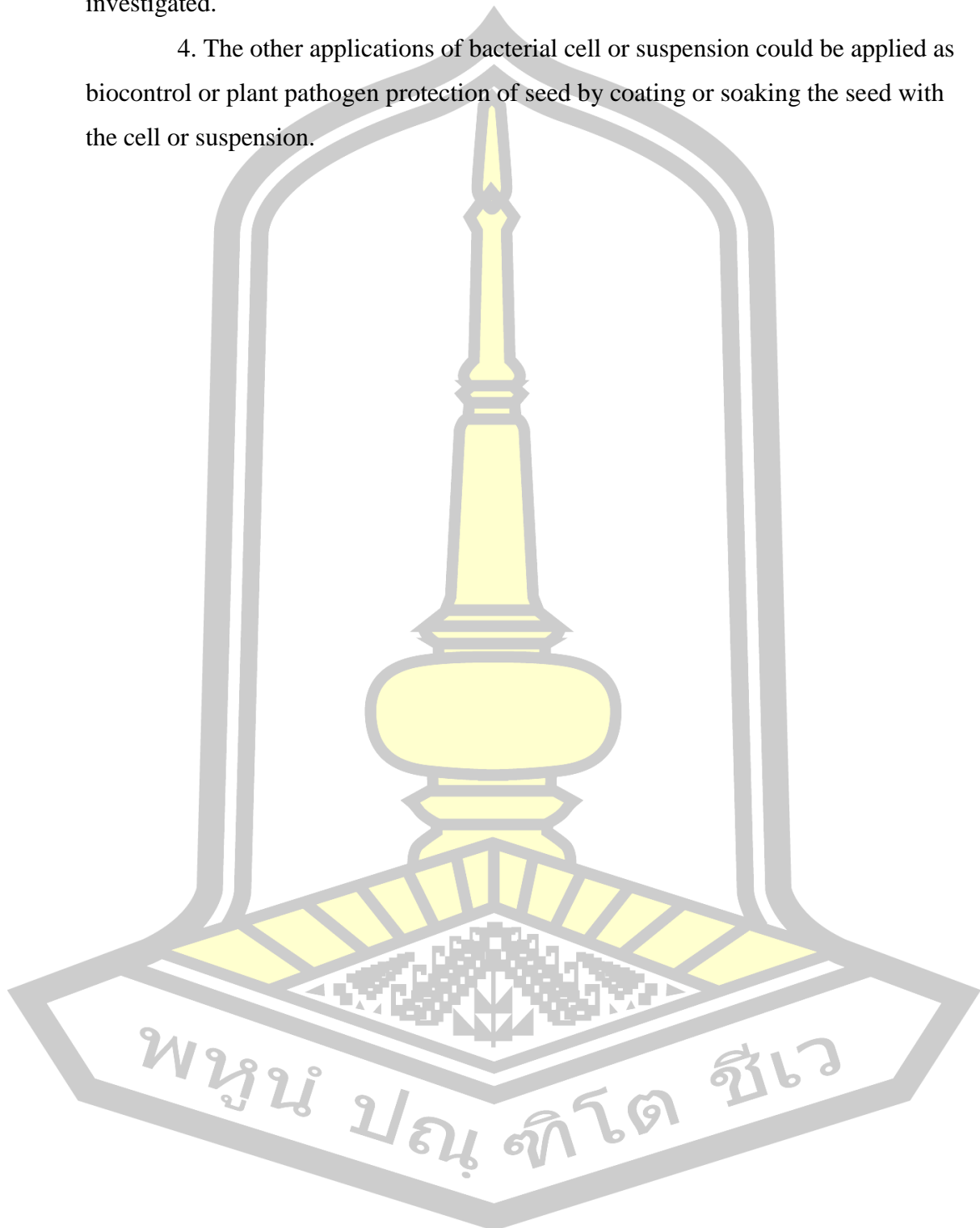
Application of EDTA, citric acid and siderophore improved the growth of marigold in the Zn/Cd contaminated soil. The crude siderophores enhanced the chlorophyll content in leaves. In comparison with the control soil, EDTA affected the Zn and Cd water solubility in the soil, whereas citric acid, siderophore and DMSO had no effect. Therefore, EDTA enhanced the Zn and Cd accumulated by marigold shoots, but citric acid and the crude siderophores did not increase the Zn and Cd accumulation. However, the problem of crude siderophore extract dissolving in water was the serious factor for this experiment. Therefore, the effect of crude siderophore extracts on Zn and Cd accumulated by marigold should be studied further.

5.3 Suggestions

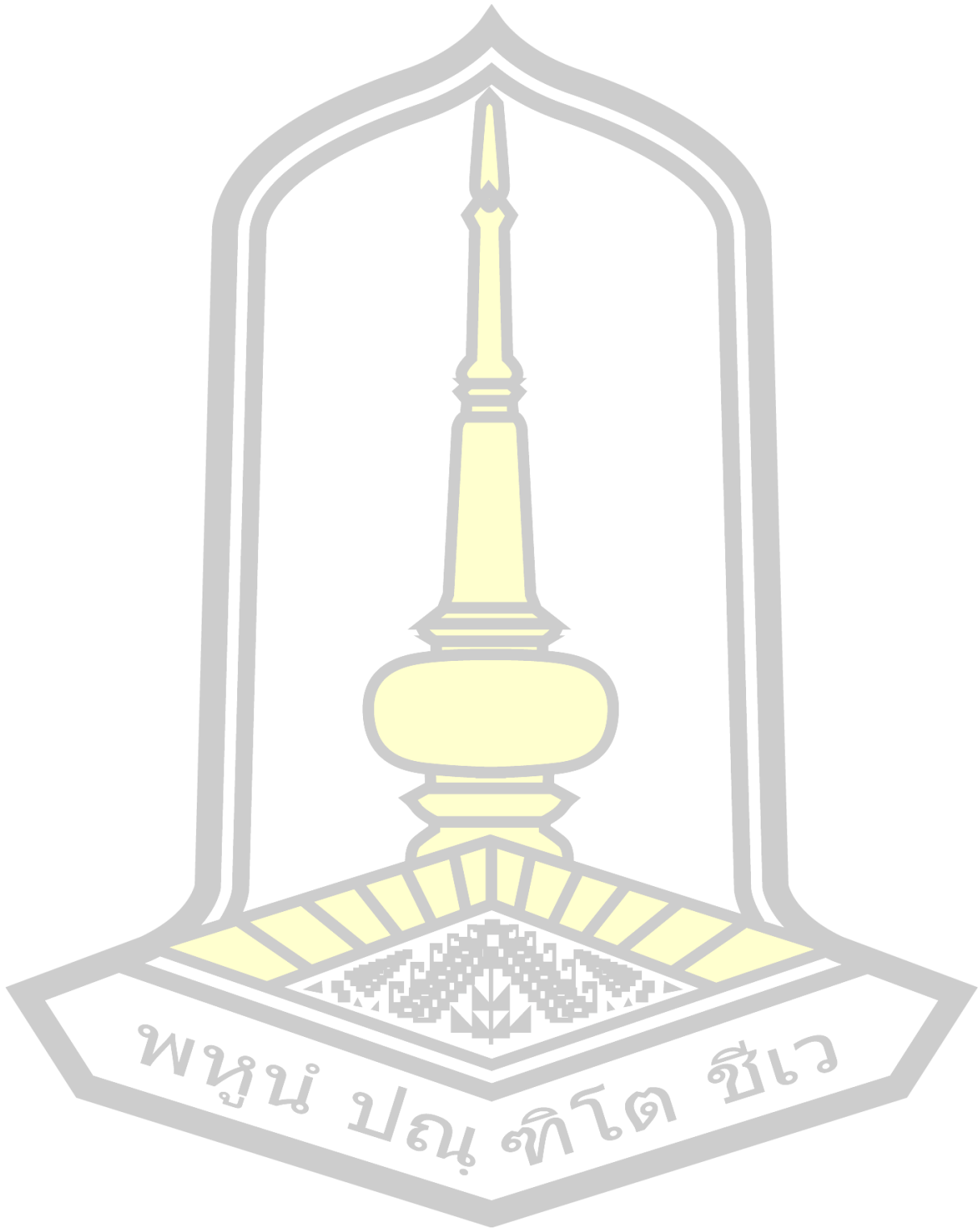
1. *Pseudomonas* siderophores should be applied as chemical standards for further study the conformation structure of siderophore during complexation with various concentration of Zn and/or Cd.
2. This research focusing on the effect of Zn and Cd on inducible siderophore production by *P. aeruginosa*. We used partition solvent extraction to separate the siderophores. However, the crude siderophore should be purified further with solid phase extraction to obtain purified compounds for study further in the unknown peaks of the LC-MS.
3. Application of siderophores in phytoextraction should be studied further by focusing on solubilizing the siderophores and how to apply it in the soil. In

addition, some effects of siderophores in phytostabilisation the Zn and Cd should be investigated.

4. The other applications of bacterial cell or suspension could be applied as biocontrol or plant pathogen protection of seed by coating or soaking the seed with the cell or suspension.



REFERENCES



REFERENCES

- Ahire JJ, Patil KP, Chaudhari BL, Chincholkar SB (2011) A potential probiotic culture ST2 produces siderophore 2,3- dihydroxybenzoylserine under intestinal conditions. *Food Chem* 127:387–393.
- Aizawa S-I, Aizawa S-I (2014) *Pseudomonas aeruginosa* — Opportunistic Pathogen in the Hospital. In: *The Flagellar World*. Elsevier, pp 60–62
- Andrews SC, Robinson AK, Rodríguez-Quñones F (2003) Bacterial iron homeostasis. *FEMS Microbiol Rev* 27:215–237.
- Anthoni U, Christophersen C, Nielsen PH, Gram L, Petersen BO (1995) Pseudomonine, an Isoxazolidone with Siderophoric Activity from *Pseudomonas fluorescens* AH2 Isolated from Lake Victorian Nile Perch. *J Nat Prod* 58:1786–1789.
- Appenroth K (2010) Definition of “Heavy Metals” and Their Role in Biological Systems. In: Sherameti I, Varma A (eds) *Soil Heavy Metals*. Springer Berlin Heidelberg, pp 19–30
- Arkhipova TN, Prinsen E, Veselov SU, Martinenko EV, Melentiev AI, Kudoyarova GR (2007) Cytokinin producing bacteria enhance plant growth in drying soil. *Plant Soil* 292:305–315.
- Atlas RM, Philp J (2005) *Bioremediation: Applied Microbial Solutions for Real-world Environmental Cleanup*. American society for Microbiology (ASM) Press, Washington DC
- Bau M, Tepe N, Mohwinkel D (2013) Siderophore-promoted transfer of rare earth elements and iron from volcanic ash into glacial meltwater, river and ocean water. *Earth Planet Sci Lett* 364:30–36.
- Beasley FC, Heinrichs DE (2010) Siderophore-mediated iron acquisition in the staphylococci. *J Inorg Biochem* 104:282–288.
- Bellenger JP, Arnaud-Neu F, Asfari Z, Myneni SCB, Stiefel EI, Kraepiel AML (2007) Complexation of oxoanions and cationic metals by the biscatecholate siderophore azotochelin. *J Biol Inorg Chem* 12:367–376.
- Bertin G, Averbeck D (2006) Cadmium: cellular effects, modifications of biomolecules, modulation of DNA repair and genotoxic consequences (a review). *Biochimie* 88:1549–1559.

- Bhargava A, Carmona FF, Bhargava M, Srivastava S (2012) Approaches for enhanced phytoextraction of heavy metals. *J Environ Manage* 105:103–120.
- Blakney AJC, Patten CL (2011) A plant growth-promoting pseudomonad is closely related to the *Pseudomonas syringae* complex of plant pathogens. *FEMS Microbiol Ecol* 77:546–557.
- Bolan N, Kunhikrishnan A, Thangarajan R, Kumpiene J, Park J, Makino T, Kirkham MB, Scheckel K (2014) Remediation of heavy metal(loid)s contaminated soils - To mobilize or to immobilize? *J Hazard Mater* 266:141–166.
- Boopathi E, Rao KS (1999) A siderophore from *Pseudomonas putida* type A1: Structural and biological characterization. *Biochim Biophys Acta - Protein Struct Mol Enzymol* 1435:30–40.
- Braud A, Jézéquel K, Lebeau T (2007) Impact of substrates and cell immobilization on siderophore activity by Pseudomonads in a Fe and/or Cr, Hg, Pb containing-medium. *J Hazard Mater* 144:229–239.
- Buckling A, Harrison F, Vos M, Brockhurst MA, Gardner A, West SA, Griffin A (2007) Siderophore-mediated cooperation and virulence in *Pseudomonas aeruginosa*. *FEMS Microbiol Ecol* 62:135–141.
- Bultreys A (2007) Siderotyping, a Tool to Characterize, Classify and Identify Fluorescent Pseudomonads. In: Varma A, Chincholkar SB (eds) *Microbial Siderophores*. Springer Berlin Heidelberg, Berlin, Heidelberg, pp 67–89
- Bultreys A, Gheysen I, De Hoffmann E (2006) Yersiniabactin production by *Pseudomonas syringae* and *Escherichia coli*, and description of a second yersiniabactin locus evolutionary group. *Appl Environ Microbiol* 72:3814–3825.
- Cajuste LJ, Cruz-Díaz J, García-Osorio C (2000) Extraction of heavy metals from contaminated soils: I. Sequential extraction in surface soils and their relationships to DTPA extractable metals and metal plant uptake. *J Environ Sci Heal - Part A Toxic/Hazardous Subst Environ Eng* 35:1141–1152.
- Carrillo-Castañeda G, Muñoz JJ, Peralta-Videa JR (2005) A spectrophotometric method to determine the siderophore production by strains of fluorescent *Pseudomonas* in the presence of copper and iron. *Microchem J* 81:35–40.
- Carson KC, Meyer JM, Dilworth MJ (2000) Hydroxamate siderophores of root nodule bacteria. *Soil Biol Biochem* 32:11–21.

- Castillo OS, Dasgupta-Schubert N, Alvarado CJ, Zaragoza EM, Villegas HJ (2011) The effect of the symbiosis between *Tagetes erecta* L. (marigold) and *Glomus intraradices* in the uptake of Copper(II) and its implications for phytoremediation. *N Biotechnol* 29:156–164.
- Chintakovid W, Visoottiviseth P, Khokiattiwong S, Lauengsuchonkul S (2008) Potential of the hybrid marigolds for arsenic phytoremediation and income generation of remediators in Ron Phibun District, Thailand. *Chemosphere* 70:1532–1537.
- Colombo C, Palumbo G, He JZ, Pinton R, Cesco S (2014) Review on iron availability in soil: Interaction of Fe minerals, plants, and microbes. *J Soils Sediments* 14:538–548.
- Cornelis P, Matthijs S (2007) *Pseudomonas* Siderophores and their Biological Significance. In: Varma A, Chincholkar SB (eds) *Microbial Siderophores*. Springer Berlin Heidelberg, Berlin, Heidelberg, pp 193–203
- Cornelis P, Matthijs S (2002) Diversity of siderophore-mediated iron uptake systems in fluorescent pseudomonads: Not only pyoverdines. *Environ Microbiol* 4:787–798.
- Cornu JY, Elhabiri M, Ferret C, Geoffroy VA, Jezequel K, Leva Y, Lollier M, Schalk II, Lebeau T (2014) Contrasting effects of pyoverdine on the phytoextraction of Cu and Cd in a calcareous soil. *Chemosphere* 103:212–219.
- Cox CD, Graham R (1979) Isolation of an iron-binding compound from *Pseudomonas aeruginosa*. *J Bacteriol* 137:357–364
- D'Souza L, Prabha D, Divya SMP, Naik CG (2008) Use of Fourier Transform Infrared (FTIR) Spectroscopy to Study Cadmium-Induced Changes in *Padina Tetrastromatica* (Hauck). *Anal Chem Insights* 91:135–143
- Dao KT, Hamer KE, Clark CL, Harshman LG (1999) Pyoverdine Production By *Pseudomonas aeruginosa*. *Ecol Appl* 9:441–448
- de-Bashan LE, Hernandez JP, Bashan Y (2012) The potential contribution of plant growth-promoting bacteria to reduce environmental degradation - A comprehensive evaluation. *Appl Soil Ecol* 61:171–189.
- Dimkpa CO, McLean JE, Britt DW, Johnson WP, Arey B, Lea AC, Anderson AJ (2012) Nanospecific inhibition of pyoverdine siderophore production in *Pseudomonas chlororaphis* O6 by CuO nanoparticles. *Chem Res Toxicol* 25:1066–1074.

- Dimkpa CO, Merten D, Svatoš A, Büchel G, Kothe E (2009a) Siderophores mediate reduced and increased uptake of cadmium by *Streptomyces tendae* F4 and sunflower (*Helianthus annuus*), respectively. *J Appl Microbiol* 107:1687–1696.
- Dimkpa CO, Merten D, Svatoš A, Büchel G, Kothe E (2009b) Metal-induced oxidative stress impacting plant growth in contaminated soil is alleviated by microbial siderophores. *Soil Biol Biochem* 41:154–162.
- Dimkpa CO, Svatoš A, Dabrowska P, Schmidt A, Boland W, Kothe E (2008) Involvement of siderophores in the reduction of metal-induced inhibition of auxin synthesis in *Streptomyces* spp. *Chemosphere* 74:19–25.
- Duckworth OW, Bargar JR, Sposito G (2009) Quantitative Structure–Activity Relationships for Aqueous Metal–Siderophore Complexes. *Environ Sci Technol* 43:343–349.
- Duffus JH (2002) “Heavy metals” a meaningless term? (IUPAC Technical Report). *Pure Appl Chem* 74:793–807.
- Edwards DC, Myneni SCB (2005) Hard and Soft X-ray Absorption Spectroscopic Investigation of Aqueous Fe(III)–Hydroxamate Siderophore Complexes. *J Phys Chem A* 109:10249–10256.
- Eghbali H, Matthijs S, Verdoold V, Gardeniers H, Cornelis P, Desmet G (2009) Use of non-porous pillar array columns for the separation of *Pseudomonas* pyoverdine siderophores as an example of a real-world biological sample. *J Chromatogr A* 1216:8603–8611.
- Ehsan S, Ali S, Noureen S, Mahmood K, Farid M, Ishaque W, Shakoob MB, Rizwan M (2014) Citric acid assisted phytoremediation of cadmium by *Brassica napus* L. *Ecotoxicol Environ Saf* 106:164–172.
- El-Fouly MZ, Sharaf AM, Shahin AAM, El-Bialy HA, Omara AMA (2015) Biosynthesis of pyocyanin pigment by *Pseudomonas aeruginosa*. *J Radiat Res Appl Sci* 8:36–48.
- Elliott RP (1958) Some Properties of Pyoverdine, the Water-soluble Fluorescent Pigment of the Pseudomonads. *Appl Microbiol* 6:241–246
- Emmanuel ESC, Ananthi T, Anandkumar B, Maruthamuthu S (2012) Accumulation of rare earth elements by siderophore-forming *Arthrobacter luteolus* isolated from rare earth environment of Chavara, India. *J Biosci* 37:25–31.

- Enyedy ÉA, Pócsi I, Farkas E (2004) Complexation of desferricoprogen with trivalent Fe, Al, Ga, In and divalent Fe, Ni, Cu, Zn metal ions: Effects of the linking chain structure on the metal binding ability of hydroxamate based siderophores. *J Inorg Biochem* 98:1957–1966.
- Gaonkar T, Bhosle S (2013) Effect of metals on a siderophore producing bacterial isolate and its implications on microbial assisted bioremediation of metal contaminated soils. *Chemosphere* 93:1835–1843.
- Gasser V, Guillon L, Cunrath O, Schalk IJ (2015) Cellular organization of siderophore biosynthesis in *Pseudomonas aeruginosa*: Evidence for siderosomes. *J Inorg Biochem* 148:27–34.
- Ghosh M, Singh SP (2005) A review on phytoremediation of heavy metals and utilization of its byproducts. *Appl Ecol Environ Res* 3:1–18.
- Glick BR (2014) Bacteria with ACC deaminase can promote plant growth and help to feed the world. *Microbiol Res* 169:30–39.
- Gutierrez-Manero FJ, Ramos-Solano B, Probanza A, Mehouchi J, Tadeo F, Talon M (2001) The plant-growth-promoting rhizobacteria *Bacillus pumilus* and *Bacillus licheniformis* produce high amounts of physiologically active gibberellins. *Physiol Plant* 111:206–211.
- Harrington JM, Bargar JR, Jarzecki AA, Roberts JG, Sombers LA, Duckworth OW (2012a) Trace metal complexation by the triscatecholate siderophore protochelin: Structure and stability. *BioMetals* 25:393–412.
- Harrington JM, Parker DL, Bargar JR, Jarzecki AA, Tebo BM, Sposito G, Duckworth OW (2012b) Structural dependence of Mn complexation by siderophores: Donor group dependence on complex stability and reactivity. *Geochim Cosmochim Acta* 88:106–119.
- Harrington JM, Winkelmann G, Haselwandter K, Crumbliss AL (2011) Fe(III)-complexes of the tripodal trishydroxamate siderophore basidiochrome: Potential biological implications. *J Inorg Biochem* 105:1670–1674.
- Haselwandter K, Häninger G, Ganzera M, Haas H, Nicholson G, Winkelmann G (2013) Linear fusigen as the major hydroxamate siderophore of the ectomycorrhizal Basidiomycota *Laccaria laccata* and *Laccaria bicolor*. *BioMetals* 26:969–979.
- Hassan HM, Fridovich I (1980) Mechanism of the antibiotic action pyocyanine. *J Bacteriol* 141:156–163

- Hawkes C V., DeAngelis KM, Firestone MK (2007) Root Interactions with Soil Microbial Communities and Processes. In: The Rhizosphere. Elsevier, pp 1–29
- Hussein KA, Joo JH (2014) Potential of siderophore production by bacteria isolated from heavy metal: Polluted and rhizosphere soils. *Curr Microbiol* 68:717–723.
- Izrael-Živković L, Rikalović M, Gojgić-Cvijović G, Kazazić S, Vrvic M, Brčeski I, Beškoski V, Lončarević B, Gopčević K, Karadžić I (2018) Cadmium specific proteomic responses of a highly resistant *Pseudomonas aeruginosa* strain. *RSC Adv* 8:10549–10560.
- Jagetiya B, Sharma A (2013) Optimization of chelators to enhance uranium uptake from tailings for phytoremediation. *Chemosphere* 91:692–696
- Jiricny N, Diggie SP, West SA, Evans BA, Ballantyne G, Ross-Gillespie A, Griffin AS (2010) Fitness correlates with the extent of cheating in a bacterium. *J Evol Biol* 23:738–747.
- Kabata-Pendias A, Pendias H (2001) Trace Elements in Soils and Plants, 3rd edn. CRC Press, Boca Raton
- Karimzadeh L, Heilmeyer H, Merkel BJ (2012) Effect of microbial siderophore DFO-B on Cd accumulation by *Thlaspi caerulescens* hyperaccumulator in the presence of zeolite. *Chemosphere* 88:683–687.
- Karimzadeh L, Nair S, Merkel BJ (2013) Effect of Microbial Siderophore DFOB on Pb, Zn, and Cd Sorption Onto Zeolite. *Aquat Geochemistry* 19:25–37.
- Kaushik MS, Singh P, Tiwari B, Mishra AK (2016) Ferric Uptake Regulator (FUR) protein: properties and implications in cyanobacteria. *Ann Microbiol* 66:61–75.
- Krämer U (2005) Phytoremediation: novel approaches to cleaning up polluted soils. *Curr Opin Biotechnol* 16:133–141.
- Krewulak KD, Vogel HJ (2008) Structural biology of bacterial iron uptake. *Biochim Biophys Acta - Biomembr* 1778:1781–1804.
- Kruft BI, Harrington JM, Duckworth OW, Jarzęcki AA (2013) Quantum mechanical investigation of aqueous desferrioxamine B metal complexes: Trends in structure, binding, and infrared spectroscopy. *J Inorg Biochem* 129:150–161.
- Krujatz F, Haarstrick A, Nörtemann B, Greis T (2012) Assessing the toxic effects of nickel, cadmium and EDTA on growth of the plant growth-promoting rhizobacterium *Pseudomonas brassicacearum*. *Water Air Soil Pollut* 223:1281–1293.

- Lal K, Minhas PS, Shipra RK, Chaturvedi RK, Yadav RK (2008) Extraction of cadmium and tolerance of three annual cut flowers on Cd-contaminated soils. *Bioresour Technol* 99:1006–1011.
- Lamichhane JR, Varvaro L, Parisi L, Audergon J-M, Morris CE (2014) Disease and Frost Damage of Woody Plants Caused by *Pseudomonas syringae*: Seeing the Forest for the Trees. *Adv Agron* 126:235–295.
- Lane TW, Saito MA, George GN, Pickering IJ.; Prince RC, Morel FMM (2005) A cadmium enzyme from a marine diatom. *Nature* 435:42
- Lebeau T, Braud A, Jézéquel K (2008) Performance of bioaugmentation-assisted phytoextraction applied to metal contaminated soils: A review. *Environ Pollut* 153:497–522.
- Liermann LJ, Kalinowski BE, Brantley SL, Ferry JG (2000) Role of bacterial siderophores in dissolution of hornblende. *Geochim Cosmochim Acta* 64:587–602.
- Lin H, Ye C, Lv L, Zheng CR, Zhang S, Zheng L, Zhao Y, Yu X (2014) Characterization of extracellular polymeric substances in the biofilms of typical bacteria by the sulfur K-edge XANES spectroscopy. *J Environ Sci* 26:1763–1768.
- Liu LZ, Gong ZQ, Zhang YL, Li PJ (2011a) Growth, Cadmium Accumulation and Physiology of Marigold (*Tagetes erecta* L.) as Affected by Arbuscular Mycorrhizal Fungi. *Pedosphere* 21:319–327.
- Liu YT, Chen ZS, Hong CY (2011b) Cadmium-induced physiological response and antioxidant enzyme changes in the novel cadmium accumulator, *Tagetes patula*. *J Hazard Mater* 189:724–731.
- Ma Y, Prasad MNV, Rajkumar M, Freitas H (2011) Plant growth promoting rhizobacteria and endophytes accelerate phytoremediation of metalliferous soils. *Biotechnol Adv* 29:248–258.
- Marschner P, Crowley D, Rengel Z (2011) Rhizosphere interactions between microorganisms and plants govern iron and phosphorus acquisition along the root axis - model and research methods. *Soil Biol Biochem* 43:883–894.
- Meesungnoen O, Nakbanpote W, Thiwthong R, Thuamnu K (2009) Plant growth promoting properties of heavy metal tolerant bacteria isolated from *Gynura pseudochina* (L.) DC.'s rhizosphere

- Meesungnoen O, Nakbanpote W, Thiwthong R, Thumanu K (2012) Zinc and cadmium resistance mechanism of *Pseudomonas aeruginosa* PDMZnCd2003. Res J Biol Sci 7:4–13.
- Meyer JM (2007) Siderotyping and Bacterial Taxonomy: A Siderophore Bank for a Rapid Identification at the Species Level of Fluorescent and Non-Fluorescent *Pseudomonas*. In: Varma A, Chincholkar SB (eds) Microbial Siderophores. Springer Berlin Heidelberg, Berlin, Heidelberg, pp 43–65
- Meyer JM (2000) Proverdines: Pigments, siderophores and potential taxonomic markers of fluorescent pseudomonas species. Arch Microbiol 174:135–142.
- Meyer JM, Abdallah MA (1978) The fluorescent pigment of *Pseudomonas fluorescens*: Biosynthesis, purification, and physicochemical properties. J Gen Microbiol 107:319–328.
- Meyer JM, Hornsperger JM (1978) Role of pyoverdine pf, the iron binding fluorescent pigment of *Pseudomonas fluorescens* in iron transport. J Gen Microbiol 107:329–331
- Miethke M, Marahiel MA (2007) Siderophore-Based Iron Acquisition and Pathogen Control. Microbiol Mol Biol Rev 71:413–451.
- Mirleau P, Delorme S, Philippot L, Meyer JM, Mazurier S, Lemanceau P (2000) Fitness in soil and rhizosphere of *Pseudomonas fluorescens* C7R12 compared with a C7R12 mutant affected in pyoverdine synthesis and uptake. FEMS Microbiol Ecol 34:35–44.
- Mizuguchi M, Nara M, Kawano K, Nitta K (1997) FT-XR study of the Ca²⁺-binding to bovine α -lactalbumin. Relationships between the type of coordination and characteristics of the bands due to the Asp COO-groups in the Ca²⁺-binding site. FEBS Lett 417:153–156.
- Morra MJ, Fendorf SE, Brown PD (1997) Speciation of sulfur in humic and fulvic acids using X-ray absorption near-edge structure (XANES) spectroscopy. Geochim Cosmochim Acta 61:683–688
- Mossialos D, Amoutzias GD (2009) Role of siderophores in cystic fibrosis pathogenesis: Foes or friends? Int J Med Microbiol 299:87–98.
- Nadal-Jimenez P, Koch G, Reis CR, Muntendam R, Raj H, Jeronimus-Stratingh, CM, Cool RH, Quax WJ (2014) PvdP is a tyrosinase that drives maturation of the pyoverdine chromophore in *Pseudomonas aeruginosa*. J Bacteriol 196:2681–2690.

- Nagata T, Oobo T, Aozasa O (2013) Efficacy of a bacterial siderophore, pyoverdine, to supply iron to *Solanum lycopersicum* plants. *J Biosci Bioeng* 115:686–690.
- Naik MM, Dubey SK (2011) Lead-enhanced siderophore production and alteration in cell morphology in a Pb-resistant *Pseudomonas aeruginosa* strain 4EA. *Curr Microbiol* 62:409–414.
- Nakbanpote W, Meesungnoen O, Prasad MNV (2016) Potential of Ornamental Plants for Phytoremediation of Heavy Metals and Income Generation. In: *Bioremediation and Bioeconomy*. Elsevier, pp 179–217
- Nakbanpote W, Panitlertumpai N, Sukadeetad K, et al (2010) Advances in Phytoremediation Research: A Case Study of *Gynura pseudochina* (L.) DC. In: Fuerstner I (ed) *Advanced Knowledge Application in Practice*. InTech, Croatia, pp 353–378
- Nehl DB, Knox OGG (2006) Significance of Bacteria in the Rhizosphere. In: Mukerji KG, Manoharachary C, Singh J (eds) *Microbial Activity in the Rhizosphere*. Springer Berlin Heidelberg, Berlin, Heidelberg, pp 89–119
- Nies DH (1999) Microbial heavy-metal resistance. *Appl Microbiol Biotechnol* 51:730–750.
- Nordberg GF (2009) Historical perspectives on cadmium toxicology. *Toxicol Appl Pharmacol* 238:192–200.
- Pages D, Rose J, Conrod S, Cuine S, Carrier P, Heulin T, Achouak W (2008) Heavy metal tolerance in *Stenotrophomonas maltophilia*. *PLoS One* 3(2) e1539.
- Panitlertumpai N, Nakbanpote W, Sangdee A, Thumanu K, Nakai I, Hokura A (2013) Zinc and/or cadmium accumulation in *Gynura pseudochina* (L.) DC. studied in vitro and the effect on crude protein. *J Mol Struct* 1036:279–291
- Parker DL, Morita T, Mozafarzadeh ML, Verity R, McCarthy JK, Tebo BM (2007) Inter-relationships of MnO₂ precipitation, siderophore-Mn(III) complex formation, siderophore degradation, and iron limitation in Mn(II)-oxidizing bacterial cultures. *Geochim Cosmochim Acta* 71:5672–5683.
- Patel AK, Deshattiwar MK, Chaudhari BL, Chincholkar SB (2009) Production, purification and chemical characterization of the catecholate siderophore from potent probiotic strains of *Bacillus* spp. *Bioresour Technol* 100:368–373.
- Patil A V., Jadhav JP (2013) Evaluation of phytoremediation potential of *Tagetes patula* L. for the degradation of textile dye Reactive Blue 160 and assessment of the toxicity of degraded metabolites by cytogenotoxicity. *Chemosphere* 92:225–232.

- Payne S (1994) Detection, Isolation and Characterization of Siderophores. *Methods Enzymol* 235:329–344.
- Peix A, Ramírez-Bahena MH, Velázquez E (2009) Historical evolution and current status of the taxonomy of genus *Pseudomonas*. *Infect Genet Evol* 9:1132–1147.
- Phaenark C, Pokethitiyook P, Kruatrachue M, Ngernsarsaruay C (2009) Cd and Zn accumulation in plants from the Padaeng zinc mine area. *Int J Phytoremediation* 11:479–495.
- Pilon-Smits E (2005) PHYTOREMEDIATION. *Annu Rev Plant Biol* 56:15–39.
- Qin Q, Li X, Wu H, et al (2013) Characterization of cadmium (^{108}Cd) distribution and accumulation in *Tagetes erecta* L. seedlings: Effect of split-root and of remove-xylem/phloem. *Chemosphere* 93:2284–2288.
- Radzki W, Gutierrez Mañero FJ, Algar E, Lucas García JA, García-Villaraco A, Ramos Solano B (2013) Bacterial siderophores efficiently provide iron to iron-starved tomato plants in hydroponics culture. *Antonie van Leeuwenhoek, Int J Gen Mol Microbiol* 104:321–330.
- Rajkumar M, Ae N, Prasad MNV, Freitas H (2010) Potential of siderophore-producing bacteria for improving heavy metal phytoextraction. *Trends Biotechnol* 28:142–149.
- Rajkumar M, Sandhya S, Prasad MNV, Freitas H (2012) Perspectives of plant-associated microbes in heavy metal phytoremediation. *Biotechnol Adv* 30:1562–1574.
- Rashmi V, ShylajaNaciyar M, Rajalakshmi R, D'Souza SF, Prabakaran D, Uma L (2013) Siderophore mediated uranium sequestration by marine cyanobacterium *Synechococcus elongatus* BDU 130911. *Bioresour Technol* 130:204–210.
- Ravel B, Newville M (2005) ATHENA, ARTEMIS, HEPHAESTUS: data analysis for X-ray absorption spectroscopy using IFEFFIT. *J Synchrotron Radiat* 12:537–541.
- Raymond KN, Dertz EA (2004) Biochemical and Physical Properties of Siderophores. In: *Iron Transport in Bacteria*. American Society of Microbiology, pp 3–17
- Rompel A, Cinco RM, Latimer MJ, McDermott AE, Guiles RD, Quintanilha A, Krauss RM, Sauer K, Yachandra VK Klein MP (1998) Sulfur K-edge x-ray absorption spectroscopy: A spectroscopic tool to examine the redox state of S-containing metabolites in vivo. *Proc Natl Acad Sci U S A* 95:6122–6127

- Rosbach S, Wilson TL, Kukuk ML, Carty HA (2000) Elevated zinc induces siderophore biosynthesis genes and a zntA-like gene in *Pseudomonas fluorescens*. FEMS Microbiol Lett 191:61–70.
- Ruangviriyachai C, Uría D, Schäfer M (2004) Structure proposal for a new pyoverdine from a Thai *Pseudomonas putida* strain 1. 18:453–458
- Sasirekha B, Srividya S (2016) Siderophore production by *Pseudomonas aeruginosa* FP6, a biocontrol strain for *Rhizoctonia solani* and *Colletotrichum gloeosporioides* causing diseases in chilli. Agric Nat Resour 50:250–256.
- Sayed RZ, Chincholkar SB (2006) Purification of siderophores of *Alcaligenes faecalis* on Amberlite XAD. Bioresour Technol 97:1026–1029.
- Sayed RZ, Patil AS, Chincholkar SB (2008) Biotechnological potential of siderophore producing microbes for sustainable agriculture. J Biotechnol 136:S262.
- Schalk IJ, Guillon L (2013) Pyoverdine biosynthesis and secretion in *Pseudomonas aeruginosa*: Implications for metal homeostasis. Environ Microbiol 15:1661–1673.
- Schalk IJ, Hannauer M, Braud A (2011) New roles for bacterial siderophores in metal transport and tolerance. Environ Microbiol 13:2844–2854.
- Schalk IJ, Mislin GLA, Brillet K (2012) Structure, Function and Binding Selectivity and Stereoselectivity of Siderophore–Iron Outer Membrane Transporters. Curr Top Membr 69:37–66.
- Schmalenberger A, Pritzkow W, Ojeda JJ, Noll M (2011) Characterization of main sulfur source of wood-degrading basidiomycetes by S K-edge X-ray absorption near edge spectroscopy (XANES). Int Biodeterior Biodegrad 65:1215–1223.
- Schwyn B, Neilands JB (1987) Universal assay for the detection and determination of siderophores. Anal Biochem 160:47–56.
- Sebat JL, Paszczyński AJ, Cortese MS, Crawford RL (2001) Antimicrobial Properties of Pyridine-2,6-Dithiocarboxylic Acid, a Metal Chelator Produced by *Pseudomonas* spp. Appl Environ Microbiol 67:3934–3942.
- Shakeri Yekta S, Gustavsson J, Svensson BH, Skjellberg U (2012) Sulfur K-edge XANES and acid volatile sulfide analyses of changes in chemical speciation of S and Fe during sequential extraction of trace metals in anoxic sludge from biogas reactors. Talanta 89:470–477.

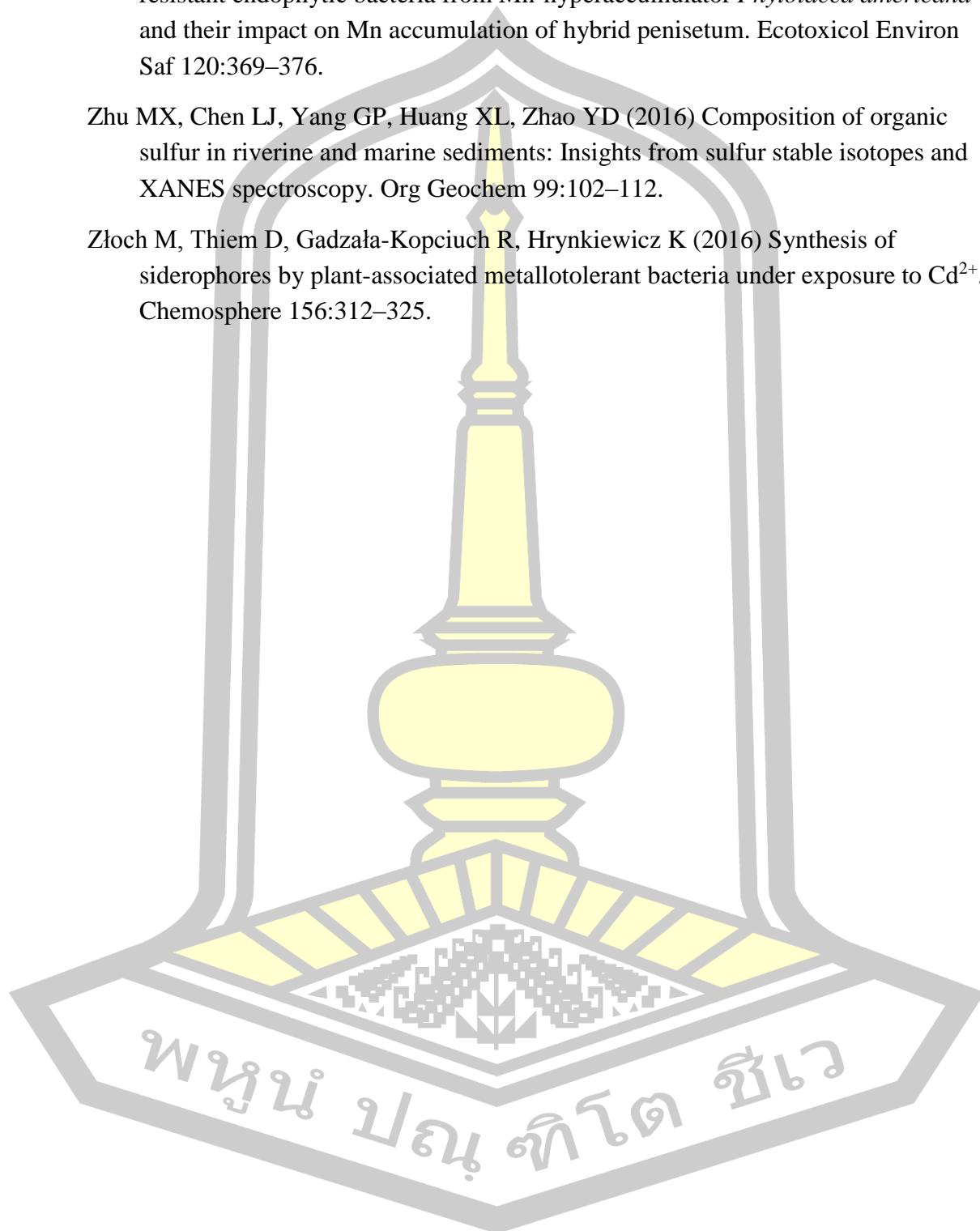
- Shrivastava A, Gupta V (2011) Methods for the determination of limit of detection and limit of quantitation of the analytical methods. *Chronicles Young Sci* 2:21.
- Singh M, Singh TA, Rathore VS (1977) Effect of dimethylsulfoxide (DMSO) in growth and zinc uptake by wheat. *J Nucl Agric Biol* 6:145–147
- Smith AW (1998) 6.13 Iron Starvation and Siderophore-Mediated iron Transport. *Methods Microbiol* 27:331–342.
- Springer SD, Butler A (2016) Microbial ligand coordination: Consideration of biological significance. *Coord Chem Rev* 306:628–635.
- Standing D, Killham K (2007) The soil environment. In: van Elsas JD, Jansson J, Trevors JT (eds) *Modern soil microbiology*. CRC Press, pp 1–22
- Stolworthy JC, Paszczyński A, Korus R, Crawford RL (2001) Metal binding by pyridine-2,6-bis(monothiocarboxylic acid), a biochelator produced by *Pseudomonas stutzeri* and *Pseudomonas putida*. *Biodegradation* 12:411–418.
- Sun B, Zhao F., Lombi E, McGrath S. (2001) Leaching of heavy metals from contaminated soils using EDTA. *Environ Pollut* 113:111–120.
- Sutton CC, da Silva G, Franks G V (2015) Modeling the IR Spectra of Aqueous Metal Carboxylate Complexes: Correlation between Bonding Geometry and Stretching Mode Wavenumber Shifts. *Chem – A Eur J* 21:6801–6805.
- Tapiero H, Tew KD (2003) Trace elements in human physiology and pathology: Zinc and metallothioneins. *Biomed Pharmacother* 57:399–411.
- Thompson SW, Molz FJ, Fjeld RA, Kaplan DI (2012) Uptake, distribution, and velocity of organically complexed plutonium in corn (*Zea mays*). *J Environ Radioact* 112:133–140.
- Tilston EL, Sizmur T, Dixon GR, Otten W, Harris JA (2010) The Impact of Land-Use Practices on Soil Microbes. In: Dixon GR, Tilston EL (eds) *Soil Microbiology and Sustainable Crop Production*. Springer Netherlands, Dordrecht, pp 273–295
- Tseng CF, Burger A, Mislin GLA, Schalk IJ, Yu SSF, Chan SI, Abdallah MA (2006) Bacterial siderophores: The solution stoichiometry and coordination of the Fe(III) complexes of pyochelin and related compounds. *J Biol Inorg Chem* 11:419–432.
- Upritchard HG, Yang J, Bremer PJ, Lamont IL, McQuillan AJ (2011) Adsorption of enterobactin to metal oxides and the role of siderophores in bacterial adhesion to metals. *Langmuir* 27:10587–10596.

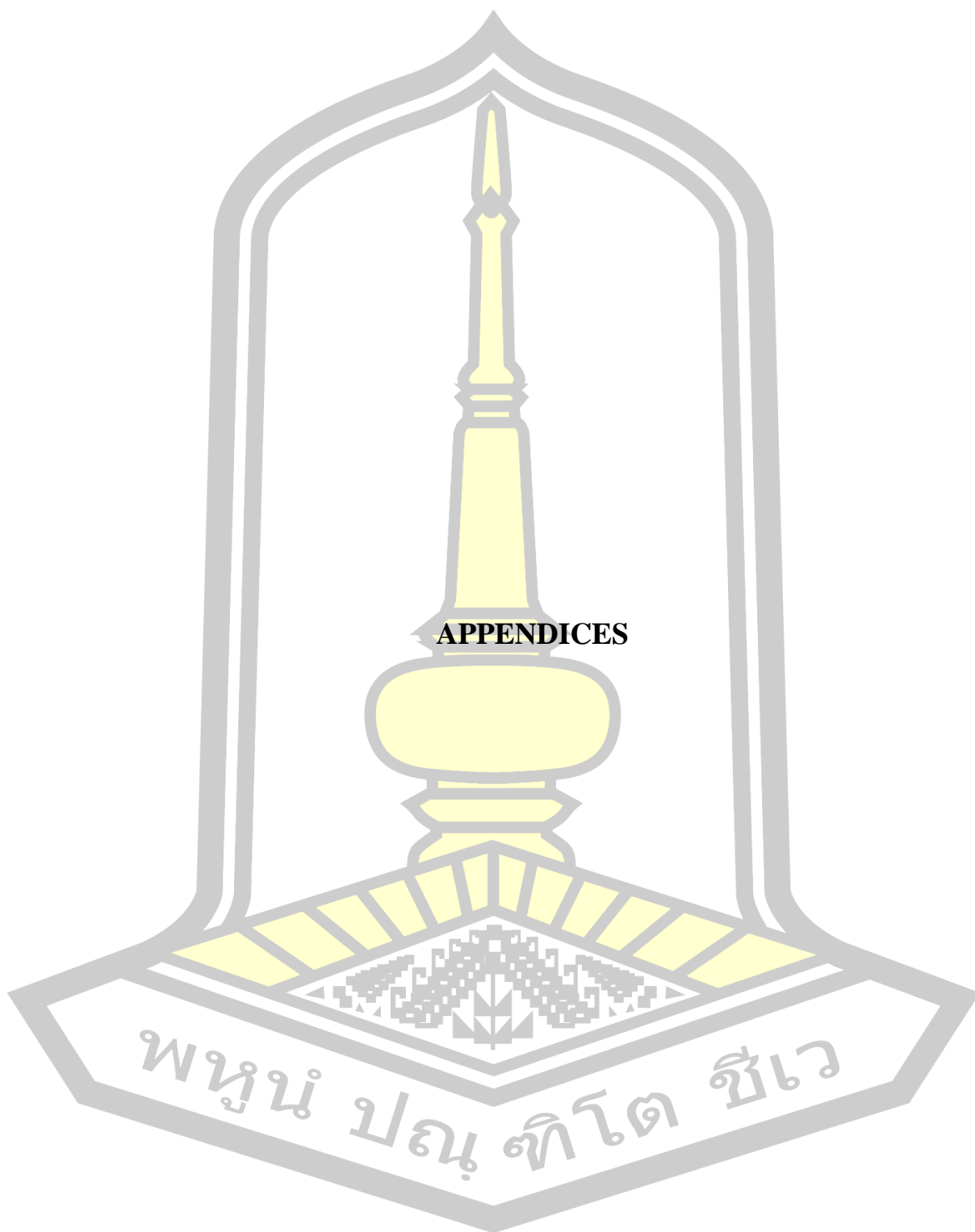
- Van Loon LC, Bakker PAHM (2006) Induced Systemic Resistance as a Mechanism of Disease Suppression by *Rhizobacteria*. In: Siddiqui ZA (ed) PGPR: Biocontrol and Biofertilization. Springer Netherlands, Dordrecht, pp 39–66
- Visca P, Colotti G, Serino L, Verzili D, Orsi N, Chiancone E (1992) Metal regulation of siderophore synthesis in *Pseudomonas aeruginosa* and functional effects of siderophore-metal complexes. Appl Environ Microbiol 58:2886–2893
- Visca P, Imperi F, Lamont IL (2007) Pyoverdine siderophores: from biogenesis to biosignificance. Trends Microbiol 15:22–30.
- Voinot A, Lemarchand D, Collignon C, Granet M, Chabaux F, Turpault MP (2013) Experimental dissolution vs. transformation of micas under acidic soil conditions: Clues from boron isotopes. Geochim Cosmochim Acta 117:144–160.
- Wei JL, Lai HY, Chen ZS (2012) Chelator effects on bioconcentration and translocation of cadmium by hyperaccumulators, *Tagetes patula* and *Impatiens walleriana*. Ecotoxicol Environ Saf 84:173–178.
- Wright W, Little J, Liu F, Chakraborty R (2013) Isolation and structural identification of the trihydroxamate siderophore vicibactin and its degradative products from *Rhizobium leguminosarum* ATCC 14479 bv. trifolii. BioMetals 26:271–283.
- Wu L., Luo Y., Xing X., Christie P (2004) EDTA-enhanced phytoremediation of heavy metal contaminated soil with Indian mustard and associated potential leaching risk. Agric Ecosyst Environ 102:307–318.
- Xie X, Wang J, Yuan H (2006) High-resolution analysis of catechol-type siderophores using polyamide thin layer chromatography. J Microbiol Methods 67:390–393.
- Yasmin S, Hafeez FY, Mirza MS, Rasul M, Arshad HMI, Zubair M, Iqbal M (2017) Biocontrol of Bacterial Leaf Blight of Rice and Profiling of Secondary Metabolites Produced by Rhizospheric *Pseudomonas aeruginosa* BRp3. Front Microbiol 8:1895.
- Yehuda Z, Hadar Y, Chen Y (2012) FeDFOB and FeEDDHA immobilized on Sepharose gels as an Fe sources to plants. Plant Soil 350:379–391.
- Zane HK, Butler A (2013) Isolation, structure elucidation, and iron-binding properties of lystabactins, siderophores isolated from a marine *Pseudoalteromonas* sp. J Nat Prod 76:648–654.
- Zhang W, Huang H, Tan F, Wang H, Qiu R (2010) Influence of EDTA washing on the species and mobility of heavy metals residual in soils. J Hazard Mater 173:369–376.

Zhang WH, Chen W, He LY, Wang Q, Sheng XF (2015) Characterization of Mn-resistant endophytic bacteria from Mn-hyperaccumulator *Phytolacca americana* and their impact on Mn accumulation of hybrid penisetum. *Ecotoxicol Environ Saf* 120:369–376.

Zhu MX, Chen LJ, Yang GP, Huang XL, Zhao YD (2016) Composition of organic sulfur in riverine and marine sediments: Insights from sulfur stable isotopes and XANES spectroscopy. *Org Geochem* 99:102–112.

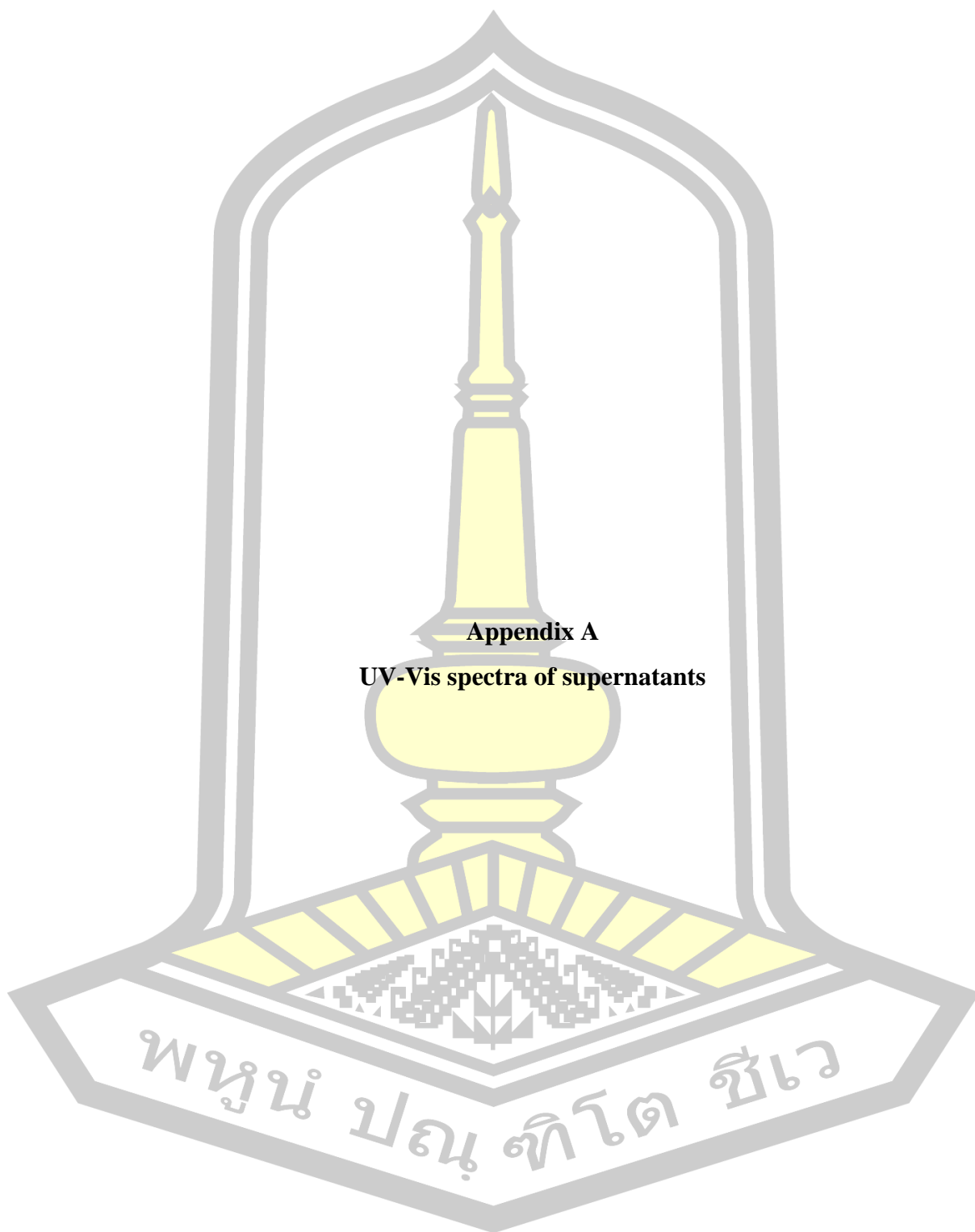
Złoch M, Thiem D, Gadzała-Kopciuch R, Hryniewicz K (2016) Synthesis of siderophores by plant-associated metallotolerant bacteria under exposure to Cd²⁺. *Chemosphere* 156:312–325.





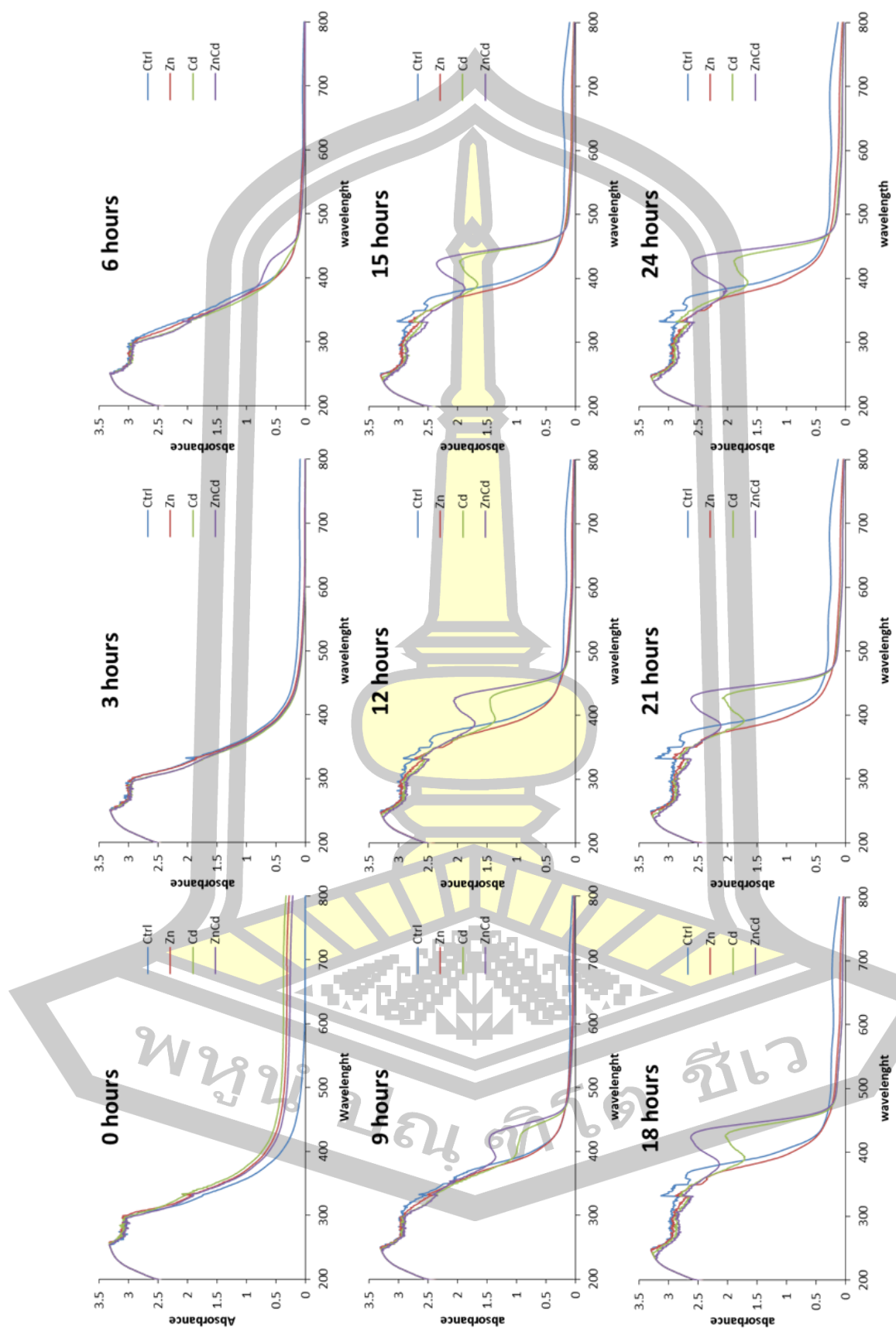
APPENDICES

พหุ ประจักษ์ วิทยา

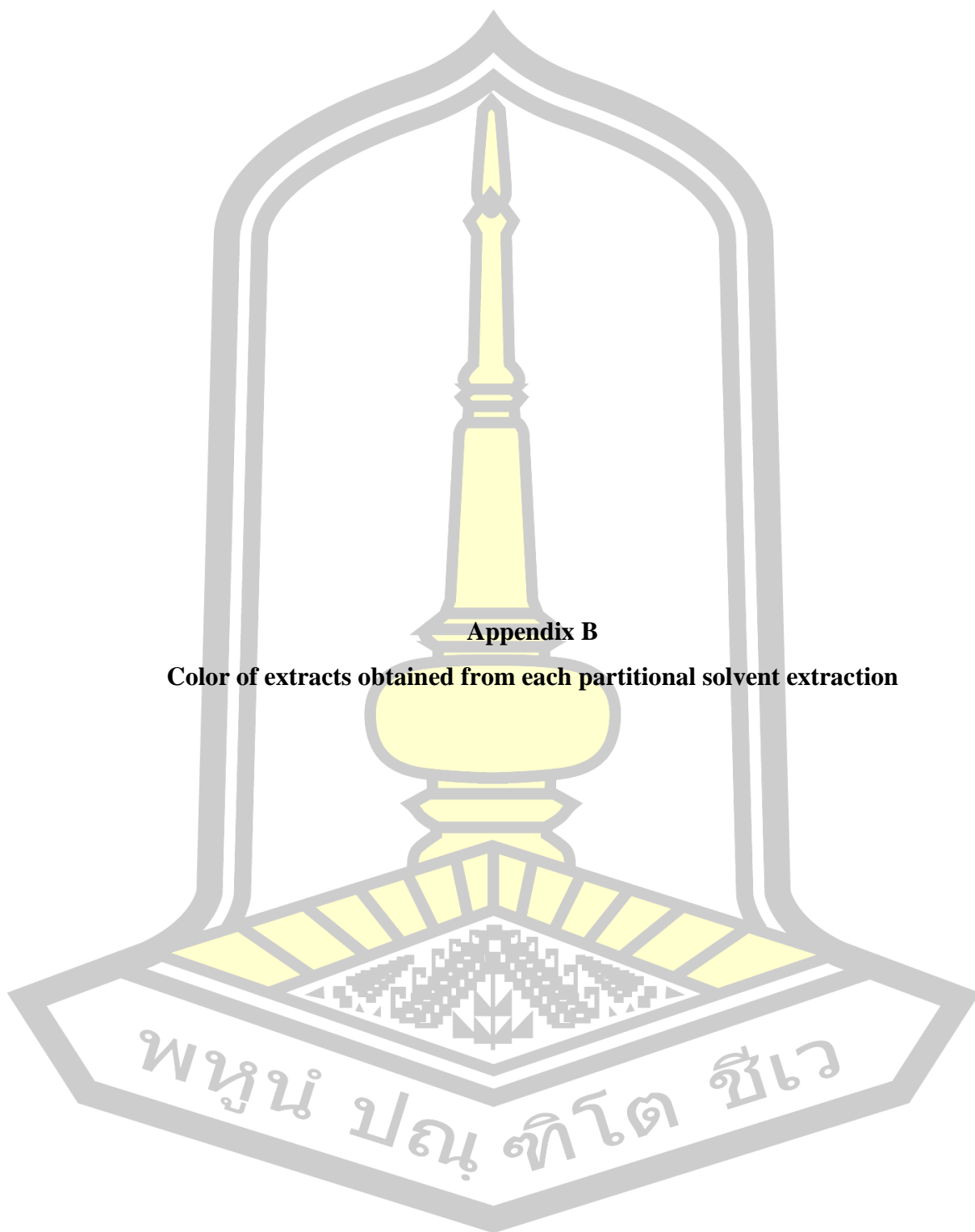


Appendix A

UV-Vis spectra of supernatants

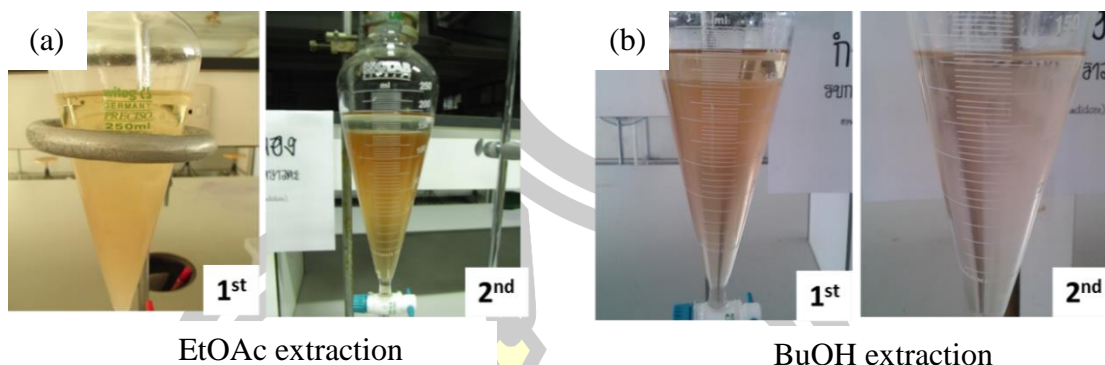


A-1 UV-Vis spectra between 200-800 nm of *P. aeruginosa* PDMZnCd2003 supernatants in each hours.

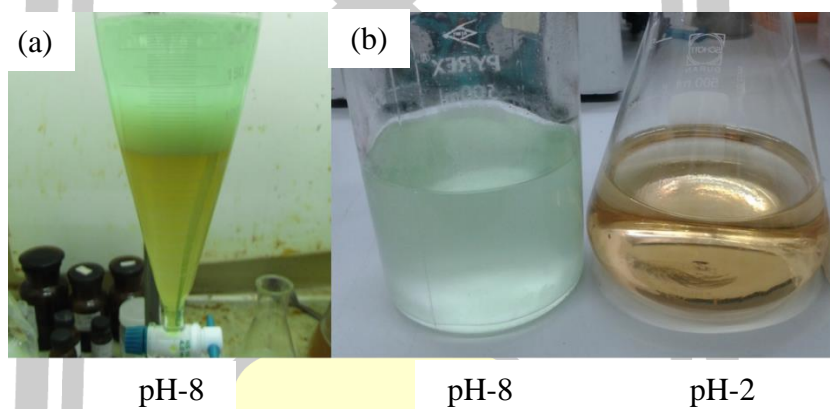


Appendix B

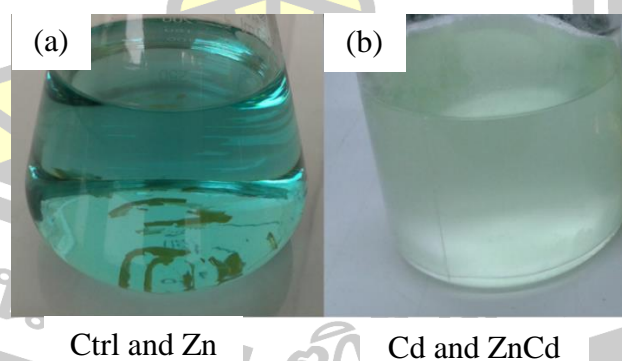
Color of extracts obtained from each partitional solvent extraction



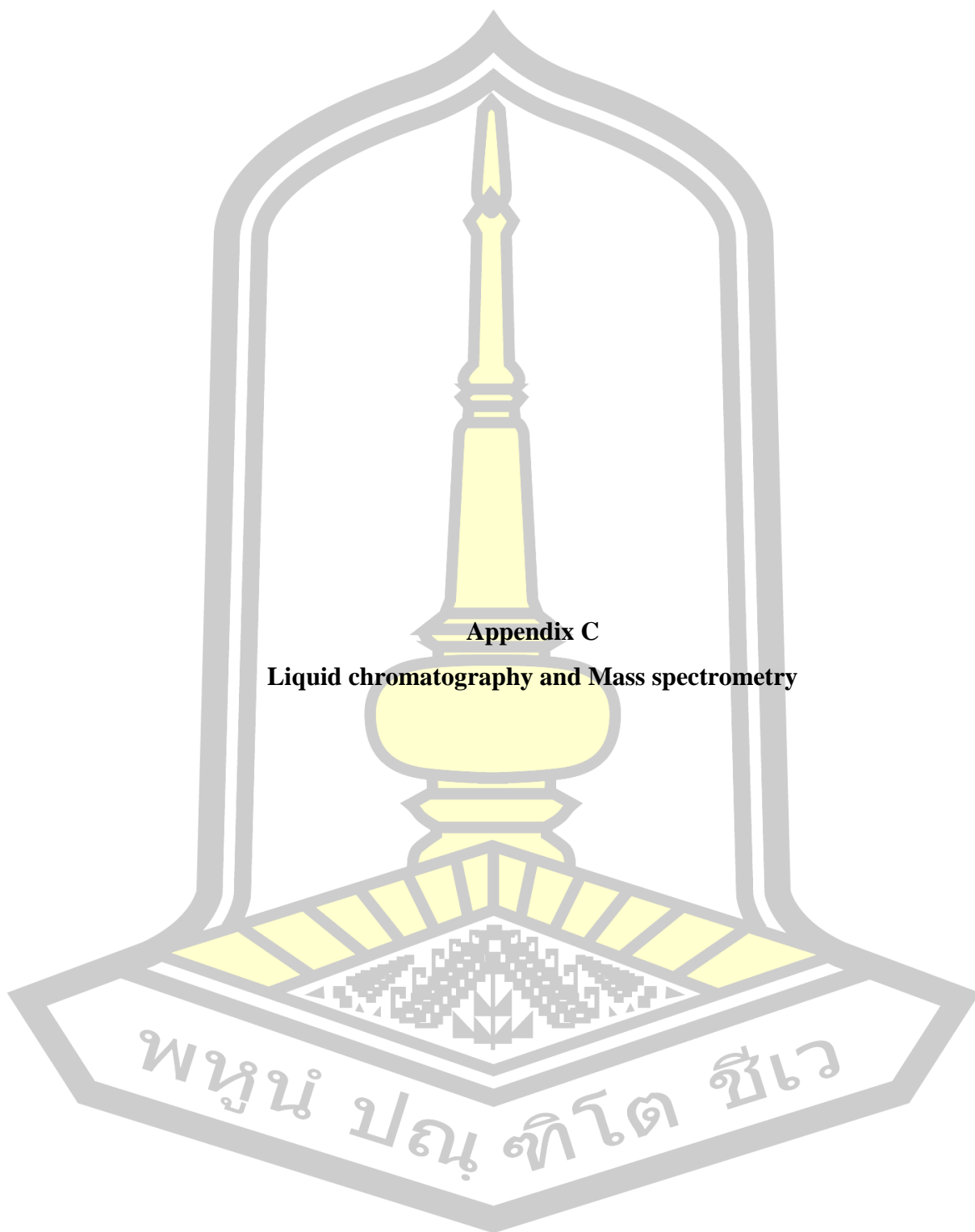
B-1 Color of pH-2 supernatants obtained from solvent extraction by (a) ethyl acetate (EtOAc) and (b) butanol (BuOH).



B-2 (b) Butanol fractions obtained from (a) the pH-8 supernatants of Zn plus Cd treatment.

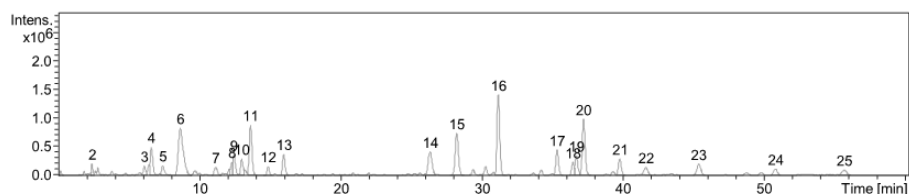


B-3 Color of butanol fractions of the pH-8 supernatants; (a) blue white fraction from control and Zn treatment, and (b) fluorescent-light green fraction from Cd and Zn plus Cd treatment.



Appendix C

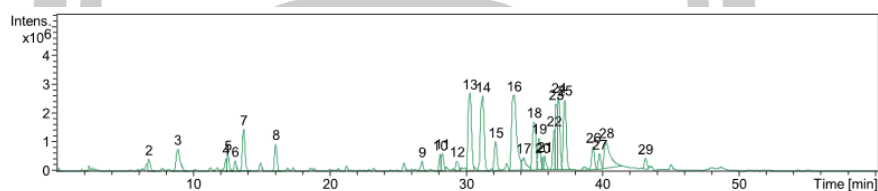
Liquid chromatography and Mass spectrometry



#	RT [min]	Prec. m/z	Prec. z	MW	Area	Height	S/N
1	0.2				524511	84008	52.5
2	2.4				1472341	202115	126.3
3	6.1				1899733	159230	99.5
4	6.6				6277184	488671	305.3
5	7.4				2264722	170955	106.8
6	8.6				20289466	825101	515.6
7	11.1				2168355	146166	91.3
8	12.3				2138054	233554	145.9
9	12.4				4399497	356165	222.5
10	13.0				3215611	286836	179.2
11	13.6				11547875	875577	547.1
12	14.9				1791117	158648	99.1
13	16.0				4564219	368957	230.5
14	26.3				7888964	411369	257.0
15	28.2				11834958	729763	456.0
16	31.1				19138808	1407934	879.7
17	35.3				6022005	437724	273.5
18	36.4				2599797	222480	139.0
19	36.7				4626791	342215	213.8
20	37.2				14196654	976608	610.2
21	39.7				4181778	290409	181.5
22	41.6				2558134	133155	83.2
23	45.3				3772274	193322	120.8
24	50.8				1970552	108800	68.0
25	55.6				2008054	89698	56.0

* Peak 1 is internal standard peak

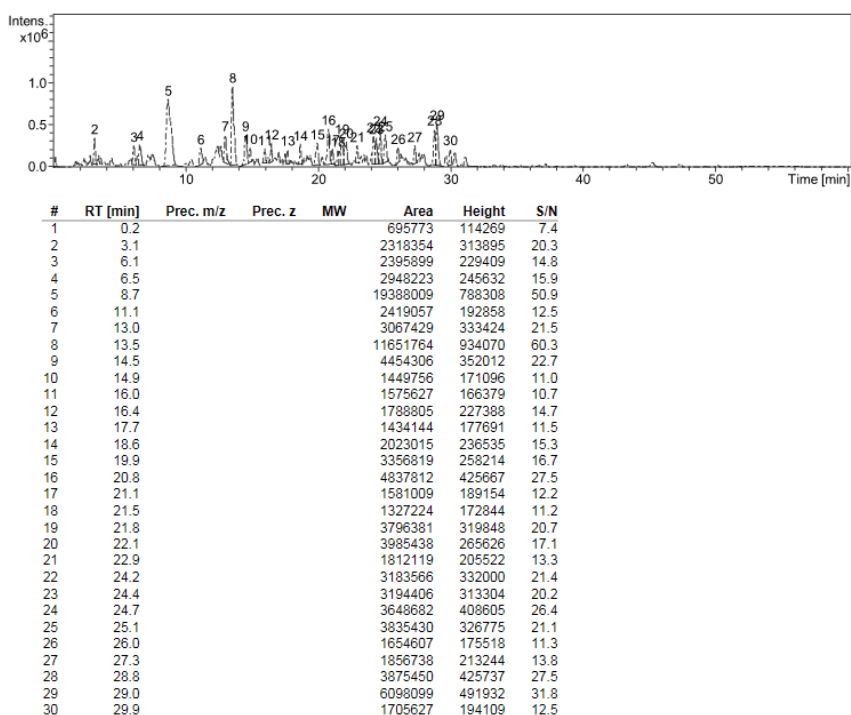
C-1 LC-MS chromatogram of ZnCd-E-2 crude extract obtained from Zn plus Cd treatment, pH-2 adjustment and ethyl acetate solvent extraction.



#	RT [min]	Prec. m/z	Prec. z	MW	Area	Height	S/N
1	0.2				704877	109752	29.0
2	6.7				5497733	421324	111.3
3	8.9				15929662	773202	204.3
4	12.4				4513637	429499	113.5
5	12.5				6408322	574783	151.9
6	13.1				4157342	359210	94.9
7	13.7				19659577	1444303	381.6
8	16.0				11909873	944660	249.6
9	26.8				4389578	335107	88.5
10	28.1				5232720	581712	153.7
11	28.2				7567611	625263	165.2
12	29.3				5034667	356806	94.3
13	30.3				47500873	2687407	710.0
14	31.2				48630732	2584979	683.0
15	32.1				14400113	999612	264.1
16	33.5				66691067	2594136	685.4
17	34.2				9702265	442450	116.9
18	35.0				28305901	1659398	438.4
19	35.3				14290866	1100662	290.8
20	35.6				3510798	436382	115.3
21	35.7				5402627	463974	122.6
22	36.4				13639870	1355411	358.1
23	36.6				20706060	2271274	600.1
24	36.8				31920747	2509959	663.1
25	37.2				37312721	2416309	638.4
26	39.3				14092658	793534	209.7
27	39.7				6998810	547979	144.8
28	40.2				28723019	899951	237.8
29	43.1				5158132	384112	101.5

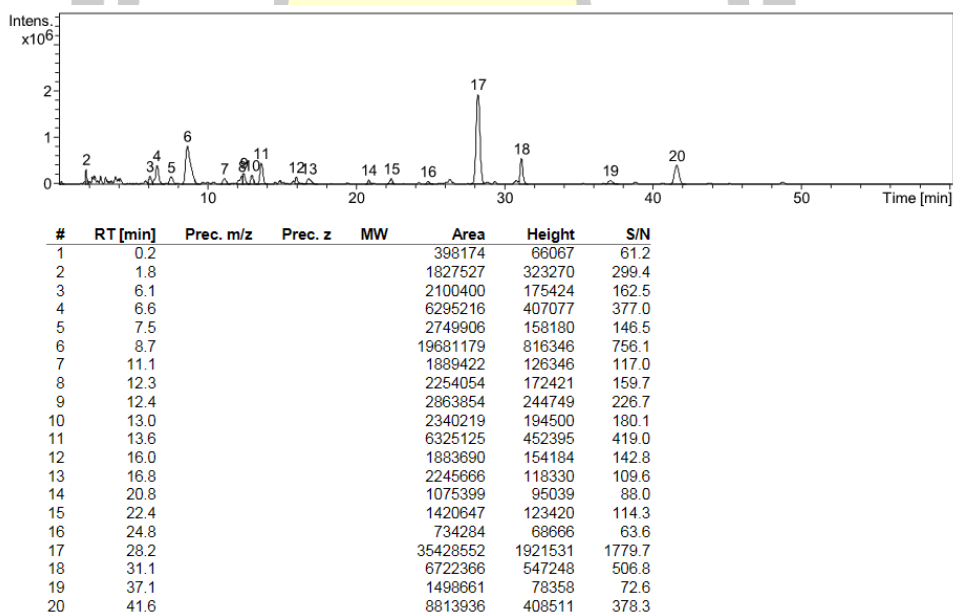
* Peak 1 is internal standard peak

C-2 LC-MS chromatogram of ZnCd-E-8 crude extract obtained from Zn plus Cd treatment, pH-8 adjustment and ethyl acetate solvent extraction.



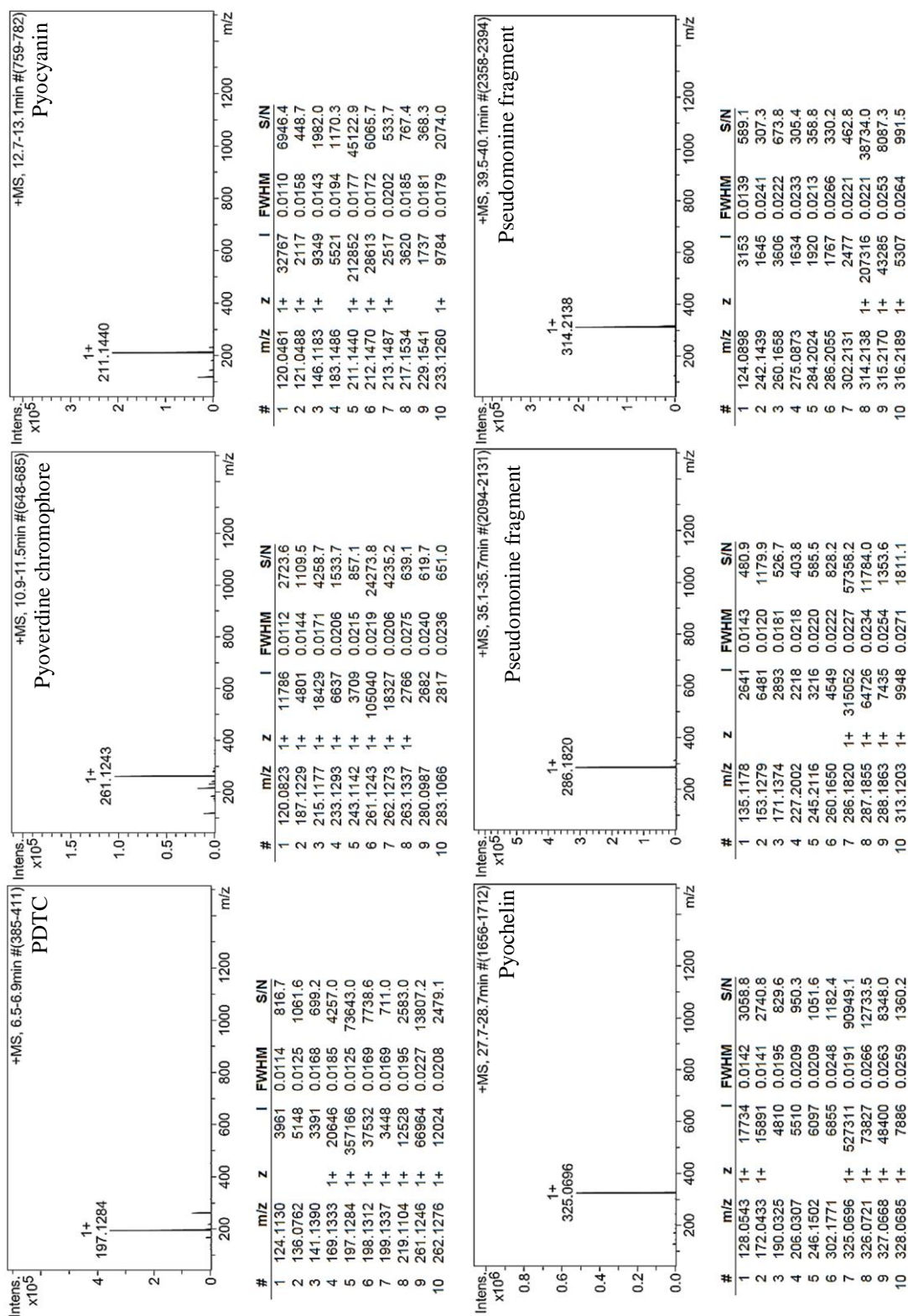
* Peak 1 is internal standard peak

C-3 LC-MS chromatogram of ZnCd-B-2 crude extract obtained from Zn plus Cd treatment, pH-2 adjustment and butanol solvent extraction.

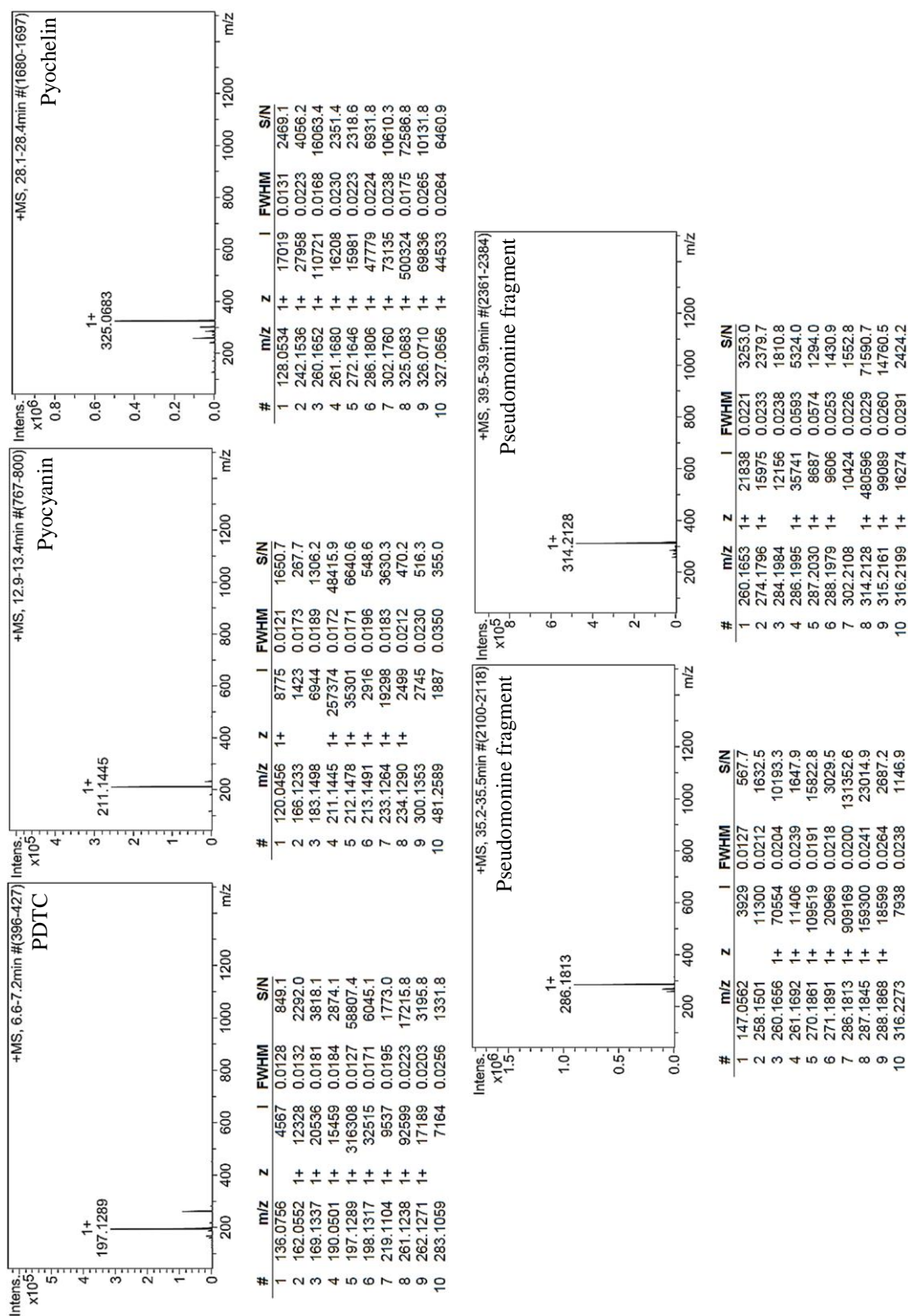


* Peak 1 is internal standard peak

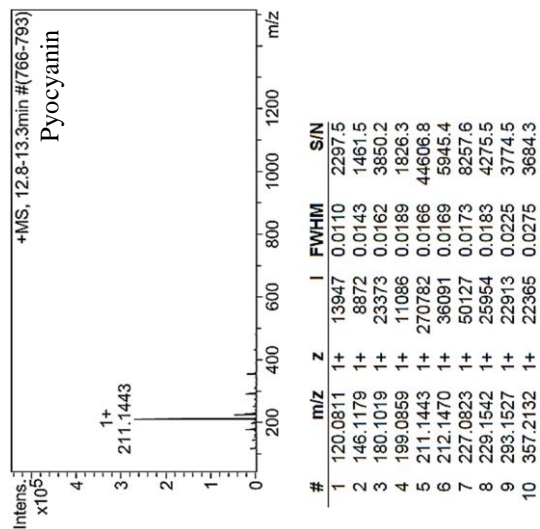
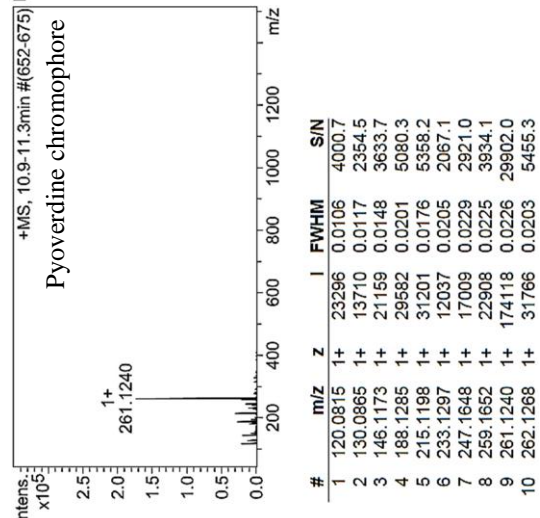
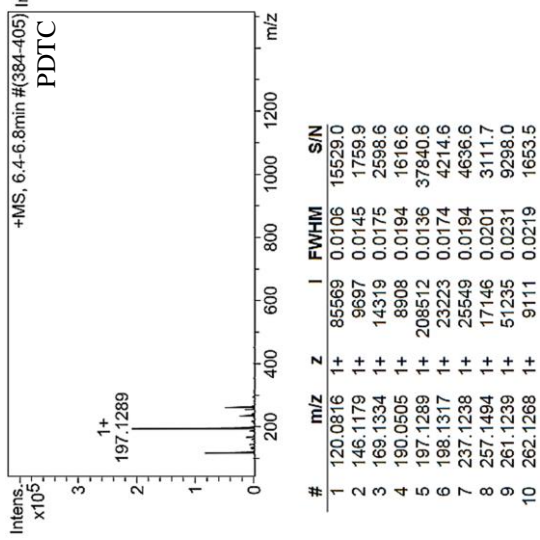
C-4 LC-MS chromatogram of ZnCd-B-8 crude extract obtained from Zn plus Cd treatment, pH-8 adjustment and butanol solvent extraction.



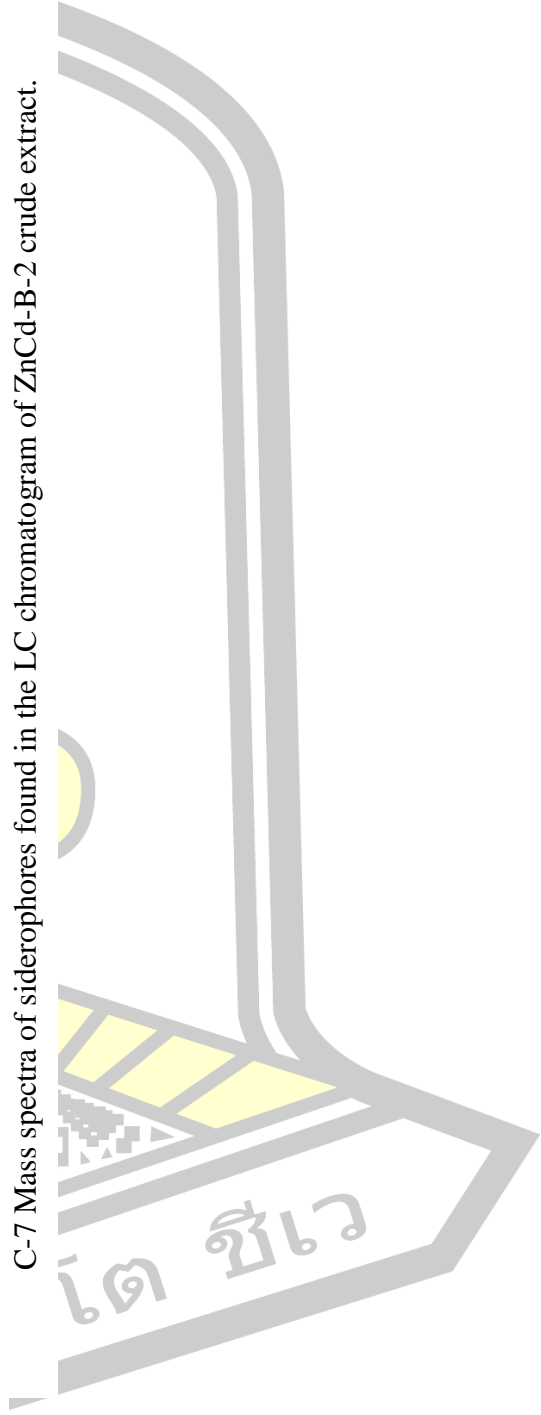
C-5 Mass spectra of siderophores found in the LC chromatogram of ZnCd-E-2 crude extract.

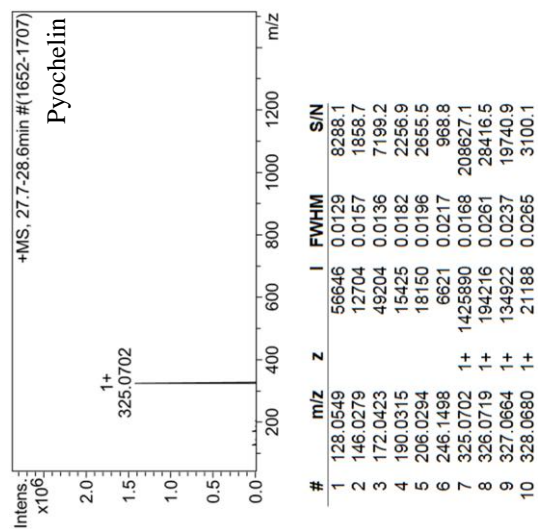
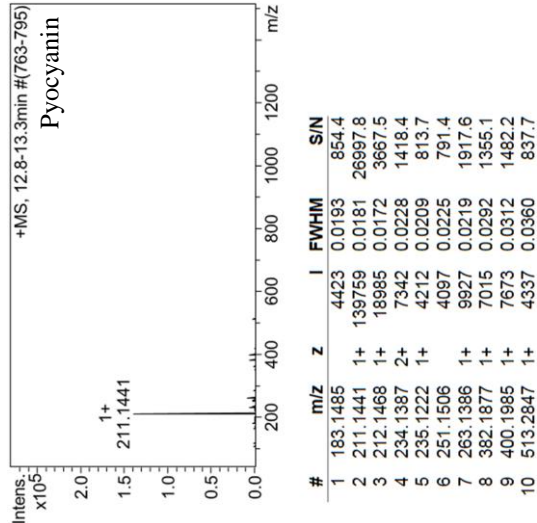
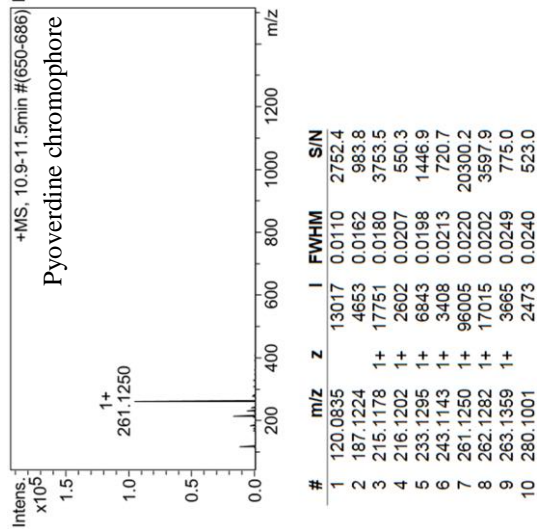
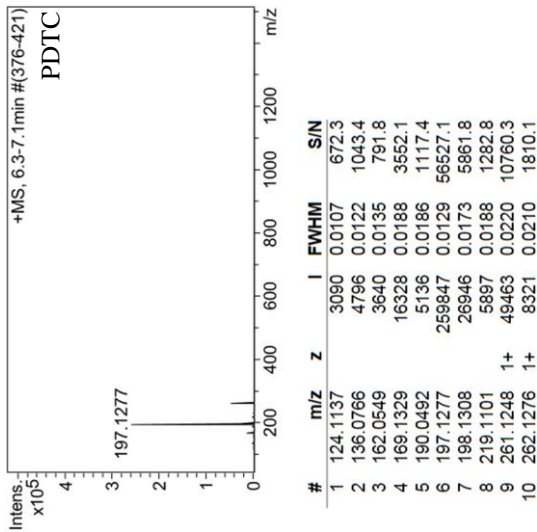


C-6 Mass spectra of siderophores found in the LC chromatogram of ZnCd-E-8 crude extract.

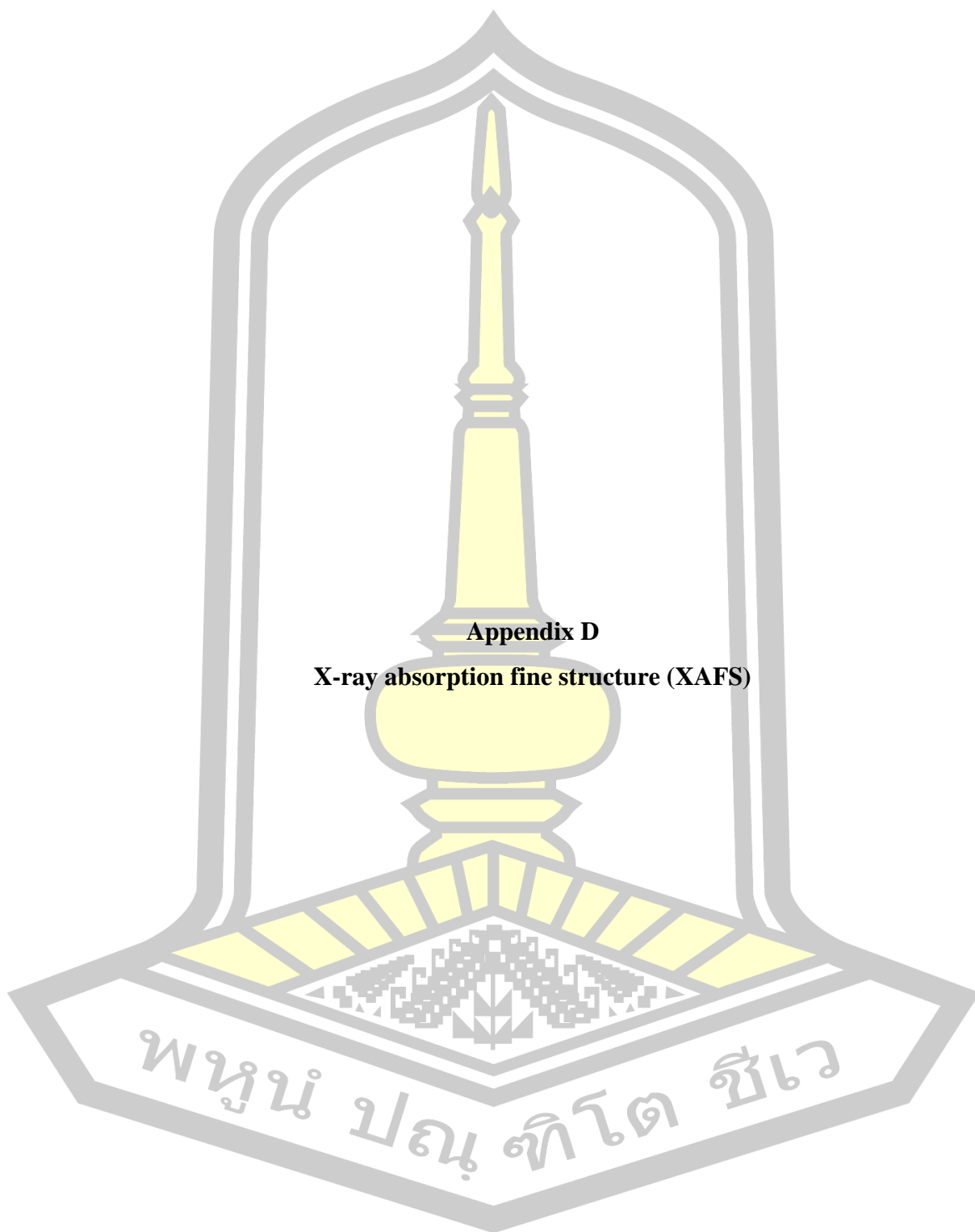


C-7 Mass spectra of siderophores found in the LC chromatogram of ZnCd-B-2 crude extract.



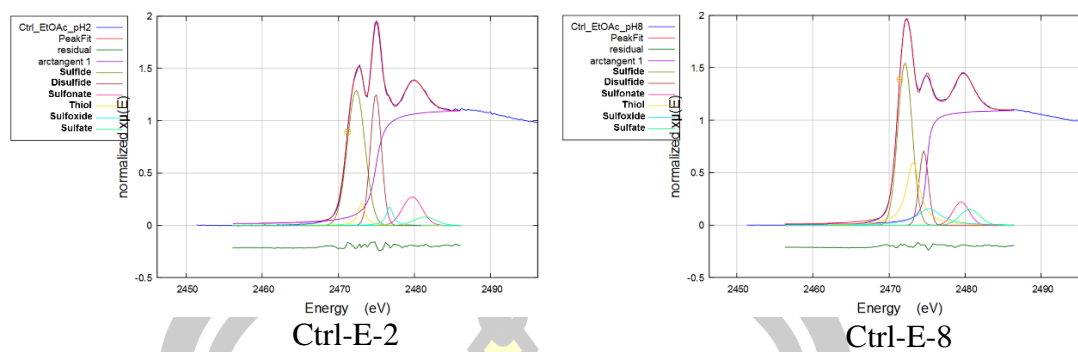


C-8 Mass spectra of siderophores found in the LC chromatogram of ZnCd-B-8 crude extract.

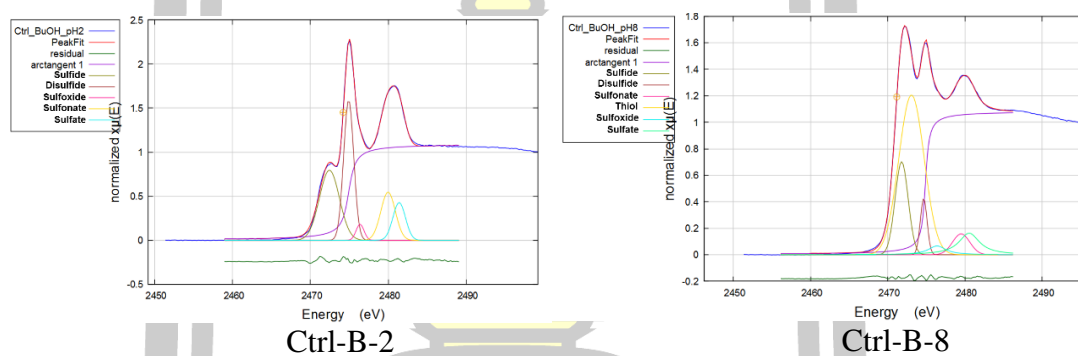


Appendix D

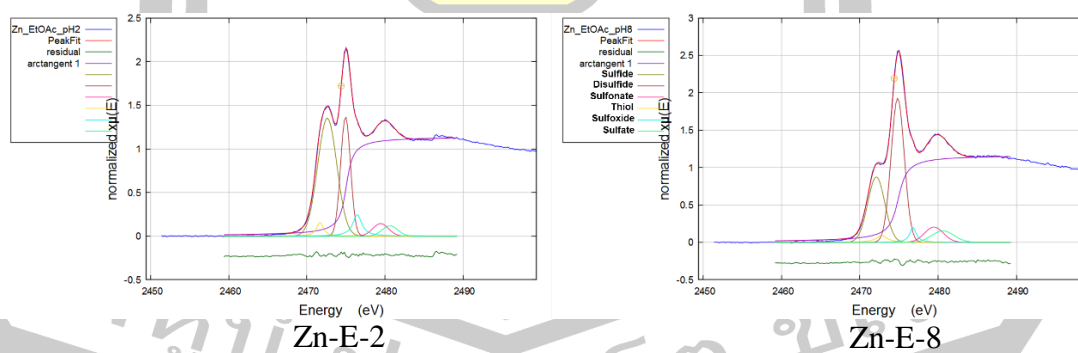
X-ray absorption fine structure (XAFS)



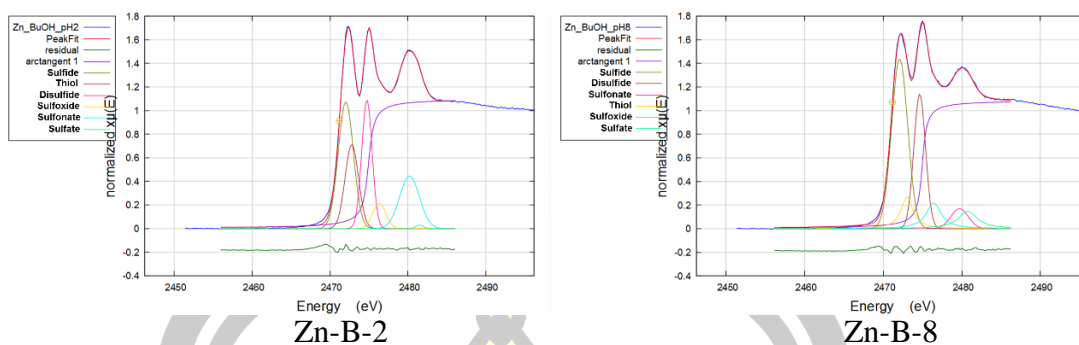
D-1 S K-edge XANES spectra of Ctrl-E-2 and Ctrl-E-8 crude extracts, and sulfur peaks fitting.



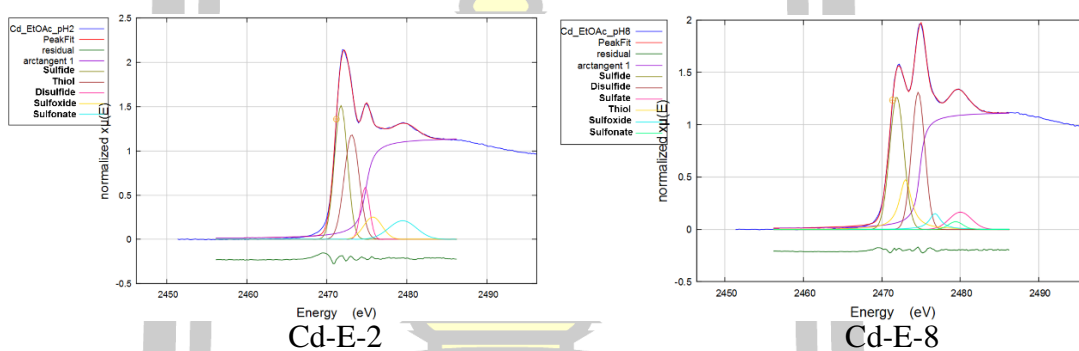
D-2 S K-edge XANES spectra of Ctrl-B-2 and Ctrl-B-8 crude extracts, and sulfur peak fitting.



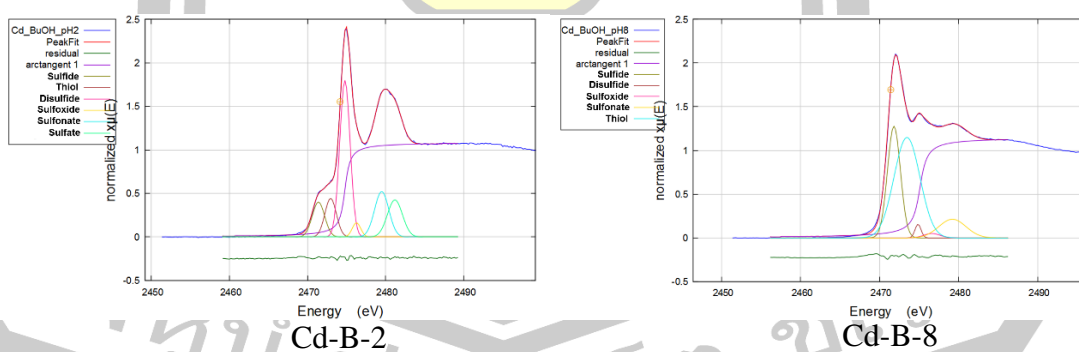
D-3 S K-edge XANES spectra of Zn-E-2 and Zn-E-8 crude extracts, and sulfur peak fitting.



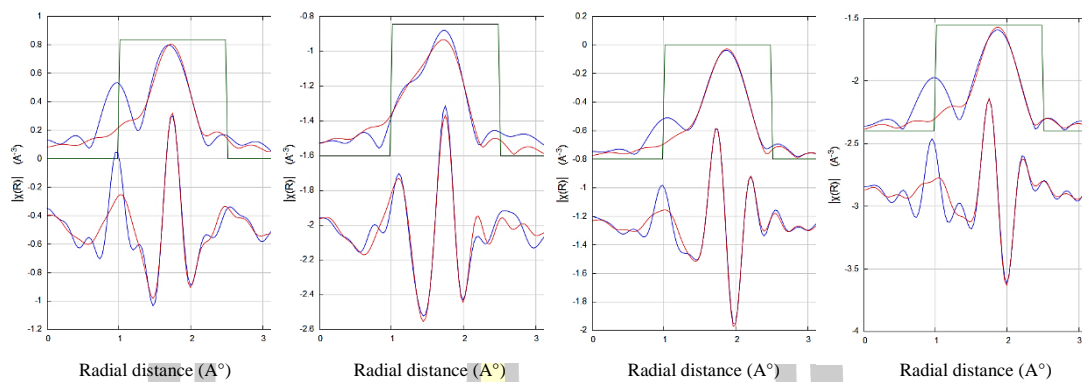
D-4 S K-edge XANES spectra of Zn-B-8 and Zn-B-8 crude extracts, and sulfur peak fitting.



D-5 S K-edge XANES spectra of Cd-E-2 and Cd-E-8 crude extracts, and sulfur peak fitting.



D-6 S K-edge XANES spectra of Cd-B-2 and Cd-B-8 crude extracts, and sulfur peak fitting.



Cd-E-8

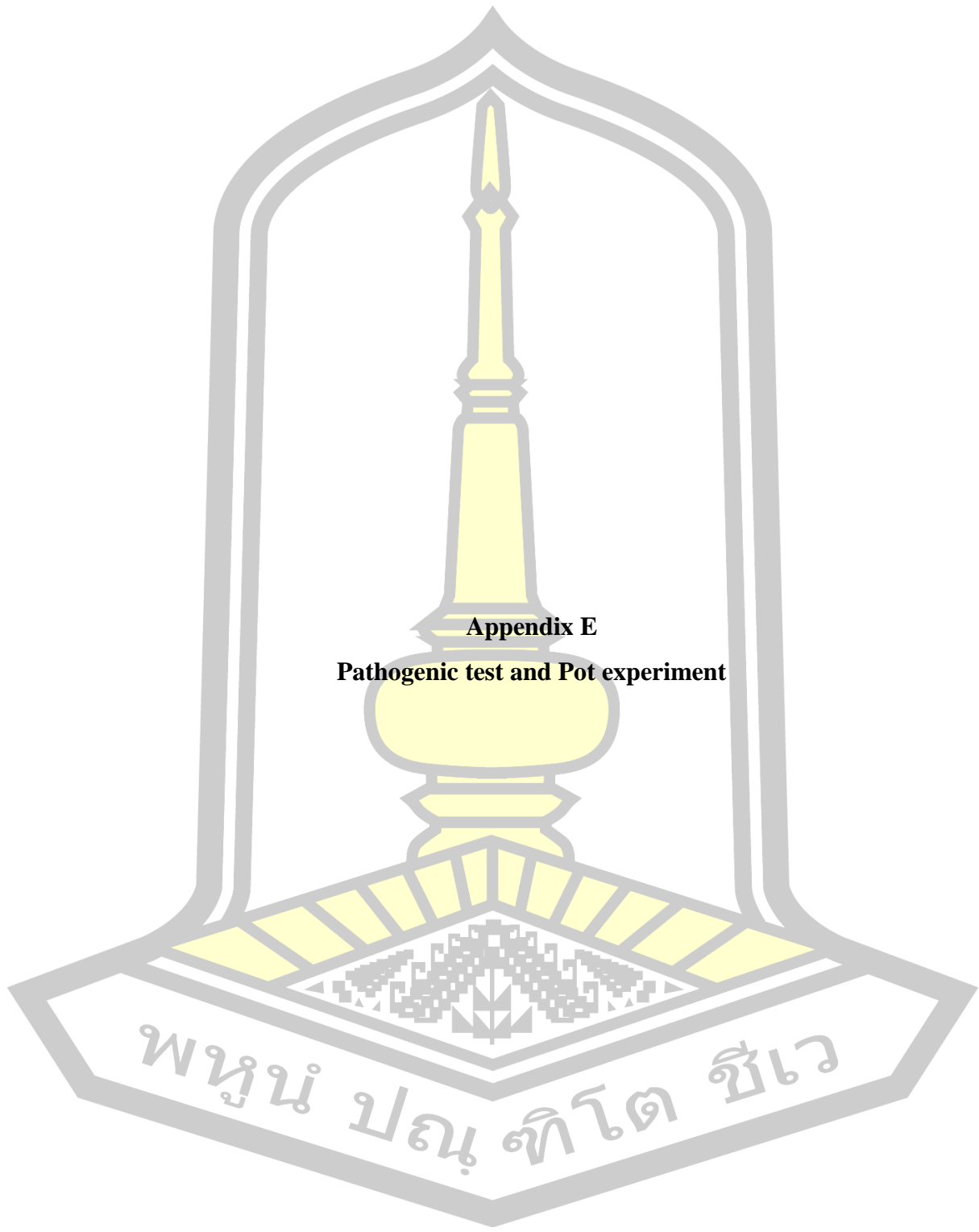
ZnCd-E-8

Cd-B-8

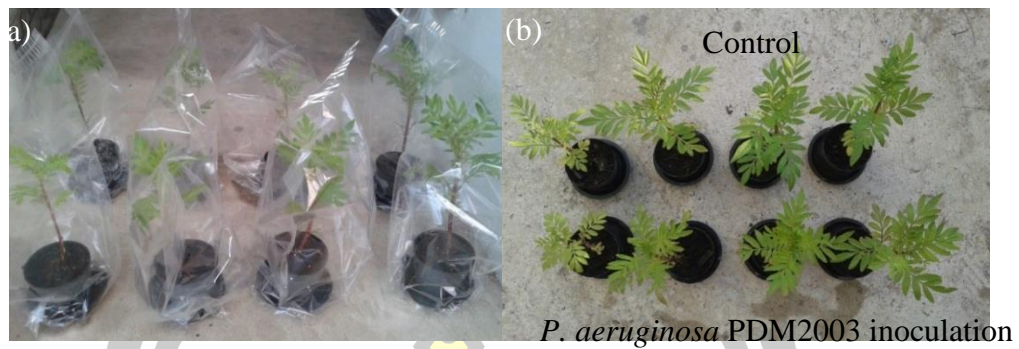
ZnCd-B-8

D-10 Cd K-edge EXAFS fitting in $\chi(R) = 1-2.5 \text{ \AA}^{-1}$ and $\chi(k) = 3-10 \text{ \AA}^{-1}$ of Cd-E-8, ZnCd-E-8, Cd-B-8 and ZnCd-B-8 crude extracts.

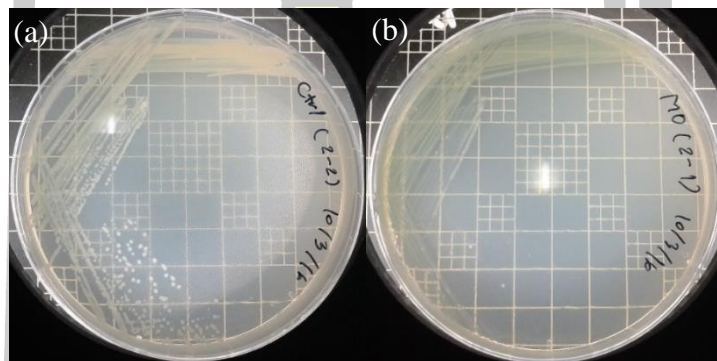




Appendix E
Pathogenic test and Pot experiment



E-1 Plant pathogenicity test (a) putting a plant in plastic bag to control moisture during incubation, and (b) control plants and plants inoculated with *P. aeruginosa* PDM2003 for 7 days.



E-2 Quadrant streak plates for bacterial detection from (a) rhizospheric soil of non-inoculated plants (control), and (b) rhizospheric soil of plants inoculated with *P. aeruginosa* PDMZnCd2004, which secrete green-fluorescence color.



E-3 Pot experiment of marigold (a) 1-month old plants, and (b) 3-months old plants in flowering stage.

BIOGRAPHY

NAME Miss Orapan Meesungnoen

DATE OF BIRTH 27 July 1986

PLACE OF BIRTH Nakhon Rachasima

ADDRESS 63/1, Moo 20, Khamrieng, Kantaravichai, Maha Sarakham, 44150, THAILAND

EDUCATION

2012-2018	Doctor of Philosophy (Biology) Mahasarakham University, THAILAND
2008-2012	Master of Science (Biology) Mahasarakham University, THAILAND
2004-2008	Bachelor of Science (Biology) Mahasarakham University, THAILAND
2001-2004	Rajsima Witthayalai school Nakhon Ratchasima, THAILAND

Research grants & awards

- Science Achievement Scholarship of Thailand, SAST
- Mahasarakham University 2016

Research output

Book Chapter

Nakbanpote W, Meesungnoen O, Prasad MNV (2015) Potential of Ornamental Plants for Phytoremediation of Heavy Metals and Income Generation In M.N.V. Prasad Ed. Bioremediation and Bioeconomy, Elsevier, USA ISBN: 978-0-12-802830-8 ISBN, 978-0-12-802830-8. Pages 179-218

Conferences

Meesungnoen O, Nakbanpote W, Klysubun W and Thumanu K (2016) Effect of pH on Siderophore extracts studied by XANES and FT-IR, Thailand synchrotron conference and exhibition 2016 (TSCE2016), February 26-28, 2016, Impact Exhibition Hall 1, Bangkok, Thailand, 94. (Poster presentation)

Meesungnoen O, Nakbanpote W, Chantiratikul P (2016) Siderophores produced by *Pseudomonas aeruginosa* PDMZnCd2003 under Zn/Cd stress, The 11th Conference on science and technology for youths, June 10-11, 2016, Bitech Bangna, Bangkok, Thailand, 303. (Poster presentation)